Design of an mRNA Vaccine Manufacturing Platform to Target *M. Tuberculosis*

A Technical Report submitted to the Department of Chemical Engineering

Presented to the Faculty of the School of Engineering and Applied Science
University of Virginia • Charlottesville, Virginia

In Partial Fulfillment of the Requirements for the Degree
Bachelor of Science, School of Engineering

Technical Project Team Members
Elliot Brna
Abbie Frost
Eliza Mills
Ian Sellors
Jason Wieder

Spring 2025

On my honor as a University Student, I have neither given nor received unauthorized aid on this assignment as defined by the Honor Guidelines for Thesis-Related Assignments

Technical Advisor

Eric Anderson, Department of Chemical Engineering

Table of Contents

1 Executive Summary

This report outlines the design and operational framework for an mRNA vaccine manufacturing facility, specifically targeting *Mycobacterium tuberculosis* (M. tuberculosis). The facility is designed to produce 10 million doses of vaccine annually. The production process involves mRNA synthesis, lipid nanoparticle (LNP) encapsulation, purification, and sterile filtration, ensuring high product quality and regulatory compliance. The plant is estimated to operate for 20 years of production with a cumulative cash flow after the 20 years of $196,047,136, with a total capital investment of $3,818,134. The estimated internal rate of return of the designed facility is 105%, thus, the design is highly profitable, while also combatting the global tuberculosis crisis.

Key Features:

- **Production Capacity:** The facility will produce 576 grams of mRNA encapsulated in lipid nanoparticles annually to be sent to external fill-to-finish operations, sufficient for 10 million vaccine doses. This includes allowances for fill-to-finish losses and ensures consistent supply to domestic and international markets.
- **Target Markets:** The vaccine is intended for healthcare workers and travelers in the U.S., as well as high-incidence regions such as Southeast Asia and Africa, which account for 70% of global TB cases.
- **Batch Scheduling:** The facility operates on a batch schedule of 24 annual runs, with each batch producing 24 grams of mRNA. This ensures efficient utilization of resources while meeting production targets.

- **Process Outline:**
    - **mRNA Synthesis:** In vitro transcription (IVT) is employed to produce mRNA strands using a T7 RNA polymerase system. A co-transcriptional capping process ensures high efficiency and stability of the mRNA product.
    - **mRNA Purification:** Sequential chromatography steps, affinity chromatography (AC) and anion exchange chromatography (AEX), remove impurities to prepare for LNP encapsulation.
    - **LNP Formation:** The mRNA is encapsulated in lipid nanoparticles using a confined impinging jet mixer (CIJM), providing protection against degradation and facilitating cellular delivery.
    - **LNP Purification:** Tangential flow filtration is used to remove excess lipids and unencapsulated mRNA, as well as to swap the buffer to improve stability and allow for cryo-preservation.

The facility adheres to stringent regulatory standards for Good Manufacturing Practices (GMP). Processes are designed to meet FDA and WHO guidelines for vaccine production, ensuring safety, efficacy, and environmental sustainability.

This facility represents a significant advancement in vaccine manufacturing technology. By leveraging modular mRNA synthesis processes and scalable LNP encapsulation techniques, it addresses the urgent need for an effective TB vaccine while maintaining flexibility for future applications against other infectious diseases.

2 Introduction

2.1 Background and Motivation

Vaccines help prevent the spread of infectious diseases, consequently reducing the impact and risk of outbreaks and lowering treatment costs. Traditional vaccines involve dead or attenuated versions of bacteria, viruses, or toxins that serve as antigens, triggering an immune response to prepare the body to recognize and fight the pathogen in the future. mRNA vaccines offer an alternative to traditional vaccines, differing from traditional vaccines because they deliver mRNA that instructs cells to produce specific antigens and trigger the immune response against the produced antigens.[1] mRNA vaccines were proposed in 1988 by Robert Malone because of the HIV/AIDS epidemic, which required a safe, long-term, and broad immune response. After decades of work and research, the COVID-19 pandemic finally offered a chance for the mRNA vaccine to make it to the market, as a quick solution was needed.[2] Pfizer (jointly with BioNTech) and Moderna created the first approved mRNA vaccines in 2020, initiating the next generation of vaccine technology.

mRNA vaccines offer high potency, safety, efficacy, capacity for rapid clinical development, and potential for rapid, low-cost manufacturing[3] mRNA vaccines can be designed and synthesized in weeks compared to traditional vaccine timelines of 10.71 years on average.[2] mRNA helps generate antigens to trigger an immune response without needing to enter the nucleus of a cell.[2] Their modular nature allows for flexible adaptation to different pathogens by altering the mRNA sequence to the desired antigen.[1] Despite these advantages, mRNA vaccines also suffer many barriers that require work as they grow in use and popularity. These include mRNA's low thermal

stability, complex delivery via lipid-based nanoparticles (LNPs), lack of standardization and public acceptance, disease and genetic variability, and possible adverse reactions.[1]

Tuberculosis (TB) is an old disease that has been found in human skeletons for thousands of years. It is caused by Mycobacterium tuberculosis, a bacillus that spreads when those sick with TB expel bacteria into the air.[4] The disease typically affects the lungs (pulmonary TB) but can affect other sites (extrapulmonary TB). There are more cases among adults than children and men than women. The COVID-19 pandemic disrupted the TB service supply chain and global reduction strategies, causing a rise in TB cases that reached a new high in 2023 at 10.8 million incident cases. The Southeast Asia and Africa regions accounted for the most TB cases in 2023, at 45% and 24%, respectively. India, Indonesia, China, the Philippines, and Pakistan are the top five countries with the highest TB burden, accounting for a collective 56% of global 2023 cases.[5]

Of the 10.8 million cases, there were an estimated 1.25 million deaths from TB in 2023. TB is the world's leading cause of death from a single infectious agent, reclaiming this title after COVID-19. Without treatment, the death rate from TB is close to 50%; however, current treatments recommended by WHO have around an 85% success rate.[5] This treatment involves a rigorous six-month regimen of four drugs, though other types of TB (e.g., drug-resistant TB) require other versions of this regimen and have lower success rates.

The only approved TB vaccine is the Bacillus Calmette-Guérin (BCG) vaccine. This vaccine prevents severe forms of TB in infants but is ineffective for adolescents and adults.[5] BCG is alternatively used as an intravesical immunotherapy treatment for early-stage bladder cancer.[6] Since 2019, Merck, BCG's sole U.S. producer and distributor, has placed the treatment under an allocation system due to increased demand; therefore, minimal quantities have been used for TB prevention in recent years (*Merck*, 2024).[7] BCG is thus insufficient, necessitating the development

of a robust TB vaccine. Currently, there are 15 unique TB vaccine candidates in clinical trials (Figure 2.1-1).[8] This includes an mRNA-based candidate, BNT164a1/BNT164b1, created by BioNTech in collaboration with the Bill and Melinda Gates Foundation.[4] The potential vaccine has recently entered Phase II trials in Germany and South Africa.[9]

Figure. 2.1-1. 2023 clinical trials pipeline for TB drugs. Adapted from Looney (2023).[8]

Our work intends to improve existing mRNA vaccine processes, address previously listed barriers, and develop an effective TB vaccine for global use.

2.2 Market Size and Plant Capacity

Our tuberculosis mRNA vaccine is intended for new healthcare workers and travelers to Southeast Asia when sold on the U.S. domestic market and will also be exported to Southeast Asia and Africa to satisfy their need for an efficacious tuberculosis vaccine, as these regions account for approximately 70% of global TB incidence.[10] Therefore, to determine our production scale, separate estimates for demand in these markets must be determined.

The CDC estimates that over 13 million people are living with latent tuberculosis in the U.S. with most incidences caused by working in healthcare, nursing homes, and homeless shelters or traveling to or from countries where TB is common.[11] Since TB has never been routinely vaccinated against in the U.S., we do not expect a widespread implementation of our product; however, we plan for our product to become an industry standard requirement for healthcare professionals and a standard recommendation for travel to high-incidence countries, specifically within Southeast Asia, like the Philippines and Vietnam.

The U.S. Bureau of Labor Statistics estimates that there are approximately 1.9 million job openings in the healthcare industry each year, and in 2023, only roughly 653,000 of them were new openings.[12,13] The number of new job openings per year serves as a good metric for our production as this quantity serves as an approximate indicator of new personnel entering the healthcare industry thus making them ideal recipients of our vaccine. Therefore, we plan to manufacture 653,000 doses each year to sell to new personnel entering the healthcare industry in the U.S.

In 2019, an estimated 4.8 million people from the U.S. visited the ASEAN region, which consists of Brunei Darussalam, Cambodia, Indonesia, Laos, Malaysia, Myanmar, Philippines, Singapore, Thailand, and Vietnam.[14] It is unrealistic to assume that all travelers to Southeast Asia will choose

to vaccinate using our product, so we plan to manufacture enough to vaccinate 30% of travelers as a conservative estimate; therefore, we plan to manufacture 1.6 million doses annually to meet this demand. We selected 2019 as the most important year to base our production quantity off because it represents travel that is unaffected by the COVID-19 pandemic; we expect travel to Southeast Asia to eventually return to this level.

In 2023, 10.8 million people became infected with TB and fell ill globally, with 45% and 24% of cases occurring in Southeast Asia and Africa, respectively.[5] We can assume that these cases were preventable by efficacious vaccination, so we can estimate that 7.45 million doses per year as our overall demand for Southeast Asia and Africa.

Combining the determined demands for new U.S. healthcare workers, U.S. travelers going to Southeast Asia, and exports to Southeast Asia and Africa, we plan to produce 10 million doses of our final mRNA vaccine annually. A single vial of our vaccine, as mentioned in the explanation of the product section, will contain a dry weight of 48 μg of our mRNA product; therefore, to produce 10 million doses, a total dry weight of 480 g of mRNA is needed, not including the additional weight contributed by the lipid nanoparticle encapsulation. However, since our process ends before fill-to-finish operations, we must increase our production quantity to account for filling losses. We will use an estimated loss from the conversion of our product from multi-dose vials to single-dose vials of 20%, which is a conservative estimate by industry professionals.[15] To conclude, to meet our outlined production demand and account for losses due to outsourcing the filling operations for our product, we plan to produce 576 g of dry weight of our encapsulated mRNA product in our facility each year.

Our final LNP-mRNA formulation will be stored at a concentration of 100 μg mRNA per mL of buffer solution. This will be the same concentration used for vial filling. Based on this

concentration for our formulation, we will produce 5760 L of LNP-mRNA vaccine product each year.

To meet this production goal, 24 batches are scheduled throughout the course of each year, with each batch producing 24 g of mRNA. The mRNA product for each batch will be suspended in 240 L of buffer to ensure a concentration of 100 μg per mL. The product for each batch will be distributed equally into three 100 L sterile bags to be frozen down to -80ºC for storage prior to being shipped to fill-to finish operations.[16]

3 Discussion

3.1 Process Flow Diagram

The LNP-mRNA vaccine manufacturing process contains several unit operations organized in a batch schedule. The process is structured in four main blocks: mRNA synthesis, mRNA purification, LNP-mRNA formation, and LNP-mRNA purification. A buffer preparation and hold area, located on the second floor of the plant, supplies all buffers needed for the process to operate. The following sections provide a design overview of each piece of equipment included in the process flow diagram (Figure 3.1-1).

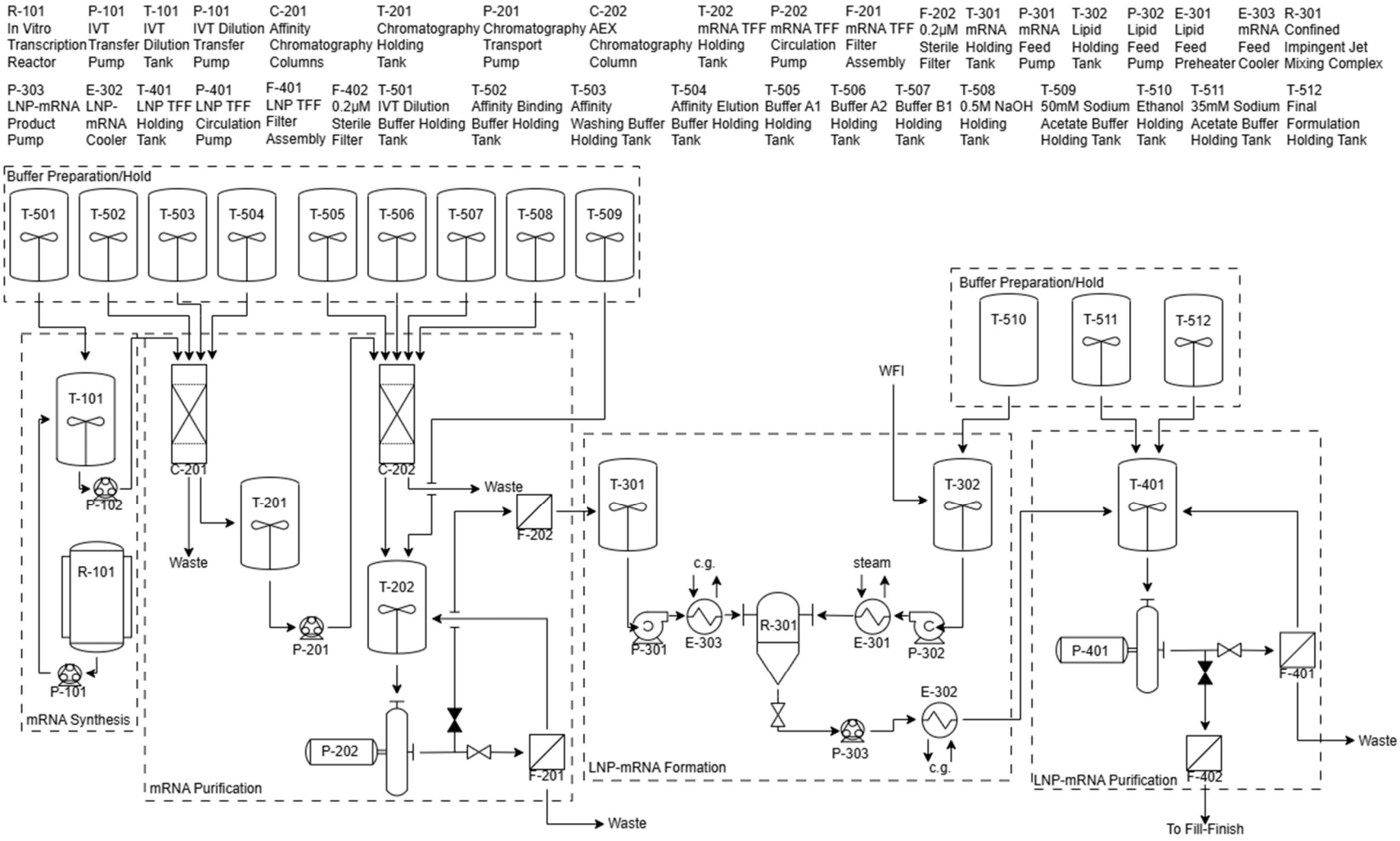

Figure 3.1-1. Process flow diagram for the LNP-mRNA vaccine manufacturing platform.

3.2 Material Balance

As a means of measuring overall process efficiency, the step yield on mRNA is estimated for each step and then the overall yield on mRNA at each point in the process is determined; this information is available in Table 3.2-1. The details of how each step yield was determined are provided in sections 3.3-5. Using the information in Table 3.2-1, the manufacturing process, including both upstream and downstream operations, is expected to have a final yield on mRNA of 38.0%, requiring that 63.20 g of target mRNA be produced per batch during mRNA synthesis to achieve the final production target of 24.00 g of target mRNA exiting the facility per batch as formulated product.

Table 3.2-1: Target mRNA yield table

Process	Step Yield (%)	Overall Yield (%)	mRNA per Batch Entering Step (g)
Transcription	80.0	80.0	63.20
Capping	95.0	76.0	50.56
Affinity Chromatography	80.0	60.8	48.03
Anion Exchange Chromatography	75.3	45.8	38.43
TFF/DF	100.0	45.8	28.94
Sterile Filtration	96.0	44.0	28.94
LNP Formation	90.0	39.6	27.78
Concentration TFF	100.0	39.6	25.00
TFF/DF	100.0	39.6	25.00
Sterile Filtration	96.0	38.0	25.00
Final Yield		**38.0**	**24.00**

3.3 *In vitro* Transcription

3.3.1 Reagents

3.3.1.1 Transcription

In vitro transcription (IVT) is a cell-free, flexible, and scalable method of mRNA synthesis. The process uses a linearized DNA template containing the sequence of interest purchased from a contracted organization, rather than produced on-site using gene-editing, *E.coli* and restriction enzymes. A bacteriophage-derived RNA polymerase then builds the target RNA sequence from the DNA strand with nucleoside triphosphates (NTPs) (Figure 3.3.1.1-1). Here, the T7 phage of E. coli is used. The T7 RNA polymerase (RNAp) binds to a sequence on the DNA template called the T7 promoter to catalyze RNA synthesis. T7 RNAp is highly specific for the T7 promoter sequence, ensuring that transcription begins at the correct site. The sequence of interest is placed downstream of the promoter. The T7 system is known for its high transcription rate, producing large amounts of RNA.[17]

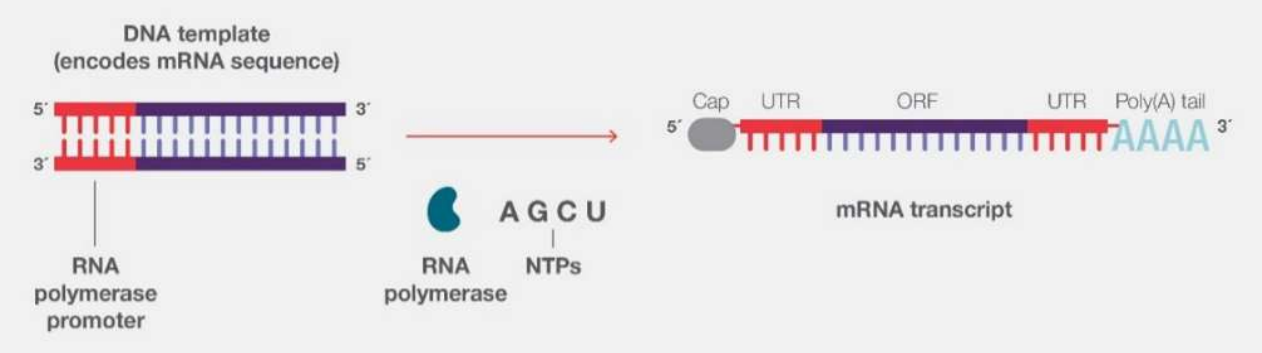

Figure 3.3.1.1-1: *In vitro* transcription (adapted from ThermoFischer)[2]

mRNA consists of a 5’ cap, coding sequence, untranslated region (UTR), and poly(A) tail (Figure 3.3.1.1-2). The 5’ cap is a modified guanine nucleotide added to the beginning of the mRNA transcript shortly after transcription begins. This cap is crucial for stability and initiating translation. The coding sequence contains instructions for synthesizing a protein, which, in the case of our

designed process, aids in tuberculosis immune response, and is transcribed from the gene's coding region. The 5' and 3' UTRs are mRNA domains that control post-transcriptional gene regulation. The poly(A) tail is a string of adenine nucleotides added to the 3' end of the mRNA after transcription. The tail plays an important role in stability and translation efficiency.[18]

Figure 3.3.1.1-2: mRNA structure (adapted from LabClinics)[4]

The reagents involved in IVT include Tris-HCl buffer, template DNA strands, nucleotides, T7 RNAp, capping analog, Magnesium chloride, ribonuclease inhibitor, dithiothreitol, spermidine, and pyrophosphatase. The Tris-HCl buffer and dithiothreitol (DTT) ensure an ideal environment for the enzymes involved with the reaction, keeping an optimal acidic environment and preventing oxidation. Equimolar amounts of nucleotides (ATP, GTP, ΨTP, CTP) are used, with pseudo uridine (ΨTP) being used to decrease anti-RNA immune response and to prevent degradation.[19] Because T7 RNAp is magnesium-dependent, magnesium chloride is added as a source for the enzyme. One of the byproducts of IVT is pyrophosphate, which is inclined to form a complex with magnesium, causing precipitate to form in the reaction. For this, pyrophosphatase is added to break down the pyrophosphate, preventing feedback inhibition and formation of magnesium-pyrophosphate precipitation.[20]

3.3.1.2 Co-transcriptional Capping

Capping the 5' end of the mRNA is essential to prevent mRNA degradation prior to delivery to the cell. The two methods usually used for the capping process are post-transcriptional capping and co-transcriptional capping. In post-transcriptional capping, capping enzymes are added once

the mRNA is synthesized from the template DNA strand. Co-transcriptional capping is a "one pot" reaction, where the capping enzymes work simultaneously with RNA polymerase to add the cap to the 5' end while the strand is synthesized. Although post-transcriptional capping gives higher yields, co-transcriptional capping is more cost-effective and is used in synthesizing the COVID-19 mRNA vaccines.[22]

The two approaches on the market for co-transcriptional capping are Anti-reverse cap analogs (ARCA) and CleanCap. Anti-reverse cap analogs create a cap-0 structure during IVT, and the process requires an additional enzyme, mRNA cap 2'-O-methyltransferase, added post IVT to reach the final desired cap-1 structure. CleanCap can create a cap-1 structure in one step during IVT. ARCA has a lower capping efficiency than CleanCap (50-80% vs >95%), but it is more cost-effective.[23] We chose to use CleanCap as our capping analog due to its high efficiency and because the cost was manageable for our system.

3.3.1.3 DNAse Treatment

After IVT and co-transcriptional capping is complete, the remaining DNA template must be digested to send the final mRNA product through purification. This is done through adding DNAse and EDTA to the reactor post IVT, where DNAse is given time to digest the remaining DNA template strand and then EDTA quenches DNAse activity and further stabilizes the mRNA for purification.[20]

3.3.2 IVT Kinetics

3.3.2.1 Reaction Equations: Initiation, Elongation, Inhibition and Termination

Transcription of mRNA from DNA is an enzymatically catalyzed polymerization reaction that occurs in 3 primary steps: initiation, elongation and termination.[24] For initiation to occur, both a

guanosine triphosphate (GTP) and a T7 RNA polymerase must form a complex with the promoter sequence of the linearized DNA template. Upon complexation, initiation can be completed, and the polymerase is irreversibly bound to the template, modeled in Equations 3.3.2.1-(1-5).

Binding of GTP to the enzyme (E), followed by complexation with the promoter (D)

$$E + GTP \rightleftarrows E \cdot GTP \quad (3.3.2.1\text{-}1)$$

$$E \cdot GTP + D \rightleftarrows E{\cdot}GTP{\cdot}D \quad (3.3.2.1\text{-}2)$$

Binding of the enzyme (E) to the promoter (D) followed by complexation with GTP

$$E + D \rightleftarrows E \cdot D \quad (3.3.2.1\text{-}3)$$

$$E{\cdot}D + GTP \rightleftarrows E{\cdot}D{\cdot}GTP \quad (3.3.2.1\text{-}4)$$

Irreversible complexation, where M_1 is the mRNA transcript of length 1

$$E{\cdot}D{\cdot}GTP \rightarrow E{\cdot}D{\cdot}M_1 \quad (3.3.2.1\text{-}5)$$

Elongation follows irreversible complexation, where the target mRNA sequence (M_n) is formed through the binding of nucleotide triphosphates (NTPs) to the T7 polymerase and cleavage of pyrophosphate molecules (PPi). Despite the simplicity of this reaction, there are many forms of inhibition which slow conversion. Competitive inhibition occurs between various NTPs which, randomly and reversibly, bind to the enzyme complex throughout transcription, slowing conversion (Equation 3.1.2.1-6,7).[24] Additionally, byproduct pyrophosphate (PPi) can bind with the enzyme complex preventing the binding of the correct NTP additional complexation with two magnesium ions causes precipitating out of the enzyme out of solution (Equations 3.1.2.1-(8-10)). As T7 polymerase is a magnesium-dependent enzyme, assisting with the cleavage of the phosphodiester bond (removal of PPi), the removal of magnesium ions from solution has severe

inhibitory effects.[25] These inhibitory effects can be reduced and avoided in the presence of an inorganic phosphatase enzymes that hydrolyze PPi into inorganic phosphate, prior to complexation and precipitation with Mg.

$$E + NTP \rightleftarrows E \cdot NTP \quad (3.3.2.1\text{-}6)$$

$$E{\cdot}D + NTP \rightleftarrows E{\cdot}D{\cdot}NTP \quad (3.3.2.1\text{-}7)$$

$$E + PPi \rightleftarrows E \cdot PPi \quad (3.3.2.1\text{-}8)$$

$$E{\cdot}D + PPi \rightleftarrows E{\cdot}D{\cdot}PPi \quad (3.3.2.1\text{-}9)$$

$$E{\cdot}D{\cdot}M_j + PPi \rightleftarrows E{\cdot}D{\cdot}M_j{\cdot}PPi \quad (3.3.2.1\text{-}10)$$

**where M_j is the mRNA transcript of length j*

The final reaction step is termination, where the RNA polymerase reaches the end of the coding region of DNA. Once reaching the target length (sequence length includes coding for the 3' poly-A tail) the enzyme-DNA-mRNA complex disintegrates as described by Eq. 3.3.2.1-11, releasing a completed mRNA strand (M_n), DNA template (D) and T7 polymerase (E) to create the next strand.

$$E{\cdot}D{\cdot}M_n \rightarrow E + D + M_n \quad (3.3.2.1\text{-}11)$$

3.3.2.2 Michaelis-Menten Approximation

To estimate the conversion of NTPs to mRNA, Equations 3.3.2.1-(1-11) were simplified using the Michaelis-Menten approximation (Equations 3.3.2.2-1&2). The Michaelis-Menten approximation assumes the reversible binding of a substrate to an enzyme followed by an irreversible product formation with the rate of product formation described in equation 3.3.2.2-2.

$$E + S \rightleftarrows E{\cdot}S \rightarrow E + P \qquad (3.3.2.2\text{-}1)$$

$$V = \frac{d[P]}{dt} = \frac{V_{max}[S]}{K_m + [S]} = \frac{V_{max}'}{K_m + [S]} \qquad (3.3.2.2\text{-}2)$$

Applying a similar approximation, we can simplify the initiation, elongation and termination steps into two steps: the reversible binding of a nucleotide to the linearized pDNA sequence and the irreversible polymerization reaction that resulting in the cleaving of a pyrophosphatase.[26,27] As it's expected that the concentration of linearized pDNA remain constant, we can re-write $V_{max}[S]$ as V_{max}'. Therefore, the expression for mRNA synthesis can be modeled using equation 3.3.2.2-3 which accounts for competition between nucleotides (NTPs).

$$\frac{d[P]}{dt} = \frac{V_{max}'}{1 + \sum_{j=1}^{N} \frac{K_{M,\,NTP,\,j}}{C_{NTP,\,j}} \left(1 + \sum_{\substack{i=1 \\ i \neq j}}^{N} \frac{C_{NTP,\,i}}{K_{I,\,NTP,\,i}}\right) + \frac{K_{M,D}}{C_D} \left[1 + \frac{K_G^I}{C_{GTP}} \left(1 + \sum_{\substack{i=1, \\ i \neq j}}^{N-1} \frac{C_{NTP,\,i}}{K_{I,\,NTP,\,i}}\right)\right]} \qquad (3.3.2.2\text{-}3)$$

However, we choose to make the simplifying assumption that all nucleotides are saturated due to the limited amount of experimental data available on inhibition coefficients for each NTP ($K_{I,\,NTP,\,i}$). This allows the elimination of the competition between NTPs term of the equation, simplifying the equation to equation 3.3.2.2-3.

$$\frac{dC_{mRNA}}{dt} = \frac{V_{max}}{1 + \frac{K_{M,ATP}}{C_{ATP}} + \frac{K_{M,CTP}}{C_{CTP}} + \frac{K_{M,GTP}}{C_{GTP}} + \frac{K_{M,UTP}}{C_{UTP}} + \frac{K_{M,D}}{C_D}\left(1 + \frac{K_G^I}{C_{GTP}}\right)} \qquad (3.3.2.2\text{-}4)$$

The following differential equations (3.3.2.2-(5-8)) model the consumption of nucleotides (assuming saturation), where n represents the number of bases per mRNA strand, and f_{NTP} represents the fraction of a specific NTP in the target mRNA sequence:

$$\frac{dC_{ATP}}{dt} = -\frac{V_{max} \cdot n \cdot f_{ATP}}{1 + \frac{K_{M,ATP}}{C_{ATP}} + \frac{K_{M,CTP}}{C_{CTP}} + \frac{K_{M,GTP}}{C_{GTP}} + \frac{K_{M,UTP}}{C_{UTP}} + \frac{K_{M,D}}{C_D}\left(1 + \frac{K_G^I}{C_{GTP}}\right)} \qquad (3.3.2.2\text{-}5)$$

$$\frac{dC_{CTP}}{dt} = -\frac{V_{max} \cdot n \cdot f_{CTP}}{1 + \frac{K_{M,ATP}}{C_{ATP}} + \frac{K_{M,CTP}}{C_{CTP}} + \frac{K_{M,GTP}}{C_{GTP}} + \frac{K_{M,UTP}}{C_{UTP}} + \frac{K_{M,D}}{C_D}\left(1 + \frac{K_G^I}{C_{GTP}}\right)} \quad (3.3.2.2\text{-}6)$$

$$\frac{dC_{GTP}}{dt} = -\frac{V_{max} \cdot n \cdot f_{GTP}}{1 + \frac{K_{M,ATP}}{C_{ATP}} + \frac{K_{M,CTP}}{C_{CTP}} + \frac{K_{M,GTP}}{C_{GTP}} + \frac{K_{M,UTP}}{C_{UTP}} + \frac{K_{M,D}}{C_D}\left(1 + \frac{K_G^I}{C_{GTP}}\right)} \quad (3.3.2.2\text{-}7)$$

$$\frac{dC_{UTP}}{dt} = -\frac{V_{max} \cdot n \cdot f_{UTP}}{1 + \frac{K_{M,ATP}}{C_{ATP}} + \frac{K_{M,CTP}}{C_{CTP}} + \frac{K_{M,GTP}}{C_{GTP}} + \frac{K_{M,UTP}}{C_{UTP}} + \frac{K_{M,D}}{C_D}\left(1 + \frac{K_G^I}{C_{GTP}}\right)} \quad (3.3.2.2\text{-}8)$$

Guanosine triphosphate (GTP), the initiating nucleotide, binds exceptionally strongly to the active site of RNA polymerase, remaining bound even in low concentrations. This inhibits transcription and limits access to enzymatic complex and promoter sequence, D. Additionally, pyrophosphate (PPi) inhibition is accounted for with the addition of inorganic phosphatase for the hydrolyzation of PPi, mitigating feedback inhibition.[24,26] The erroneous consumption of NTPs from abortive transcription is not explicitly modeled in equations 3.1.2.2-(4-7), but is incorporated in the final yield assumption, where only 80% of the produced mRNA corresponds to the target sequence. Guanosine triphosphate (GTP), the initiating nucleotide, binds exceptionally strongly to the active site of RNA polymerase, remaining bound even in low concentrations, inhibiting transcription and limiting access to enzymatic complex and promoter sequence, D. Additionally, pyrophosphate (PPi) inhibition is accounted for with the addition of inorganic phosphatase for the hydrolyzation of PPi, mitigating feedback inhibition.[24,26] The erroneous consumption of NTPs from abortive transcription is not explicitly modeled in equations 3.3.2.2-(4-7), but is incorporated in the final yield assumption, where only 80% of the produced mRNA corresponds to the target sequence.

3.3.2.3 Fractional conversion and final mass concentrations

The simplified Michaelis-Menten-based kinetic model provides a useful framework for estimating mRNA synthesis in an IVT reactor, however; its accuracy depends on assumptions regarding

enzyme kinetics, inhibition effects, and coefficient estimations.[26] Transcription rates are highly dependent on promoter concentration and identity, as well as batch-to-batch variability in RNA polymerase, with results varying by several orders of magnitude across different studies.[24,26] To establish reasonable estimates for reagent conversion and batch size requirements, representative average parameters were selected for each coefficient, as shown in Table 3.1.2.3-1, are chosen to estimate reagent conversion and requirements per batch. The simplified Michaelis-Menten-based kinetic model provides a useful framework for estimating mRNA synthesis in an IVT reactor, however; its accuracy depends on assumptions regarding enzyme kinetics, inhibition effects, and coefficient estimations.[26] Transcription rates are highly dependent on promoter concentration and identity, as well as batch-to-batch variability in RNA polymerase, with results varying by several orders of magnitude across different studies.[24,26] To establish reasonable estimates for reagent conversion and batch size requirements, representative average parameters were selected for each coefficient, as shown in Table 3.3.2.3-1, are chosen to estimate reagent conversion and requirements per batch. However, coefficient values varied widely across the field and need to be experimentally determined for the optimization of this *in vitro* transcription process prior to manufacturing.

Table 3.3.2.3-1: Estimated coefficients for Michaelis-Menten approximation of IVT kinetics

Parameter	Definition	Estimation
V_{max}'	Maximum transcription rate for promoter sequence D	0.358 μM/min
$K_{M, ATP}$	Michaelis-Menten constant for ATP (½ concentration of ATP required to reach maximum transcription rate)	140.4 μM
$K_{M, CTP}$	Michaelis-Menten constant for CTP (½ concentration of CTP required to reach maximum transcription rate)	71.5 μM
$K_{M, GTP}$	Michaelis-Menten constant for GTP (½ concentration of GTP required to reach maximum transcription rate)	165.5 μM

Parameter	Definition	Estimation
$K_{M,\ UTP}$	Michaelis-Menten constant for ψTP (½ concentration of ψTP required to reach maximum transcription rate)	101.5 μM
$K_{M,\ D}$	Michaelis-Menten constant for promoter (½ concentration of promoter sequence required to reach maximum transcription rate (widely varying based on promoter))	0.22 μM
K_G^I	Dissociation constant for initial GTP binding to the promoter region D	0.025 μM
$C_{NTP,\ i}$ (t=0)	Initial concentration of nucleotide (each NTP, i = ATP, CTP, GTP, ψTP)	10 x 10^3 μM
C_D	Concentration of promoter (linearized pDNA, constant)	0.024 μM

To solve equations 3.3.2.2-(3-7), estimating nucleotide conversion and final mRNA yield, numerical integration techniques were implemented to model the time-dependent behavior of nucleotide consumption and mRNA synthesis over the 6-hour reaction time to (designed to optimize conversion and minimize unused nucleotides).

Starting with 10 mM concentrations of each nucleotide and $\frac{10\ \mu g\ pDNA}{.2\ mL\ Tris\ buffer}$ (corresponding to ~0.024 μM pDNA) results in a final mRNA concentration of 9.4 μM (19.7 g/L) , as depicted in Figures 3.3.2.3-1 and 3.3.2.3-2. The production of 9.4 μM mRNA corresponds to near-complete nucleotide conversion, assuming equimolar nucleotide availability in the 4,250-nucleotide target sequence.

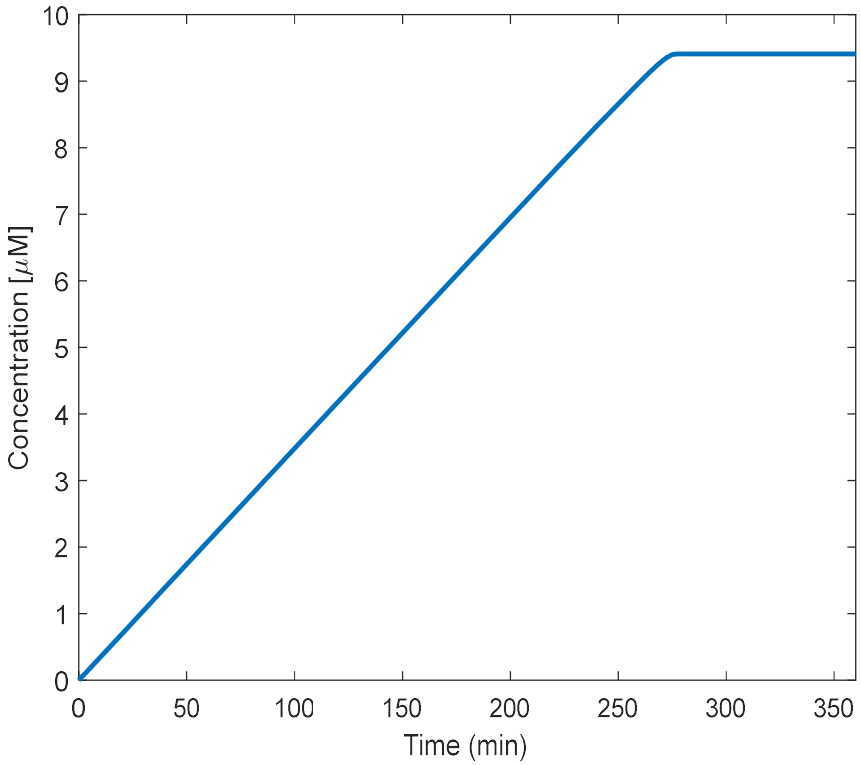

Figure 3.3.2.3-1: Production of mRNA over a 6-hour (360 min) reaction period.

This estimate is subject to variation due to factors such as final RNA nucleotide composition, target sequence length, and promoter selection for the linearized plasmid DNA (pDNA). The time-dependent production of mRNA over the 6-hour reaction is illustrated in Figure 3.3.2.3-1, while nucleotide consumption trends are shown in Figure 3.3.2.3-2).

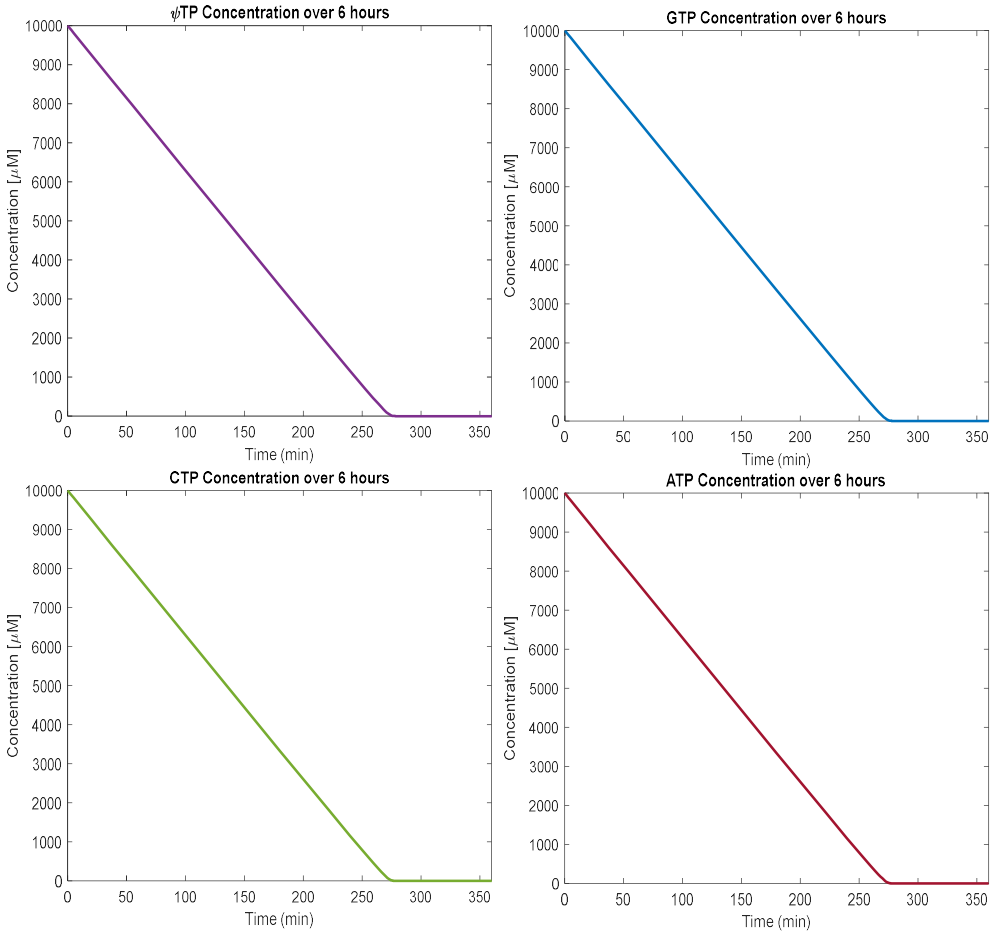

Figure 3.3.2.3-2: Consumption of nucleotides over the 6-hour reaction period.

Following transcription, deoxyribonuclease (DNAse) and EDTA are added to degrade the DNA template and inactivate the enzymes, ensuring that undesired template strands and enzymes were removed prior to further purification. The reagents and their respective quantities used during IVT are listed in Table 3.3.2.3-2, where 1 U (unit) represents the amount of enzyme required to catalyze the conversion of one micromole of substrate per minute under specified conditions.

As depicted in Figures 3.3.2.3-1 and 3.3.2.3-2, the production of 9.4 µM mRNA corresponds to near-complete nucleotide conversion, assuming equimolar nucleotide availability in the 4,250-nucleotide target sequence.

Table 3.3.2.3-2: Mass balance for materials used during IVT.

Species	IVT Reagents	IVT Products
Tris-HCl (g)	20.8	20.8
$MgCl_2$ (g)	15.7	15.7
DTT (g)	5.1	5.1
Nucleotides (g)	64.12	0.01
Spermidine (g)	0.96	0.96
Pyrophosphatase (U)	3210	3210
DNA Template (mg)	160.5	0
RNAase inhibitor (U)	3210000	3210000
T7 Polymerase (U)	40125000	40125000
CleanCap capping agent (g)	14.71	14.67
DNAase (U)	160.5	160.5
EDTA (g)	4.8	4.8
mRNA product (g)	0	48.03
DNA oligonucleotides (g)	0	160.5
Immunogenic Impurities (g)	0	12.008

Of the total mRNA produced (19.7 g/L), the Michaelis-Menten model does not account for aborted transcripts or double-stranded RNA byproducts. Based on experimental observations from similar IVT systems, we estimate that 95% of the synthesized mRNA contains the CleanCap modification, allowing for efficient separation during downstream processing. Of this fraction, approximately 80% corresponds to the correct target sequence, resulting in a final concentration of ~15 g/L of capped, functional mRNA product.

3.3.3 Reactor Specifications

3.3.3.1 Reactor Information

The IVT reactor we will be using is the Broadley James 5 L, 316L stainless steel bioreactor with a working volume range of 1.5-3.75 L, ideal for our 3.3 L working volume. The system includes pH and temperature sensors to maintain the process within a pH range of 7.5-8.0 and at a temperature of 37°C. The vessel, made of borosilicate glass, has an inner height of 254 mm and

inner diameter of 160 mm. A silicone heating blanket keeps the reactor at 37°C, with the jacket utilizing 9.4 W (see section 3.7.1.1). The impeller will be a scoping marine-style impeller from Chemglass Life Sciences. It has a diameter of 59 mm and will operate at 105 rpm for a total power output of 11.4 mW (equation 3.3.3.1).

$$P = K_T n^3 D^5 \rho = 3\left(\frac{105\,rpm}{60}\right)^3 (0.059\,m)^5 \left(994\,\frac{kg}{m^3}\right) = 11.4\,mW \qquad (3.3.3.1)$$

3.3.3.2 IVT Procedure

According to methods developed by Whitley et al. and Guo et al., the IVT reaction begins by combining the ingredients for the transcription buffer in the reactor and heating the mixture to 37°C using the heating jacket. Once the mixture reaches 37°C, an enzyme mixture is added. The transcription buffer and enzyme mixture are incubated and mixed for 6 hours. After this, DNase is added, and the mixture is incubated and mixed for an additional 2 hours. Finally, EDTA is added, and the mixture is incubated and mixed for 15 minutes. The entire process is carried out at 37°C, with a pH range of 7.5–8.0, and an impeller speed of 105 rpm. [28,29]

The following ingredients are listed as final concentrations and are based off values from national and international studies on optimizing yield, these values are also summarized above in Table 3.3.2.3-2.[28,29] The transcription buffer consists of 40 mM Tris-HCl, 50 mM $MgCl_2$, 10 mM dithiothreitol (DTT), 2 mM spermidine, 0.001 U/μL pyrophosphatase, and 10 mM NTPs (including ATP, GTP, CTP, and ΨTP). Nuclease-free water is added to bring the total working volume to 3.3 L. The enzyme mixture contains 50 ng/μL linearized DNA template, 1 U/μL RNase inhibitor, 12.5 U/μL T7 polymerase, and excess 4 mM CleanCap. After the incubation and mixing steps, 1 U of DNase per mg of linearized DNA template is added, followed by the addition of 5 mM EDTA, as outlined above.[24,29–31]

3.4 LNP Formation

3.4.1 Selection of Drug Delivery Vehicle

For an mRNA vaccine to be effective, the mRNA molecules must overcome both extracellular and intracellular obstacles to produce proteins of interest. Extracellularly, mRNA needs to evade nuclease degradation in physiological fluids. Post administration, the formulation must clear the innate immune response from monocytes. Intracellularly, mRNA must reach the target cell and enter the cell through endocytosis. Once inside the cell, the mRNA must perform endosomal escape to reach the cytoplasm, allowing protein translation to take place.[32]

Because of the threat of immune response and degradation, mRNA vaccines require a delivery vehicle to ensure safety, stability, and release into the cytoplasm. There are multiple delivery methods that have been tested in mRNA vaccines, which include direct injection of mRNA, conjugation with polymers or peptides, transfection of dendritic cells, and lipid nanoparticle entrapment.[33]

Direct injection of mRNA involves dissolving mRNA into a buffer and injecting straight into the body. Naked-mRNA-based vaccines have been tested in clinical trials but experience limited efficacy due to mRNA degradation. Peptide and polymer-based adjuvants have also been tested in clinical trials. The peptide adjuvant Protamine has been tested extensively with mRNA; however, results showed Protamine to be an ineffective adjuvant as the mRNA was poorly translated within the cells. Polymer-based adjuvants have shown promising results, but questions about toxicity and biodegradability hinder their further development as delivery vehicles. Transfection of dendritic cells involves electroporation of dendritic cells to disrupt the cell membrane and allow intracellular mRNA delivery. Issues such as cost, efficacy, and scalability make the technology unfeasible for

an industrial vaccine process. Other methods, such as cationic nano-emulsion and use of virus-like particles, show promise in preclinical trials, but have not been fully developed and tested.[34]

Lipid nanoparticle (LNP) encapsulation has shown its success as an mRNA delivery vehicle, seen in Moderna's mRNA-1273 and Pfizer's BNT162b COVID-19 vaccines. LNPs are the ideal delivery method for mRNA vaccines, because they protect mRNA from both intracellular and extracellular obstacles. They are biocompatible and lack a sufficient foreign body response, degrade in the body into nontoxic counterparts, entrap mRNA efficiently, and allow for cell uptake and endosomal escape into the cytoplasm.[35]

The benchmark formulation for LNPs contributes to the stability and efficacy of mRNA delivery and involve cationic lipids, ionizable lipids, phospholipids, cholesterol, and polyethylene glycol (PEG) lipids. The positive charges of the cationic lipids interact with the mRNA in encapsulation and stimulate an innate immune response within the body. Ionizable lipids are pH-sensitive, which prevents interactions in the neutral environment surrounding blood cells and promotes endosomal escape in the lower pH of endosomes. Phospholipids, specifically phosphatidylcholine, have been shown to stabilize nanoparticle structure. Cholesterol stabilizes the nanoparticle by adding rigidity to the membrane. PEG-lipids decrease particle aggregation due to their size, having a large effect on overall particle size.[32]

3.4.2 Mechanics of Lipid Nanoparticle Formation

The mRNA-LNP drug substance is created by mixing an aqueous phase containing purified mRNA with an organic phase containing lipids under controlled conditions. Electrostatic interactions between the anionic mRNA and ionizable lipids, along with hydrophobic interactions between lipid groups, enable the encapsulation of mRNA through self-assembly.[3,36] This nanoprecipitation

process is highly dependent on rapid and homogeneous mixing of the two streams, impacting key LNP parameters such as size distribution and mRNA encapsulation efficiency.[37]

LNP size and mRNA encapsulation efficiency (EE) are primarily regulated by the flow rates, ratio of lipids, and stream ratios. Uniform mixing of streams ensures consistent distribution of particle sizes and high encapsulation efficiencies.[36] Conversely, inadequate mixing can lead to large disparities in particle size and larger losses of mRNA. Thus, the mixing process plays a critical role in vaccine functionality and efficacy.

LNP size, referring to particle diameter, plays a significant role in mRNA delivery, biodistribution, and efficacy, with varying sizes optimal for different therapeutic targets. Small, uniform LNPs with diameters between 80-120 nm are ideal for effective cellular uptake and minimizing off-target side effects following intramuscular injection.[38] Precise size and properties of LNPs are achieved through careful control of stream flow rates and the composition of the lipid-containing, organic stream. Higher flow rates and faster mixing speeds result in smaller, more uniform particle size by encouraging nanoprecipitation and minimizing lipid aggregation.[39,40] Consistent flow rates and lipid ratios allow for repeatable LNP size and performance, critical for vaccine products.

The lipid composition is selected to balance stability and delivery efficiency (controlled release of mRNA). Ionizable lipids, such as DLin-MC3-DMA (MC3), play a crucial role by providing an environment-dependent cationic charge (determined by pKa), which can electrostatically interact with the anionic mRNA for encapsulation. These lipids neutralize with pH changes, stabilizing the LNP and preventing aggregation. During endocytosis (absorbance into the cytoplasm), the low pH of the endosomes (~5) induces protonation, destabilizing the endosome membrane and facilitating the release of mRNA into the cytoplasm. Phospholipids, like DSPC, enhance cellular uptake by stabilizing the LNP structure. Cholesterol improves membrane fluidity and permeability while

enhancing structural stability by tightly packing between other lipid components. PEGylated lipids, such as DMG-PEG_{2000}, provide hydrophilic tails that protrude from the LNP surface, preventing aggregation, and rapid clearance by the kidneys and reducing protein adsorption. [38] These components are combined in a benchmark molar ratio of 50:10:38.5:1.5 for ionizable lipid, phospholipid, cholesterol, and PEGylated lipid, respectively .[41,42] This formulation has been shown to be effective for mRNA encapsulation and release with each LNP encapsulating between two and three mRNA strands.[43]

In addition to LNP size, encapsulation efficiency (EE) is a key parameter as optimization minimizes loss of target mRNA strands, increasing process throughput and cost-effectiveness. EE is the percentage of mRNA encapsulated within LNPs relative to the total mRNA initial present in the formulation and can be determined by attaching a fluorescent compound to the mRNA and measuring the absorbance.[44] Typical EE values exceed 85%, with efficiency largely influenced by the nitrogen-to-phosphate (N/P) ratio, which reflects the molar ratio of ionizable lipid to mRNA. Optimal N/P ratios typically range from 3-8, balancing the electrostatic interactions necessary for encapsulation while minimizing excess lipid.[43] However, due to the unknown sequence and molecular weight and charge of the target mRNA, optimization of this value is not possible.

To ensure high EE, a higher ratio of 60:1 (w/w) for ionizable lipid to mRNA is required. This high ratio maximizes encapsulation efficiency by providing an excess of ionizable lipids to complex with the mRNA. [43] While increasing the lipid-to-mRNA ratio enhances EE, it also raises the likelihood of forming empty LNPs. However, empty LNPs have been shown to act as adjuvants and not greatly impact vaccine safety, making this approach justifiable.[45] Despite the high ratio of ionizable lipids to mRNA, a conservative estimate for EE (90%) allows for determination of

upstream product requirements. This estimate balances the need for high yield with the variability associated with mRNA sequence characteristics and process conditions.

As previously stated, LNP encapsulation of mRNA requires controlled mixing to achieve desired properties, which can be accomplished through two main methods: turbulent jet mixing and microfluidic mixing (Figure 3.3.2-1).[37]

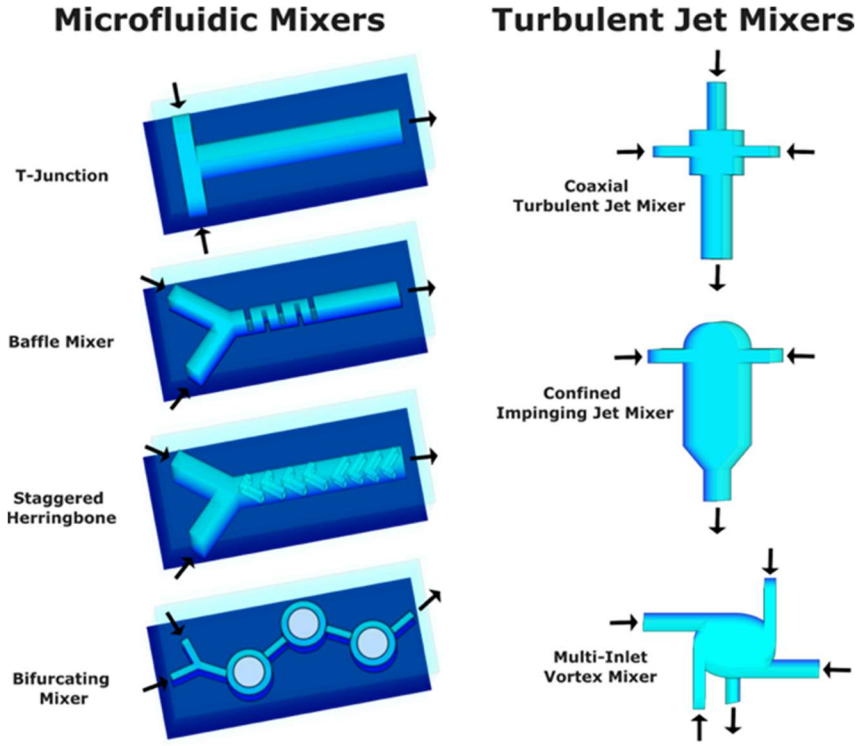

Figure 3.4.2-1. Various geometries of microfluidic and turbulent mixers. Adapted from Nguyen (2023).[46]

Microfluidic mixing employs microscale chips with channels that direct, mix, or separate fluids using continuous laminar flow. Mixing occurs through diffusion between adjoining streams, and the small scale of microfluidics allows for precise control but requires low sample volumes, typically in the microliter (μL) range.[39] Various geometries of microfluidic mixers exist as seen in the first column of Figure 3.3.2-1, some inducing turbulence or featuring longer channels for enhanced mixing. However, due to their low throughput, these systems are primarily used in research and development rather than large-scale commercial production.[37]

In contrast, turbulent jet mixing occurs when liquids collide at high velocities, generating intense turbulence and shear forces at the impingement point (point of collision). This collision creates eddies and vortices that result in chaotic interactions, producing homogeneous solutions. Turbulent mixing is characterized by its speed and ability to achieve uniform nanoparticle size through rapid fluid interactions. Different geometries, such as impinging jet and multi-inlet vortex, are used to introduce collisions at various speeds and positions, enhancing mixing efficiency.[37,39,47]

One effective approach to turbulent mixing is the use of a confined impinging jet mixer (CIJM), which involves two input streams that collide at high velocity in a mixing chamber. As shown on the second column in Figure 3.4.2-1, CIJMs offer several advantages over other turbulent and microfluidic mixers. Their mixing chambers are typically around half a centimeter in diameter, about ten times larger than those used in microfluidic systems, making CIJMs easily scalable. They enable continuous operation, high throughputs and are widely researched for flash nanoprecipitation uses (unlike multi-inlet vortex mixers), enhancing scalability for large-scale manufacturing. Unlike other high-shear mixers, which can cause mRNA degradation due to heat, CIJMs rapidly dissipate heat through fast mixing and precise temperature controls. Additionally, CIJMs allow for fine-tuning of input stream flow rates, shear forces, and mixing conditions, providing flexibility in manipulating LNP size and encapsulation efficiency.[37] These advantages make CIJMs the ideal choice for our LNP-mRNA encapsulation process.

3.4.3 Confined Impinging Jet Mixer: Theory

Confined impinging jet mixers (CIJMs) are specialized turbulent mixing devices designed for nanoprecipitation. In a CIJM, two streams (solvent and anti-solvent) collide at high velocities in a confined mixing chamber, as diagramed in Figure 3.4.3-1, resulting in turbulent fluid regimes that ensure uniform mixing.

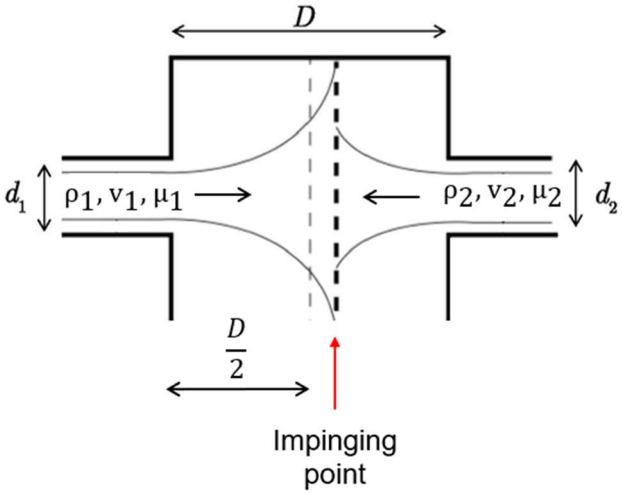

Figure 3.4.3-1. Simplified design of a confined impinging jet mixer.

CIJMs are effective for producing LNPs through a process known as flash nanoprecipitation, where mixing induces supersaturation, leading to nucleation and controlled particle growth.[37,44] This process is highly dependent on maintaining a Damköhler number (Da) << 1, ensuring that the mixing time is significantly shorter than the combined times for nucleation and particle growth (Equation 3.4.3-1).

$$\mathrm{Da} = \frac{\tau_{mix}}{\tau_{nucleation\ and\ aggregation}} \qquad (3.4.3\text{-}1)$$

Maintaining a constant Da number, less than 1, throughout scale-up allows for repeatable results. However, the calculation of aggregation and nucleation times require detailed kinetic information about LNP formation—considering factors like supersaturation, nucleation theory, and particle

diffusivity—that require experimentation, proprietary knowledge, and computational simulations around micromixing and mesomixing, which is beyond the scope of this work.

Another method for achieving desired mixing levels is maintaining flow rates within a range of critical Re numbers, such as 10,000-100,000 as summarized by Devos et al. in 2025, which ensures nanoparticles of a diameter ~100 nm.[48] The Reynolds number is calculated in Equation 3.4.3-2 as the summation of the Reynold's numbers of the colliding streams.

$$\mathrm{Re} = \sum_{i=1}^{n} \frac{\rho_i \cdot v_i \cdot d_i}{\mu_i} \tag{3.4.3-2}$$

where

$\rho_i =$ density of stream i

$v_i =$ linear velocity of stream i

$d_i =$ nozzle diameter of jet i

$\mu_i =$ viscosity of stream i

High Reynolds numbers enable rapid and homogeneous mixing that results in uniform nanoparticle size. As illustrated in Figure 3.4.3-2, smaller LNPs are produced at higher Reynolds numbers, emphasizing the importance of maintaining flow values within this range.

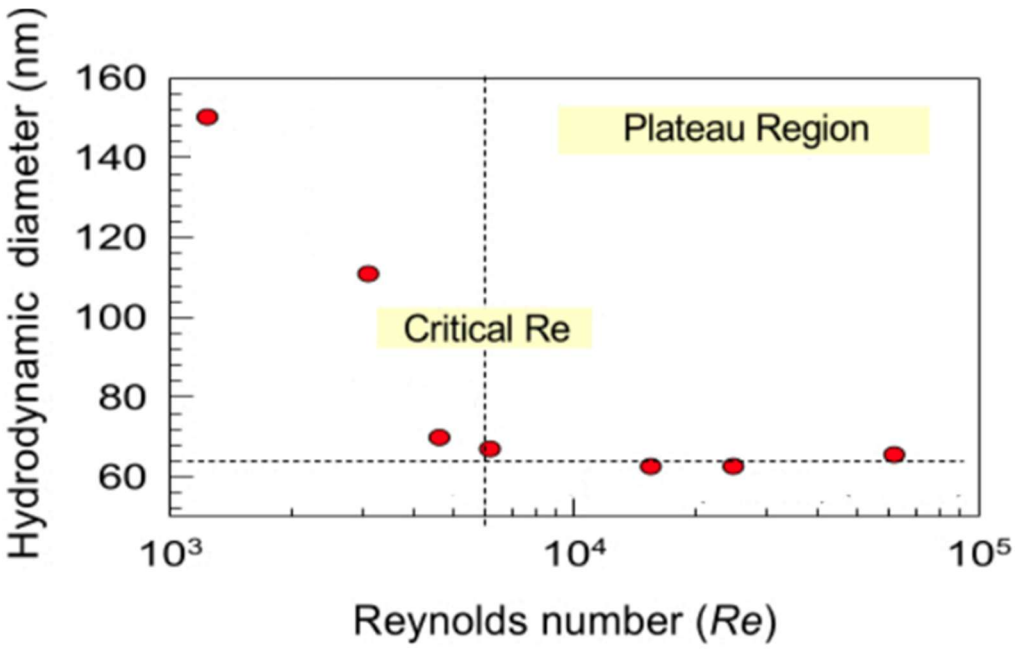

Figure 3.4.3-2. LNP hydrodynamic diameter versus Reynolds number. Adapted from Subraveti et al.'s work (2024).

Proper design of a CIJM relies on balancing the input jets to ensure that the impingement point (Figure 3.4.2-1), where the flows collide, is centered within the mixing chamber. An off-center impingement point can cause uneven mixing, and potential clogging of the jets.[49] The location of the impingement point depends on the fluid properties—namely viscosity, density, and flow rate—and can be adjusted by altering nozzle diameters and stream velocities. Three methods are commonly used to estimate the impingement point: the elastic analogue model, which approximates jets as springs that balance forces at the impingement point; the jets kinetic energy model, which considers the kinetic energy of each stream at the point of collision; and the jets momentum model, which balances the momentum of the colliding streams.[40,49] The momentum model is particularly effective for fluids with differing viscosities like 90% EtOH (v/v) and 50 mM acetate buffer.[48] Balancing stream momentum using jets momentum model, results in Equation 3.4.3-3 where r_s is the ratio of the streams moment, ρ is the fluid density, v is the flow velocity, d

is the nozzle diameter, and D is the mixing chamber diameter (stream 1 is the more viscous solution).[49]

$$\sqrt{\frac{\rho_2}{\rho_1}} r_s \frac{\mathrm{Re}_1}{\mathrm{Re}_2} \frac{d_2}{d_1} = \frac{8\mathrm{D} + \mathrm{Re}_1 \mathrm{d}_1}{8\mathrm{D} + \mathrm{Re}_2 \mathrm{d}_2}, \text{ where } \mathrm{r_s} = \frac{\rho_1 \cdot \mathrm{v}_1^2 \cdot \mathrm{d}_1}{\rho_2 \cdot \mathrm{v}_2^2 \cdot \mathrm{d}_2} \quad (3.4.3\text{-}3)$$

Using the relationship between parameters described in Equation 3.4.3-2 ensures that the jets collide symmetrically, maximizing mixing efficiency and minimizing the risk of clogging.

3.4.4 Confined Impinging Jet Mixer: Final Design Specifications

The final design of the confined impinging jet mixer (CIJM) was developed to optimize mRNA encapsulation in LNPs while maintaining consistent particle size and high throughput. Several general design rules guided the selection of chamber diameter (D), chamber height, nozzle height, and exit pipe diameter, all of which were determined based on the diameters of the input nozzles (Figure 3.3.4-1).[37,40] The final design of the confined impinging jet mixer (CIJM) was developed to optimize mRNA encapsulation in LNPs while maintaining consistent particle size and high throughput. Several general design rules guided the selection of chamber diameter (D), chamber height, nozzle height, and exit pipe diameter, all of which were determined based on the diameters of the input nozzles (Figure 3.4.4-1).[37,40]

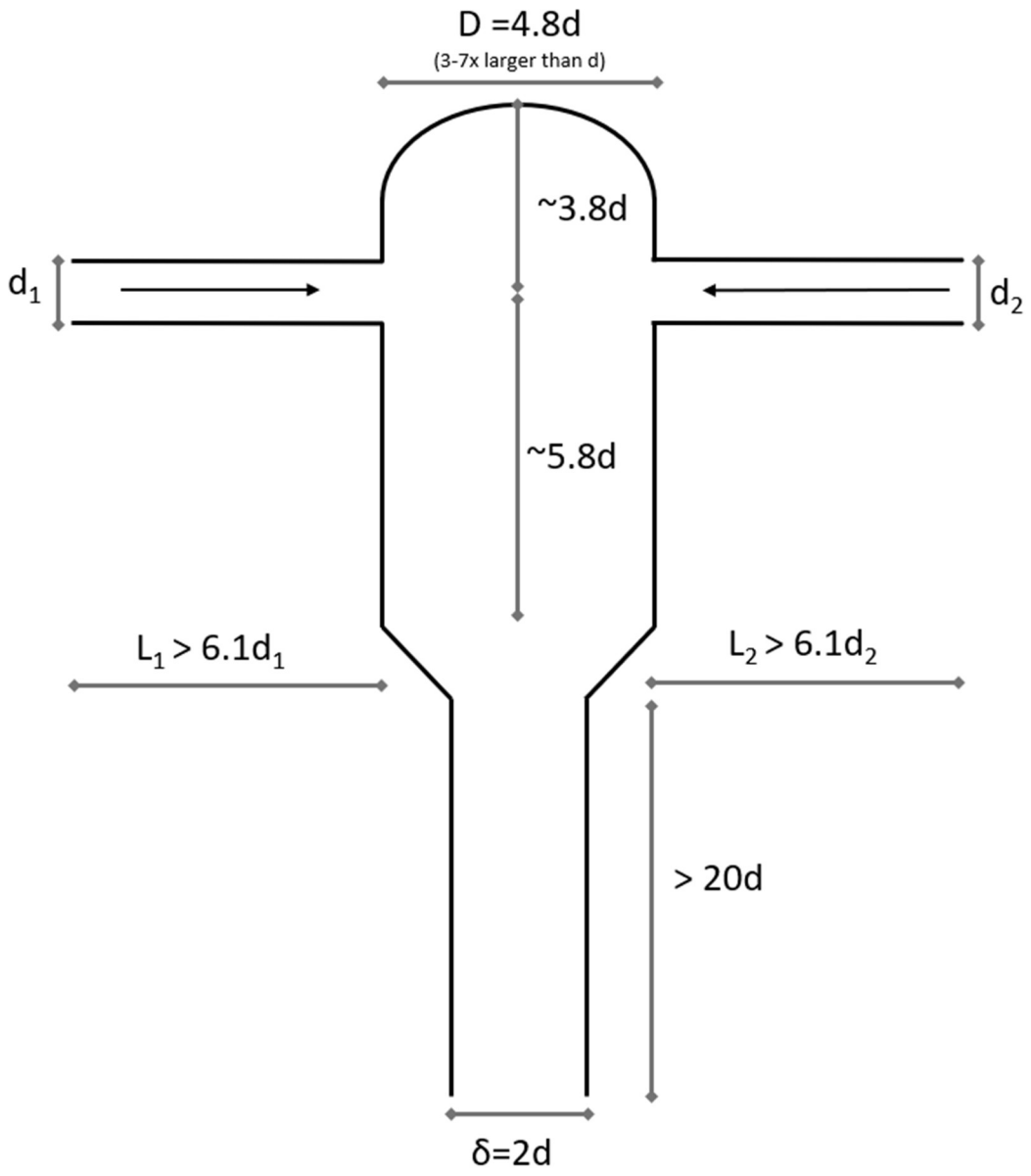

Figure 3.4.4-1. General design characteristics for confined impinging jet mixers used for flash nanoprecipitation.

This ensures the establishment of steady turbulent flow following diameter changes at the nozzle inlets and mixer outlet. The confinement volume of the mixing chamber was optimized to promote homogeneous mixing, minimizing recirculation zones and ensuring uniform nanoprecipitation. Free impinging jet mixers, which lack an enclosed chamber, were avoided due to their inefficiency in pharmaceutical applications. Symmetrical mixers were chosen due to their simplified design

and demonstrated effectiveness in achieving uniform LNP size distributions, as supported by previous experimental studies.[50]

The specifications for temperatures and mass concentrations of lipids and mRNA were selected to achieve the necessary supersaturation conditions for LNP, maximize mRNA encapsulation efficiency and stabilized inlet streams. Lipid concentrations were calculated to remain just below saturation levels when entering the mixing chamber. Heating the mixture to 60ºC ensures complete solubilization while maximizing the degree of supersaturation upon contact with the colder aqueous mRNA stream which is stored at 4ºC for stabilization purposes.[36,41] This supersaturation initiates rapid nucleation and controlled nanoprecipitation. The lipid mixture, described in Table 3.4.4-1, maintains the benchmark molar ratio of ionizable lipid, phospholipid, cholesterol, and PEGylated lipid at 50:10:38.5:1.5, with total lipid concentrations of 130 mmol/L and 76.3 mg/mL.

Table 3.4.4-1. Inlet concentration of lipids in 90% EtOH (v/v)

Lipid	Lipid Type	Molar %	Molar Concentration (mmol/L)	Mass Concentration (mg/mL)	Saturation Concentration (mg/mL)
DLin-MC3-DMA (MC3)	Ionizable	50	65	41.7	195
DSPC	Phospholipid	10	13	10.3	12.5
Cholesterol	Steroid	38.5	50.05	19.4	20
DMG-PEG_{2000}	PEGylated	1.5	1.95	4.9	125
Total		**100**	**130**	**76.3**	–

The identified ionizable lipid (DLin-MC3-DMA) concentration was the key to determining the mRNA stream's mass concentration to achieve a 60:1 weight ratio, optimizing the encapsulation efficiency. The molar mass of the mRNA sequence was estimated to be similar to that of Pfizer's COVID-19 vaccine (~4250 nucleotides)[51] with equal amounts of each nucleotide present, resulting in a final concentration of 0.70 mg/mL.

Specific chamber dimensions, as shown in Figure 3.4.4-2, were chosen for a symmetric CIJM based on designs from established flash nanoprecipitation studies.[40]

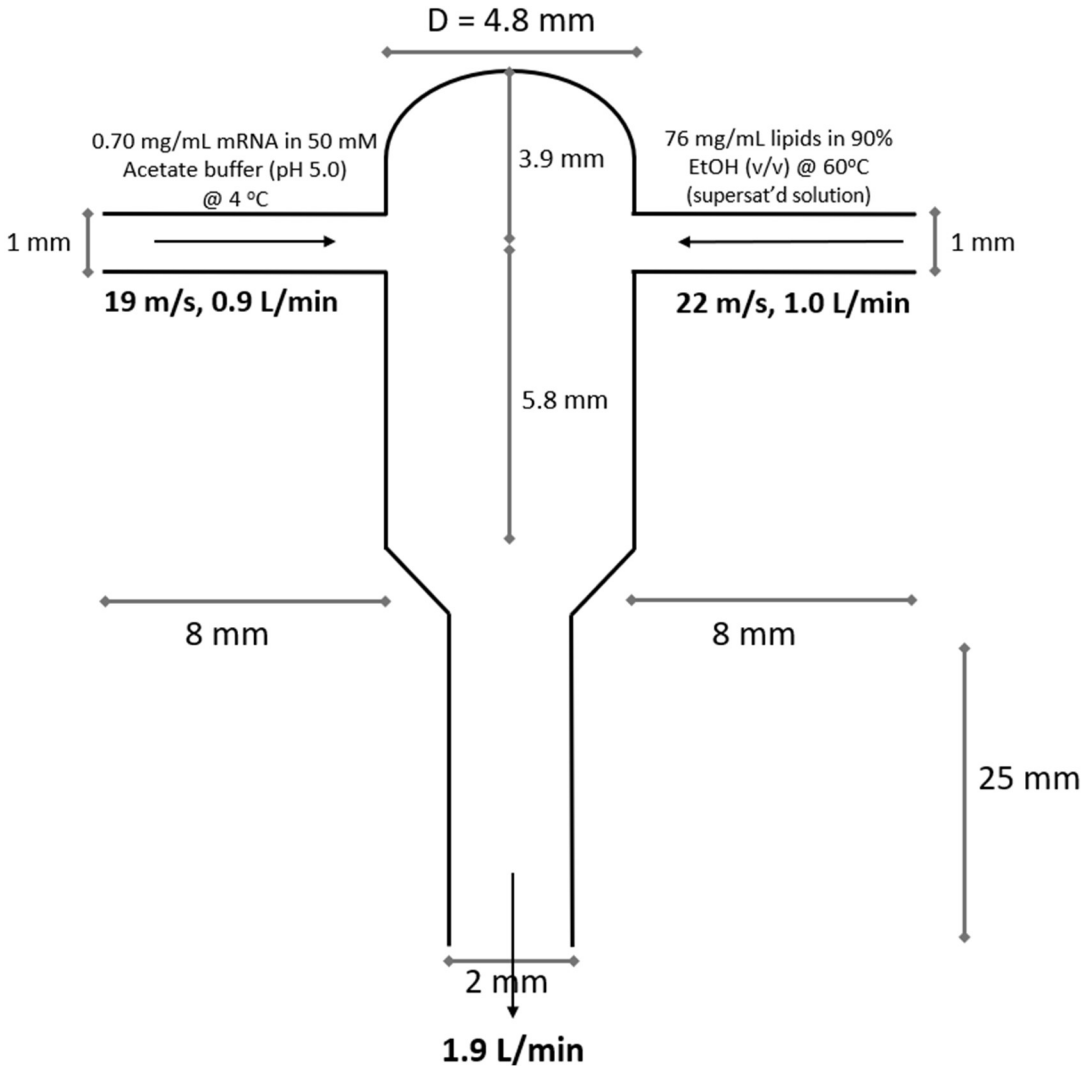

Figure 3.4.4-2. Confined impinging jet mixer dimensions.

The identification of chamber dimensions left two design process variables: the inlet velocities of the lipid and mRNA streams. The velocity of the lipid stream was selected to contribute approximately half of the desired Reynolds number within the critical range of 10,000 to 100,000, ensuring turbulent flow and rapid mixing. The target volumetric flow rate of 1.9 L/min was selected to align with the capabilities of commercial CIJM systems, such as those manufactured

by KNAUER, from which the mixers will likely be purchased. Aspen Plus simulations were used to estimate the density and viscosity of the solutions at operating temperatures. Although the simulation did not account for the effects of lipid and mRNA solutes on viscosity, we assumed the estimates were sufficient to perform a momentum balance to ensure an impinging point at the center of the mixing chamber (Equation 3.4.3-3). These calculations resulted in final inlet velocity of the aqueous mRNA solution of 19 m/s and a total Reynolds number of ~42,000 expected to produce a uniform LNP size between 80-120 nm.

To meet the production target of 25 g of encapsulated mRNA per batch, the required amount of mRNA to be processed through the CIJM is calculated by accounting for unencapsulated mRNA the encapsulation efficiency. Assuming a conservative EE estimate of 90%, approximately 27.78 g of mRNA is needed to produce 25 g of encapsulated product, obtained equation 3.4.4-1.

$$\text{Required mRNA throughput} = \frac{\text{mRNA per batch target}}{\text{Encapsulation efficiency}} = \frac{25\ \text{g}}{0.90} = 27.78\ \text{g} \qquad (3.4.4\text{-}1)$$

With the mRNA concentration set at 0.70 mg/mL and the inlet volumetric flow rate of 0.90 L/h, the time to process 27.78 g of mRNA is calculated using equation 3.4.4-2.

$$t = \frac{\text{required mRNA}}{\text{Volumetric flow rate} \times \text{mass concentration}} = \frac{27{,}780\ \text{mg}}{900\ \text{mL/min} \times 0.70\ \text{mg/mL}} = 44.1\ \text{min} \quad (3.4.4\text{-}2)$$

The length of this process, approximately 45 min, ensures that batch production demands are met in an efficient and practical manner from a workflow standpoint.

3.4.5 Dilution of CIJM Effluent

The goal of diluting the LNP-mRNA solution leaving the impinging jet mixer is to reduce the ethanol concentration to 5% w/v. An ethanol concentration of 5% w/v has been shown to sufficiently limit the degradation of LNPs following formation.[40,41,52]

Sodium acetate buffer at a concentration of 0.287% w/v is fed from tank T-502 to tank T-401 to dilute the LNP-mRNA mixture. The volume of sodium acetate buffer needed for sufficient dilution is determined by calculating the mass of ethanol leaving the impinging jet mixing operation. Using equation 3.2.5-1, 84,780 g of EtOH leaves the impinging jet mixer.

$$m_{EtOH} = \rho_{EtOH} V_{EtOH} \tag{3.4.5-1}$$

where

$\rho_{EtOH} = 789\ {}^{g}/_{L}$ @ 25℃

$V_{EtOH} = 39.69\text{L}$ (Volume of EtOH in T-302)

Knowing the mass of ethanol in tank T-402 that must be diluted the final tank volume is calculated using equations 3.4.5-2 and 3.4.5-3. From here, it is seen that 543 L of sodium acetate buffer must be added to tank T-402 to dilute the ethanol concentration to 5% w/v. This volume of sodium acetate buffer is added at once following completion of impinging jet mixing.

$$V_{f,tank} = \frac{m_{EtOH}}{C_{f,EtOH}} \tag{3.4.5-2}$$

$$V_{Added} = V_{f,tank} - V_{i,tank} \tag{3.4.5-3}$$

where

$C_{f,EtOH} = 5\%\ \text{w/v}$

$V_{i,tank} = 84\ \text{L}$

The final concentration of each species in tank T-401 following dilution is calculated using the new tank volume and is summarized in Table 3.4.5-1.

Table 3.4.5-1. Summary of batch characteristics following dilution phase of LNP purification

Parameter	Before	After
Tank Volume (L)	84	626
C_{mRNA} (% w/v)	0.0332	0.0039
C_{EtOH} (% w/v)	37.4	5.00
C_{NaOAc} (% w/v)	0.136	0.267

3.5 Purification Processes

3.5.1 Chromatography

Following the IVT and capping reactions, the target mRNA must be purified to remove any impurities from the solution prior to LNP encapsulation. To effectively remove all impurities from the solution, two sequential chromatography steps are employed: affinity chromatography (AC) and anion exchange chromatography (AEX). Both chromatography steps are operated in bind-and-elute mode, a diagram for which is depicted in Figure 3.5.1-1.

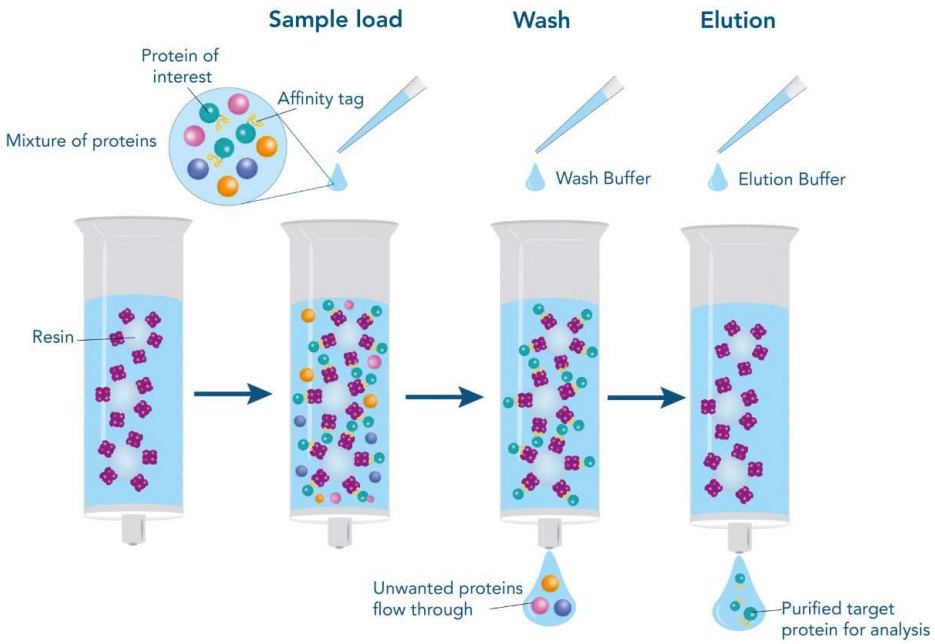

Figure 3.5.1-1 Diagram of affinity chromatography process operated in bind-and-elute mode. Adapted from QYAOBIO (2025).[53]

When a chromatography column is operated in bind-and-elute mode, a mixture of proteins containing the target protein and any other impurities, like oligonucleotides in the case of IVT products, is loaded into the column, where the target protein binds to the resin. A wash buffer then run through the column, causing species not bound to the resin to flow through the column and be discarded as waste, while the target molecules remains bound. Then, an elution buffer that disrupts

the binding of the target protein to the resin is passed through the column, eluting anything left bound to the resin and collected as product.

The first of the two chromatography steps, AC, removes any uncapped species, like reaction enzymes, oligonucleotides, and any uncapped mRNA from the IVT mixture; this is explained in further detail in section 3.5.1.1. However, immunogenic impurities, like double-stranded RNA (dsRNA), hairpin RNA, RNA-DNA hybrids, which resemble the structure of the target mRNA will bind to the affinity resin and elute with the target mRNA due to also being capped, therefore, the second chromatography step, AEX, is a necessary polishing step, the details for which are in section 3.5.1.2.

3.5.1.1 Affinity Chromatography

The resin selected for the AC process is the CIMmultus® Oligo DT resin by Sartorious. The functional ligands of this resin are deoxythymidine (DT) nucleotides, which form a stable hybrid with the terminal poly-adenine sequence, also known as the poly(A) tail, of the target mRNA under high ionic strength conditions, which is controlled by the salt concentration in the buffer. (Sartorius, 2022). The poly(a) tail that is important for this process is added to the mRNA transcripts during the co-transcriptional capping step of the IVT reaction and is used biologically to prevent enzymatic degradation in the cytoplasm once delivered to patients. As the capping reaction that polyadenylates the target mRNA will also provide a poly(A) to any off-target RNA species, like

double-stranded mRNA, RNA-DNA hybrids, and hairpin RNA, these species will also bind to the column under high strength ionic conditions. As the ionic strength of the column conditions is reduced by reducing the salt concentration in the buffer, the hybridization between the poly(A) tails and the resin is interrupted and the mutual repulsion of the oligoDT's and the mRNA's negatively charged backbones is enough to unbind the mRNA and allow for elution out of the column. The change in binding of the mRNA to the oligoDT resin at high and low salt concentrations is depicted in Figure 3.5.1.1-1.[54]

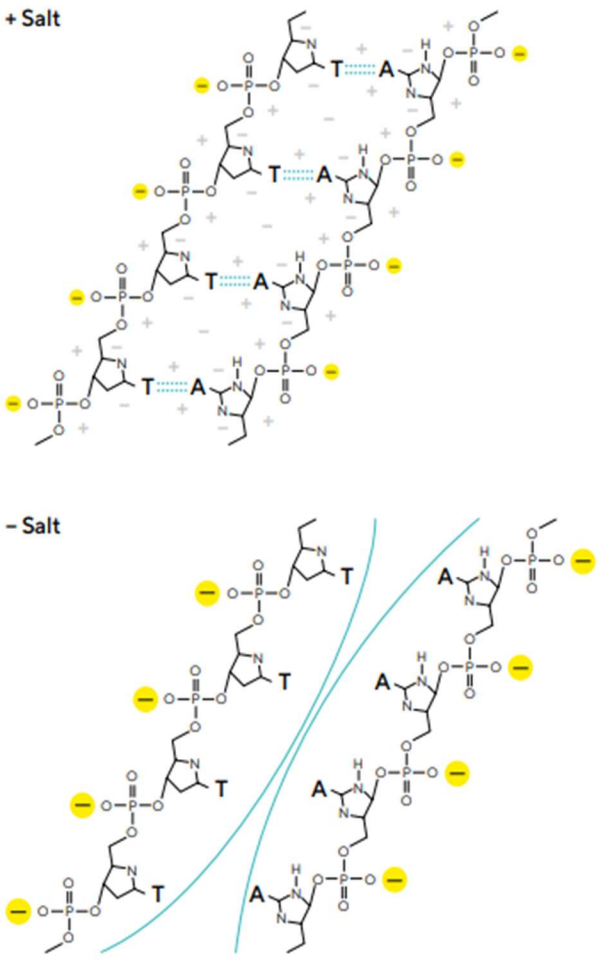

Figure 3.5.1.1-1 Schematic for binding of mRNA to Oligo DT resin at high and low salt conditions. Adapted from Sartorius (2022).

The AC process is operated in 5 five steps: equilibration, loading, binding, washing, and elution. During the equilibration phase, a high salt concentration is passed through the column to prepare the resin for binding with the mRNA in the IVT mixture. During the loading phase, the IVT mixture with added salt is passed into the column, where any species with a poly(A) tail will begin to bind to the resin. During the binding phase, a large volume of high salt concentration buffer is passed through the column, which strengthens the binding between the resin and species with poly(A) tails, while any other impurities−including enzymes, oligonucleotides, DNA templates, incomplete mRNA transcripts, uncapped mRNA, etc.

–will elute out of the column. Though the output buffers from the elution steps are discarded as waste here, it is possible to purify remaining reaction enzymes for continued use, however, this is outside the scope of this facility. After binding, in the washing phase, a buffer of reduced salt concentration is passed through the column to reduce any non-specifically bound contaminants that may have remained in the column at high-salt concentrations.[55] During the elution phase, a low-salt concentration buffer is used to free the mRNA from the column and pass any species with a poly(A) tail out of the column; the solution collected during the elution phase is passed into a hold tank so it can be prepared for the next chromatography step. All steps in the chromatography process are carried out at a pH of 7.0. The exact compositions of all buffers in this process are available in Table 3.5.1.1-1.

Table 3.5.1.1-1 AC buffer compositions

Equilibration Buffer	50 mM Na-phosphate, 250 mM NaCl, 2 mM EDTA
Loading Buffer	IVT mix, 50 mM Na-phosphate, 1M NaCl
Binding Buffer	50 mM Na-phosphate, 250 mM NaCl, 2 mM EDTA
Wash Buffer	50 mM Na-phosphate, 2 mM EDTA
Elution Buffer	10 mM Tris

A representative chromatogram for this process is depicted in Figure 3.5.1.1-2.

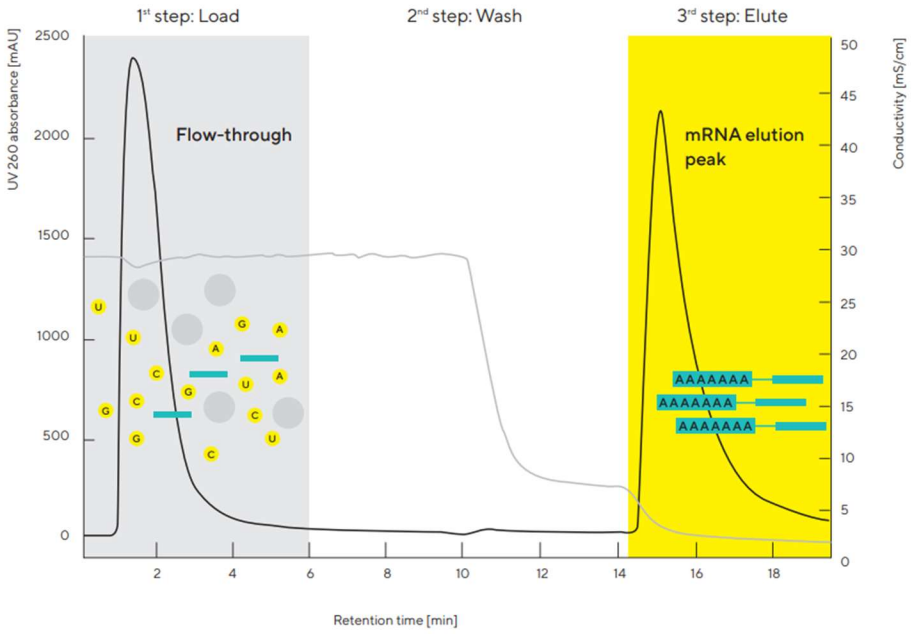

Figure 3.5.1.1-2. Example chromatogram for AC process. Adapted from Mencin et al. (2022).[56]

Rather than use a single manually packed column, the affinity chromatography unit is designed to operate using numerous CIMmultus™ Oligo dT18 8000 mL monolithic columns in parallel, which is the largest commercially available pre-packed column of this resin type. To determine the resin volume necessary to purify the 48.03 g of mRNA per batch from the IVT process, Equation 3.5.1.1-1 was used, with an estimated binding capacity of 2 g/L, which was found experimentally by BIA Separations.[55]

$$V_R = \frac{m_{mRNA}}{BC} \tag{3.5.1.1-1}$$

where

V_R = Resin volume (L)

m_{mRNA} = Mass of mRNA entering column per batch (g)

BC=mRNA binding capacity ($\frac{g}{L}$)

From this calculation, 24.02 L of resin are necessary, so the AC process is designed to use four 8000 mL monoliths operated in parallel, rather than operating three columns at their maximum

binding capacity. Thus, the total resin volume is higher than necessary (32 L), and the process can bind up to 64 g of mRNA per batch, if necessary.

The design operating flow rate for all steps of the affinity chromatography process is 0.5 CV/min. To verify this flow rate is acceptable, Darcy's Law (Equation 3.5.1.1-2) is used to calculate a 5.35 bar pressure drop for each column, which is below the maximum operating pressure of 7 bar for the monoliths used in the process; therefore, our operating flow rate is acceptable.

$$\Delta P = \frac{v\mu L}{k} \qquad (3.5.1.1\text{-}2)$$

where

$\Delta P = \text{Pressure drop (Pa)}$

$\mu = \text{Fluid viscosity (Pa·s)}$

$v = \text{Superficial velocity (m/s)}$

$L = \text{Column length (m)}$

$k = \text{Column permeability (m}^2\text{)}$

The fluid viscosity is assumed to be constant and equivalent to water, which is the main component of all process buffer solutions, at ambient temperature (0.001 Pa s) to remain consistent with the assumptions made during the design for the LNP formation process. The column permeability is assumed to be 1.00E-12 m^2, which is a conservative estimate for monolithic columns. It is important to note that the true values for these parameters must be determined experimentally, which must be done once the plant is fully built. Therefore, the realistic pressure drop may be greater than the calculated pressure drop if column permeability is lower than estimated or the fluid viscosity is higher than estimated. In this case, the operating flow rate would need to be

reduced to ensure the pressure drop is less than the maximum operating pressure drop of 7 bar. The superficial velocity used in Equation 3.5.1.1-2 is found using Equation 3.5.1.1-3.

$$\mu = \frac{V_c \dot{v}}{\pi(\frac{D_c}{2})^2} \tag{3.5.1.1-3}$$

where

$\mu = \text{Superficial velocity (m/s)}$

$\dot{v} = \text{Operating flow rate (CV/s)}$

$V_c = \text{Column volume (m}^3\text{)}$

$D_c = \text{Column Diameter (m)}$

The volumes of buffer and time required for each step of the AC, as well as the overall processing time (62 minutes) and the total buffer volumes used per batch are displayed in Table 3.5.1.1-2.

Table 3.5.1.1-2 Chromatographic procedure for AC process

Process Step	**Column Volumes**	**Time required (min)**	**Volume of Buffer per Column (L)**	**Total Volume per Batch (L)**
Equilibriation	10	20	80	320
Sample loading	1	2	8	32
Binding	8	16	64	256
Washing	4	8	32	128
Elution	8	16	64	256
	Total Time:	62	**Total Volume:**	992

The number of column volumes and buffer compositions used for each step align with the mRNA purification experiment performed by BIA Separations using an equivalent monolith.[55] These parameters were chosen to be equivalent to ensure that the mRNA yield found during this experiment (80%) would be the most accurate estimate for the AC process yield as possible.

Therefore, the 48.03 g of mRNA entering the AC step from IVT is expected to be reduced to 38.43 g leaving the process in the product solution.

The material balance around the AC process is displayed in Table 3.5.1.1-3.

Table 3.5.1.1-3 Material balance for AC

	Inflows		Outflows	
Species	**IVT Products**	**AC Buffer Addition**	**AC Waste**	**AC Products**
Tris-HCl (g)	20.8	403.5	20.8	403.5
MgCl2 (g)	15.7	0.0	15.7	0.0
DTT (g)	5.1	0.0	5.1	0.0
Nucleotides (g)	0.0	0.0	0.0	0.0
Spermidine (g)	1.0	0.0	1.0	0.0
Pyrophosphatase (U)	3210.0	0.0	3210.0	0.0
RNAase Inhbitor (U)	3210000.0	0.0	3210000.0	0.0
T7 Polymerase (U)	40125000.0	0.0	40125000.0	0.0
Capping Agent (g)	14.7	0.0	14.7	0.0
DNAase (U)	160.5	0.0	160.5	0.0
EDTA (g)	4.8	411.5	416.3	0.0
mRNA Product (g)	48.0	0.0	9.6	38.4
DNA Oligonucleotides (g)	160.5	0.0	160.5	0.0
Immunogenic Impurities (g)	12.0	0.0	0.0	12.0
Na-Phosphate (g)	0.0	5817.9	5817.9	0.0
NaCl (g)	0.0	8785.5	8785.5	0.0
Arginine (g)	0.0	0.0	0.0	0.0
Sodium Acetate (g)	0.0	0.0	0.0	0.0
Volume (L)	3.2	988.8	736.0	256.0

3.5.1.2 Anion Exchange Chromatography

Following AC, the product solution contains mRNA-associated impurities, also called immunogenic impurities, like double stranded RNA, hairpin RNA, and RNA-DNA hybrids, that bound and eluted alongside the target mRNA. It is necessary to remove these immunogenic impurities, as they are commonly recognized by the body's innate immune system as a pathogen associated molecular pattern, thus triggering an immune response that can lead to inflammation and toxicity.[57] Anion exchange chromatography for the purification of mRNA from immunogenic impurities exploits the differences in the charge densities of the species resulting from the varying structures of their negatively charged phosphate backbone, visualized in Figure 3.5.1.2-1, which interact reversibly with the positively charged resin.

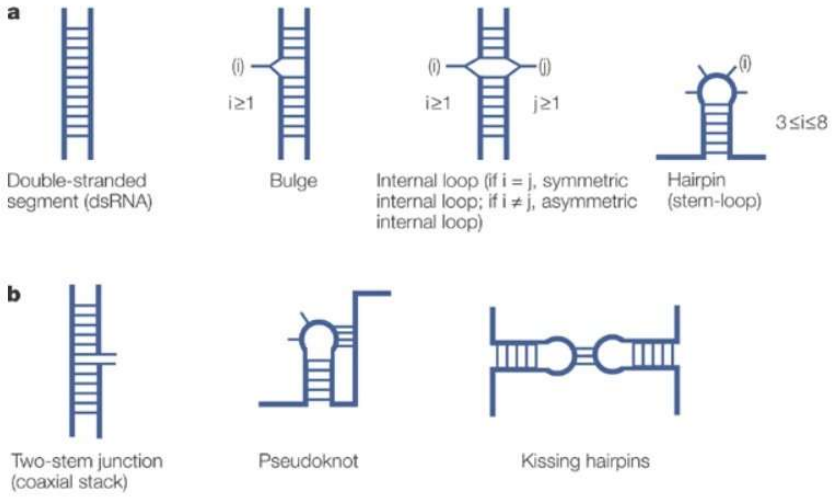

Figure 3.5.1.2-1 Structures of possible mRNA-related impurities. Adapted from Tian et al. (2004).[58]

During the AEX process, a salt gradient is applied to the column, where ions in the buffer compete with the negatively charged RNA species for binding to the positively charged resin. Molecules with weaker interactions, such as single-stranded RNA, elute first at lower salt concentrations. As the ionic strength increases, molecules with higher charge densities and stronger binding, such as double-stranded RNA (dsRNA) or RNA-DNA hybrids, are sequentially displaced and eluted. This

selective elution ensures that mRNA and its immunogenic impurities are separated based on their binding affinities, enabling efficient purification of target mRNA.

The AEX process uses Eshumo Q, which is a strong anion exchange resin by Sigma Aldrich. Eshmuno Q was selected since it has been determined to be effective at purifying mRNA from mRNA-associated impurities in an experiment performed by Millipore Sigma. This experiment found an optimal elution profile using Eshmuno Q resin that led to a 100% reduction in dsRNA and an mRNA yield of 75.3%; thus, the buffer compositions, buffer volumes, and elution profile for the AEX process are designed to be equivalent to this experiment to achieve comparable results.[59] The buffer compositions for AEX are displayed in Table 3.5.1.2-1.

Table 3.5.1.2-1 Buffer compositions for AEX

A1	50 mM Tris, 150 mM NaCl, pH 8.0
A2	50 mM Tris, 0.5M Arginine, pH 9.0
B1	50 mM Tris, .5 M Arginine, 2 M NaCl, pH 11.0

The AEX process will be operated in 8 steps: equilibration, loading, two washes, and four elution steps. To begin with, the column is equilibrated with a low-salt concentration buffer (Buffer A1) to prepare the column to bind with the RNA species. In the loading phase, the 256 L of solution from AC are passed through the column, where any RNA species will bind to the strong anion exchange resin. The first wash is performed using low-salt concentration buffer (Buffer A1) to wash away loosely bound impurities. The second wash uses another low-salt concentration buffer (Buffer A2), this time containing arginine, which serves to further remove non-specifically bound contaminants and stabilize the mRNA during the chromatographic process.[57] The four-step elution process in the AEX procedure uses a stepwise increase in salt concentration to selectively elute RNA species based on their binding strength to the positively charged resin. In Elution 1, a buffer with moderate salt concentration (40% Buffer B1) begins to release weakly bound impurities, such

as small RNA fragments or loosely associated contaminants. Elution 2 increases the salt concentration (70% Buffer B1), which displaces moderately bound species, including some structured RNA impurities like hairpin RNAs. Elution 3 (90% Buffer B1) targets strongly bound species, such as mRNA with its high charge density and larger size, ensuring its efficient recovery. Finally, Elution 4 (100% Buffer B1) ensures complete removal of any remaining tightly bound material, including residual impurities.

As the chromatographic procedure outlined by Millipore Sigma does not specify exactly which RNA species elute during each elution step, the AEX process is designed such that all elution buffer is collected as a conservative estimate. The exact range that must be collected to only capture the target mRNA will be found through experimental testing once the facility is constructed. The ideal capture range will be determined by analyzing the chromatogram for the mRNA spike, which is represented by the sharp blue peak observed in Millipore Sigma's experiment in Figure 3.5.1.2-2.

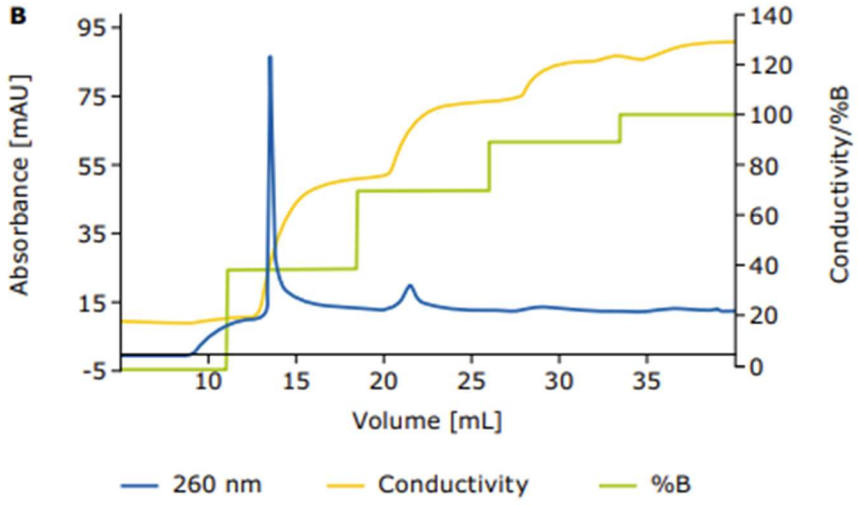

Figure 3.5.1.2-2. Chromatogram for mRNA purification from mRNA-related impurities using a 4-step elution profile. Adapted from Millipore Sigma (2024).[59]

Figure 3.5.1.2-2 suggests that most of the target mRNA will elute during the first elution step; however, to avoid making any downstream collection tanks too small, the entire volume of all four elution steps is assumed to be the collection range for AEX.

The minimum reported binding capacity for mRNA in AEX studies is 10 g/L; therefore, this value will serve as a conservative estimate of the binding capacity for mRNA on the Eshmuno Q resin. Thus, the necessary resin volume to capture the 38.43 g of mRNA from AC is 3.84 L, which is found using Equation 3.3.1.1-1. Due to the small resin volume, AEX can be accomplished using a single pilot scale manually packed column, the specifications for which are in Table 3.5.1.2-2.

Table 3.5.1.2-2 AEX column specifications

Column Selection	Cytiva Axichrom
Maximum Bed Height (mm)	300
Inner Diameter (mm)	140
Volume (L)	4.62
Maximum Operating Pressure (bar)	6

The design operating flow rate for the AEX is 0.3 CV/min (1.39 L/min). To verify this operating flow rate is allowable for the AEX process, Darcy's Law (Equation 3.5.1.1-2) is used to calculate the pressure drop across the column. Like AC, the fluid viscosity is assumed to be equivalent to water at ambient temperature to align with the assumptions made during LNP formation design. Also, the column permeability is assumed to be 1.00E-12 m^2, as this serves as a conservative estimate for manually packed columns. The superficial velocity for the AEX process is 0.0015 m/s, which is found using Equation 3.5.1.1-3. Using these values, the estimated pressure drop across the AEX column is 4.50 bar, which is below the maximum operating pressure of the column (6 bar); the design operating flow rate is acceptable.

As mentioned in Section 3.5.1.1, the values for column permeability and fluid viscosity must be determined experimentally once the facility is complete. The operating flow rate may need to be

reduced in the case that the column permeability is lower than estimated or the fluid viscosity is significantly higher than estimated.

The chromatographic procedure for AEX is available in Table 3.5.1.2-3. As mentioned earlier in this section, the number of column volumes for each process step was chosen to align with the experiment performed by Millipore Sigma, with the only major difference occurring in the lengthened loading phase.[59] The column volumes required for the loading phase are determined by the volume of solution collected during AC (256 L) and the design operating flow rate for AEX (1.39 L/min). The total time required for all steps of the AEX process is 334.8 minutes.

Table 3.5.1.2-3 Chromatographic procedure for AEX

Process Step	Column Volumes	Time Required (min)
Equillibriation	5	16.7
Loading	55.4	184.8
Wash 1	5	16.7
Wash 2	5	16.7
Elution 1 (40% B1)	7.5	25.0
Elution 2 (70% B1)	7.5	25.0
Elution 3 (90% B1)	7.5	25.0
Elution 4 (100% B1)	7.5	25.0
	Total Time:	**334.8**

The material balance for the AEX process is displayed in Table 3.5.1.2-4

Table 3.5.1.2-4 Material balance for AEX.

	Inflows		Outflows	
Species	AC Products	AEX Buffer Addition	AEX waste	AEX Product
Tris-HCl (g)	403.5	3654.9	2966.6	1091.7
mRNA Product (g)	38.4	0.0	9.5	28.9
Immunogenic Impurities (g)	12.0	0.0	12.0	0.0
NaCl (g)	0.0	15097.3	2648.9	12448.4
Arginine (g)	0.0	11061.6	2011.2	9050.4
Volume (L)	256.0	207.8	325.3	138.5

3.5.2 Tangential Flow Filtration

Tangential flow filtration (TFF) is a purification process in which fluid is continuously flowed past a filter, allowing the permeate to be discarded while retaining larger particles in the retentate. For this process, the desired product is contained in the retentate. Unlike traditional filtration methods, tangential flow prevents filter clogging by sweeping particles off the filter surface.[60]

This process operates in two distinct modes: concentration and diafiltration.[60] In concentration mode, no buffer is added to the system, and the permeate is sent to waste, effectively reducing the batch volume. In contrast, diafiltration involves the continuous addition of buffer to the TFF system at the same rate as the permeate removal, allowing for efficient buffer exchanges.

Tangential flow filtration plays a critical role in the purification of both mRNA and lipid nanoparticles in this process, ensuring the removal of impurities while maintaining the integrity of the final product.

3.5.2.1 Concentration

Concentration is utilized at two stages in the LNP-mRNA production process. During mRNA purification, it is applied after chromatography to achieve the batch volume required for the impinging jet mixer. In LNP purification, concentration is used to reduce the batch volume, ensuring the mRNA reaches the target concentration of 0.01% w/v in the final formulation. When designing each concentration system, it is important to determine the batch time required to complete the concentration process and quantify the material lost as waste. These calculations are nearly identical for both mRNA and LNP concentration and are described below.

A key parameter in TFF systems is the rejection coefficient (σ). The rejection coefficient describes what fraction of a species is retained by the membrane. A rejection coefficient of 1 indicates the species is completely retained while a rejection coefficient of 0 means the species passes straight

through the membrane. A T-Series Cassette with a Delta regenerated cellulose membrane using a MWCO of 100kDa is used to perform each TFF in this process.[61,62] A MWCO of 100kDa was selected, as both LNPs and mRNA tend to be significantly over this size threshold and will not be lost through the filter as a result.[63–65] Therefore, the rejection coefficients for this TFF process is assumed to be 1 for the LNPs and mRNA and 0 for all other species.

Filter size for each of the TFF steps was determined based on the volume of fluid handled. The LNP TFF system processes a lot more fluid than the mRNA TFF system, resulting in selected filter areas of 2.5m^2 and 0.5m^2, respectively (Table 3.5.2.1-1). Permeate flux through the filter was estimated based on a study by Cytiva Life Sciences using the T-Series Cassette with a 100kDA Delta RC membrane.[61] Both mRNA and LNP concentration run at constant trans-membrane pressure (TMP) of 20 bar and feed flowrate of 450 LHM allowing for permeate flowrate and crossflow flowrate to be determined from Figure 3.5.2.1-1. Crossflow flowrate is calculated by subtracting the feed flowrate by the permeate flowrate.

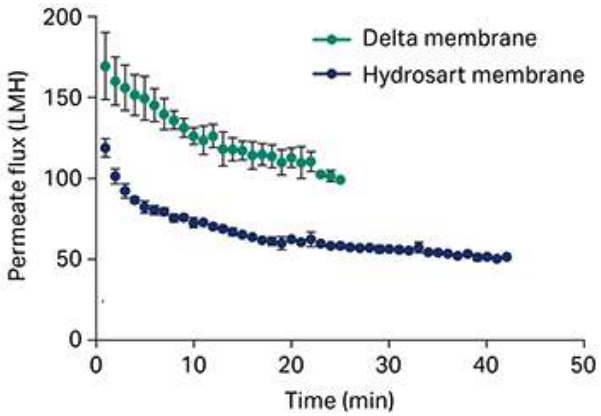

Figure 3.5.2.1-1. Permeate flux over time during concentration at 20 bar TMP and feed flowrate of 450LHM

Table 3.5.2.1-1. Operating conditions during concentration

Parameter	mRNA Concentration	LNP Concentration
Filter Area (m^2)	0.5	2.5
TMP (psi)	20	20
Feed Flowrate (L/h)	225	1125
Permeate Flowrate (L/h)	60	300
Crossflow Flowrate (L/h)	165	825

To find the time required to complete each concentration, a concentration factor is first calculated based on the initial volume in the tank and the desired final volume (equation 3.5.2.1-1). Final product concentration and yield can then be determined using equations 3.5.2.1-2 and 3.5.2.1-3.

$$CF = \frac{V_0}{V_f} \tag{3.5.2.1-1}$$

$$C_{f,product} = C_{i,product}(CF)^{\sigma} \tag{3.5.2.1-2}$$

$$Yield = (CF)^{\sigma-1} \tag{3.5.2.1-3}$$

where

$V_0 =$ Initial Tank Volume (L)

$V_f =$ Final Tank Volume (L)

$C_f =$ Final Product Concentration (% w/v)

$C_i =$ Initial Product Concentration (% w/v)

$\sigma =$ Rejection Coefficient

Processing time is calculated based on the filter area, average permeate flux, and concentration factor of the process (equation 3.5.2.1-4). Filter size specifications differ between mRNA and LNP concentration as mentioned previously in Table 3.5.2.1-1.

$$t = \frac{V_0 - V_f}{Au_{p,avg}} \tag{3.5.2.1-4}$$

where

$\mathrm{t} =$ Batch Time (hrs)

$\mathrm{A} =$ Membrane Area (m^2)

$\mathrm{u_{p,avg}} =$ Average Filtrate Flux ($\mathrm{L/m^2/hr}$)

Throughout the concentration process, the solution is assumed to be well mixed. Considering this and the fact that the rejection coefficients for the buffer components and all other non-product

components are assumed to be 0, the concentration of each of these components in the permeate stream is equivalent to that in the retentate stream. The mass of each species sent to waste is determined by multiplying the amount of filtrate generated by the concentration of each species in solution (Equation 3.5.2.1-5).

$$m_{x,w} = V_{Filtrate} C_x \quad (3.5.2.1\text{-}5)$$

where

$m_x = \text{Mass of Species x Sent to Waste (g)}$

$V_{Filtrate} = \text{Volume of Filtrate Generated (L)}$

$C_x = \text{Concentration of Species x (g/L)}$

The workflow described above is used to calculate the processing time and waste characteristics for both mRNA and LNP concentration. In mRNA concentration, mRNA product from IVT is retained in the system while buffer salts from chromatography flow through the membrane. In LNP concentration, the LNP-encapsulated mRNA is retained in the system while ethanol and acetic acid flow through the membrane. Both processes aim to reduce the batch volume to obtain the mRNA concentration necessary for later in the process or the final product (Table 3.5.2.1-2).

Table 3.5.2.1-2. Summary of batch characteristics following concentration

Parameter	mRNA Concentration	LNP Concentration
Initial Tank Volume (L)	138.54	620
Final Tank Volume (L)	39.69	240
Initial C_{mRNA} (%w/v)	0.0209	0.00399
Final C_{mRNA} (%w/v)	0.0729	0.0104
Processing Time (hr)	1.65	1.29

Waste generated during each concentration process is calculated from equation 3.5.2.1-5 and summarized in the table below. Water accounts for the volume of each stream.

Table 3.5.2.1-3. Summary of waste characteristics following concentration

Species	mRNA Concentration	LNP Concentration
Volume (L)	98.86	386.2
Tris-HCl (g)	779	0
Sodium Acetate (g)	0	1223
Sodium Chloride (g)	8883	0
Arginine (g)	6458	0
Ethanol (g)	0	19312

3.5.2.2 Diafiltration

Following each concentration step, diafiltration is used to replace the buffer the product is suspended in. After mRNA concentration, the buffer is exchanged to 50mM sodium acetate to bring the solution to a pH of 5 necessary for lipid nanoparticle formation. Two diafiltration steps follow LNP concentration. The first diafiltration replaces the remaining ethanol in solution with 35mM sodium acetate buffer. The second diafiltration replaces the sodium acetate buffer with the final formation buffer consisting of tris buffer and sucrose. This two-step diafiltration approach for lipid nanoparticles has been shown to provide improve LNP storage stability, decrease the amount of empty LNPs, and enhance transfection efficiency.[66]

During each diafiltration, buffer is continuously added to the tank throughout the process at the same rate permeate leaves the filter ($Q_D = Q_P$). As a result, the batch volume remains constant while the product is retained by the membrane, and smaller molecules, including the buffer components, are removed through the permeate and sent to waste. The same T-Series Cassette with a Delta regenerated cellulose membrane with a MWCO of 100kDa used in concentration is used to perform each diafiltration.[61,62] Like with concentration, the rejection coefficients (σ) for this TFF process will be assumed to be 1 for the LNP-mRNA and 0 for all other species.

LNP and mRNA purification each have their own TFF skid that performs both concentration and diafiltration. As a result, the membrane area used in each diafiltration remains the same as used in concentration, 2.5m^2 for LNPs and 0.5m^2 for mRNA (Table 3.5.2.2-1). Permeate flux through the filter was estimated based on a study by Cytiva Life Sciences using the T-Series Cassette with a 100kDA Delta RC membrane.[61] Based on the operating conditions of each diafiltration process (trans-membrane pressure and feed flowrate) permeate flux through the membrane can be estimated (Figure 3.5.2.2-1).[61] Once permeate flux for each diafiltration system is calculated, crossflow flowrate and processing time for the process can be determined. Similar to mRNA and LNP concentration, calculating processing time and waste stream characteristics is nearly identical for both mRNA and LNP diafiltration and is described below.

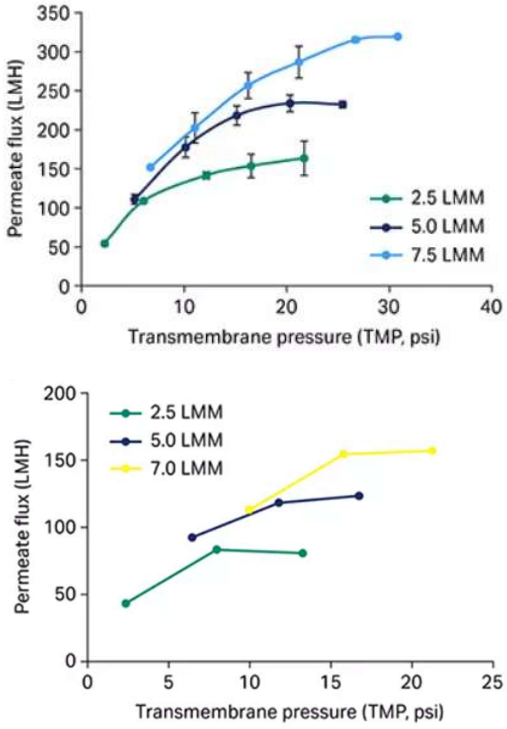

Figure 3.5.2.2-1. Permeate flux during diafiltration as a function of TMP and feed rate for (A) mRNA (B) LNPs.[54]

Table 3.5.2.2-1. Operating conditions during diafiltration

Parameter	mRNA NaOAc Diafiltration	LNP NaOAc Diafiltration	LNP F.F. Diafiltration
Filter Area (m^2)	0.5	2.5	2.5
TMP (psi)	10	20	20
Feed Flowrate (L/h)	450	1050	1050
Permeate Flowrate (L/h)	100	375	375
Crossflow Flowrate (L/h)	125	675	675

For each diafiltration process, yield is calculated based on reducing the concentration of a specific species to a desired level (Equation 3.5.2.2-1). For mRNA 50mM NaOAc diafiltration, yield is set to 0.01 to ensure a sufficient volume of sodium acetate buffer is added to the process. During the first LNP diafiltration, yield of ethanol is based on reducing the final concentration of ethanol in solution drops to 0.5% w/v in compliance with FDA guidelines.[67] For the second LNP diafiltration, a solution containing tris buffer and sucrose is added to the tank until the concentration of sodium acetate buffer drops to 0.04% w/v, consistent with AstraZeneca formulations.[68]

$$Yield = \frac{C_{f,x}}{C_{i,x}} \tag{3.5.2.2-1}$$

where

$C_{f,x}$ = Final Concentration of Species x (% w/v)

$C_{i,x}$ = Initial Concentration of Species x (% w/v)

Once the yield for each diafiltration process is determined, the volume of buffer that must be added to the system can be calculated (Equation 3.5.2.2-2). When considering the initial tank volume, this enables the number of diavolumes used in the diafiltration to be determined (Equation 3.5.2.2-3).

$$V_D = -V_0 \ln(yield) \tag{3.5.2.2-2}$$

$$Diavolumes = \frac{V_D}{V_0} \tag{3.5.2.2-3}$$

where

V_D=Diafiltration Volume (L)

V_0 = Initial Tank Volume (L)

Based on the volume of buffer added, the total time to complete each diafiltration is found by considering the membrane area and permeate flux (Equation 3.5.2.2-4). As stated earlier,

membrane specifications differ between mRNA and LNP diafiltration and are summarized in Table 3.5.2.2-1.

$$t = \frac{V_D}{A \cdot u_{p,avg}} \tag{3.5.2.2-4}$$

The final concentration of each species in solution following diafiltration can be found through a material balance with the resulting equations shown below. Equation 3.5.2.2-5 models the concentration of a species following a diafiltration if it is contained in the buffer added to the system. Equation 3.5.2.2-6 calculates the final concentration of each species assuming they are not present in the buffer added.

$$C_{x,f} = \frac{C_{x,feed}}{(1-\sigma)} + (C_{x,0} - \frac{C_{x,feed}}{(1-\sigma)})\exp\left(-\frac{V_D}{V_0}(1-\sigma)\right) \tag{3.5.2.2-5}$$

$$C_{x,f} = C_{x,0}\exp\left(-\frac{V_D}{V_0}(1-\sigma)\right) \tag{3.5.2.2-6}$$

where

$C_{x,f} =$ Final Concentration of Species x (g/L)

$C_{x,0} =$ Starting Concentration of Species x (g/L)

$C_{x,feed} =$ Feed Concentration of Species x (g/L)

$V_D =$ Diafiltration Volume (L)

$V_0 =$ Initial Tank Volume (L)

The composition of the waste generated throughout each diafiltration is calculated through the material balance depicted in equation 3.5.2.2-7.

$$m_{x,w} = V_t C_{x,0} + V_D C_{feed} - V_x C_{x,f} \tag{3.5.2.2-7}$$

where

$m_x =$ Mass of Species x Sent to Waste (g)

$V_t = \text{Tank Volume (L)}$

$V_D = \text{Diafiltration Volume (L)}$

$C_{x,0} = \text{Starting Concentration of Species x (g/L)}$

$C_{x,f} = \text{Final Concentration of Species x (g/L)}$

$C_{x,feed} = \text{Feed Concentration of Species x (g/L)}$

The workflow described above is used to calculate the processing time and waste characteristics for both mRNA and LNP diafiltrations. Product concentration remains constant throughout diafiltration due to a constant batch volume and rejection coefficient of 1 for LNPs and mRNA. A breakdown of how the concentrations of non-product species change because of each diafiltration is depicted in Table 3.5.2.2-2.

Table 3.5.2.2-2. Summary of batch characteristics following diafiltration

Parameter	**mRNA NaOAc Diafiltration**		**LNP NaOAc Diafiltration**		**LNP F.F. Diafiltration**	
	Before	*After*	*Before*	*After*	*Before*	*After*
Tank Volume (L)	39.69	39.69	240	240	240	240
C_{Tris} (%w/v)	0.778	0.008	0	0	0	0.129
C_{NaOAc} (%w/v)	0	0.406	0.317	0.290	0.290	0.04
C_{NaCl} (%w/v)	8.99	0.089	0	0	0	0
$C_{Arginine}$ (%w/v)	6.53	0.065	0	0	0	0
C_{EtOH} (%w/v)	0	0	5	0.5	0.5	0.069
Processing Time (hr)	1.83		1.47		1.27	

Waste generated during each diafiltration process is calculated from equation 3.5.2.2-7 and summarized in the Table 3.5.2.2-3. Water accounts for the volume of each stream.

Table 3.5.2.2-3. Summary of waste characteristics throughout diafiltration

Species	mRNA NaOAc Diafiltration	LNP NaOAc Diafiltration	LNP F.F. Diafiltration
Volume (L)	182.8	552.6	475.4
Tris-HCl (g)	309.6	0	402.7
Sodium Acetate (g)	580.7	1650	599.9
Sodium Chloride (g)	3530	0	0
Arginine (g)	2567	0	0
Ethanol (g)	0	10800	1034
Sucrose (g)	0	0	13426

3.5.3 Sterile Filtration

Sterile filtration is designed to ensure that the mRNA product is free from microorganisms and other contaminants. Two sterile filtration steps are incorporated into the process: the first occurs at the end of mRNA purification, and the second takes place at the end of LNP purification. Following mRNA sterile filtration, bioburden reduction is achieved, though the product is not claimed to be completely sterile. This bioburden reduction helps maintain mRNA stability by removing potential contaminants that could degrade the mRNA.[69] After the final LNP sterile filtration, the product is considered sterile, ensuring compliance with federal regulations.[70]

A Sartopore 2 XLG filter (0.2 μm pore size) is used to perform both mRNA and LNP sterile filtrations. Due to the large size of mRNA-LNPs, there are typically significant product loss issues associated with the usage of industry-standard, 0.22 μm sterile filters; however, a study performed by Messerian et al. found that the Sartopore 2 XLG filter (0.2 μm pore size) can be used to effectively sterile filter mRNA-LNPs at reasonable transmembrane pressure drops (TMP) with high yields (> 96%).[71] The final sterile filtration unit, F-402, is designed to operate using Sartopore 2 XLG cartridges with a control loop to maintain constant TMP to replicate the results observed by Messerian et al. The sterile filtration unit for mRNA, F-202, operates under the same conditions as F-402.

Figure 3.5.3-1 displays that filtration of mRNA-LNPs using the Sartopore 2 XLG leads to significant filter fouling behavior, as filtrate flux decreases sharply and resistance increases sharply as volumetric throughput increases. To overcome this issue, the sterile filtration process is operated at the highest constant TMP studied by Messerian et al. (20 psi) to increase the volumetric throughput at which significant fouling behavior occurs, and numerous filters of large filtration area (1.6 m^2) are used to reduce the necessary volumetric throughput per filter.

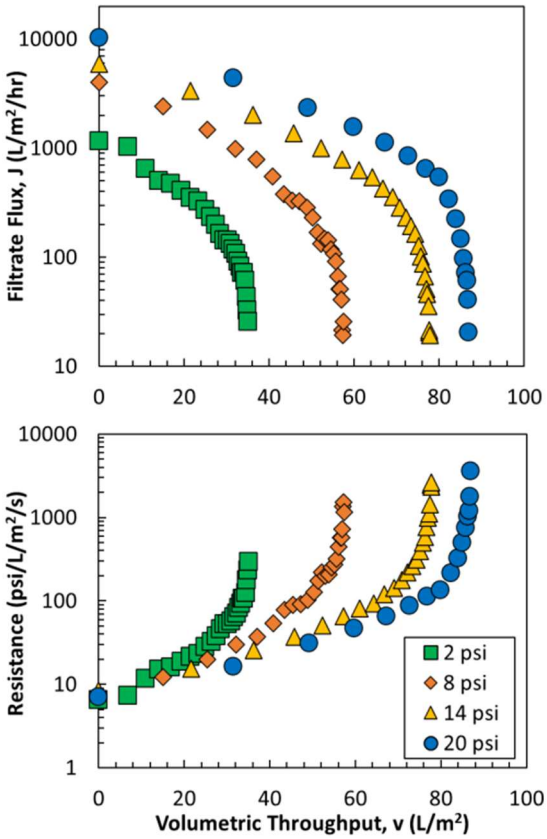

Figure 3.5.3-1. Filtrate flux (upper panel) and resistance (lower panel) as a function of the volumetric throughput during constant pressure filtration using Sartopore 2 XLG capsules at constant TMPs of 2, 8, 14, and 20 psi. Adapted from Messerian et al. (2022).

240 L of mRNA-LNP solution passes through the F-402 per batch, therefore, if a single filter with 1.6 m^2 filtration area were used, then the total volumetric throughput would be 150 L/m^2, greatly exceeding the volumetric throughput at which the filter flux drops aggressively when operated at a constant TMP of 20 psi, as seen in Figure 3.5.3-1. Instead, F-402 uses 3 filters operated in parallel to reduce the total volumetric throughput per filter to 50 L/m^2, reducing the fouling behavior and allowing for an approximation of the time-average filtrate flux (6250 LHM) as the region from 0 to 50 L/m^2 in the upper panel of Figure 3.5.3-1 is approximately linear.

As for mRNA sterile filtration through F-202, only 39.69 L of mRNA solution pass through each batch. Due to the smaller filtrate volume than LNP sterile filtration, only 1 filter is used operating

with a volumetric throughput of 25L/m^2. Average filtrate flux through this filter is approximated to be 7500 LMH (Figure 3.5.3-1). The data selected from Figure 3.5.3-1 used to calculate the average filtrate flux for each sterile filtration process is depicted in Table 3.5.3-1.

Table 3.5.3-1. Calculation of time-average filtrate flux using linear approximation

Volumetric Throughput (L/m^2)	**Filtrate Flux (LMH)**	
	mRNA Sterile Filtration	*LNP Sterile Filtration*
0	10000	10000
25	5000	-
50	-	2500
Average:	**7500**	**6250**

The processing time for each sterile filtration is calculated based on the filtrate volume, filtrate flowrate, and number of filter cartridges used (Equation 3.5.3-1).

$$t_{processing} = V/U_f(A * n) \qquad (3.5.3\text{-}1)$$

where

$t_{processing}$ = Processing Time (s)

V = Total Filtrate Volume (L)

U_f = Filtrate Flux (L/m^2/s)

A = Effective Filtration Area per Filter (m^2)

n = Number of Filters Cartridges

The mRNA yield of both sterile filtrations is conservatively estimated to be 96% based on the minimum yield observed by Messerian et al.[21] Using this yield value and Equation 3.5.3-2, the mass of mRNA remaining in the sterile filters can be determined (Table 3.5.3-2).

$$m_{mRNA,in} * (\%\ yield) = m_{mRNA,out} \qquad (3.5.3\text{-}2)$$

where

$m_{mRNA,in}$ = The mass of mRNA entering sterile filter (g)

$m_{mRNA,out}$ = The mass of mRNA leaving sterile filter (g)

Table 3.5.3-2. Mass balance of mRNA surrounding sterile filtration

Parameter	mRNA Sterile Filtration	LNP Sterile Filtration
Yield (%)	96	96
Input mRNA (g)	28.94	25
Output mRNA (g)	27.78	24
mRNA lost in filter (g)	1.16	1

The stream balance around each sterile filter is summarized in Table 3.5.3-3, with the only difference in the streams occurring in the reduction of mRNA concentration due to the mass of mRNA remaining in the filter cartridges each batch.

Table 3.5.3-3. Stream balance around sterile filters

Parameter	mRNA Sterile Filtration		LNP Sterile Filtration	
	Entering	*Leaving*	*Entering*	*Leaving*
Volume (L)	39.69	39.69	240	240
C_{mRNA} (%w/v)	0.0729	0.07	0.0104	0.0100
C_{Tris} (%w/v)	0.008	0.008	0.129	0.129
C_{NaOAc} (%w/v)	0.406	0.406	0.04	0.04
C_{NaCl} (%w/v)	0.089	0.089	0	0
$C_{Arginine}$ (%w/v)	0.065	0.065	0	0
C_{EtOH} (%w/v)	0	0	0.069	0.069
$C_{sucrose}$ (%w/v)	0	0	4.310	4.310
Processing Time (s)	11.9		28.8	

The maximum allowable front pressure (MAFP) for the sterile filtration process is a critical parameter to determine the pumping requirements to push the fluid through each filter. Using Equation 3.5.3-3, the MAFP for each sterile filter is 3.4 bar, which is the maximum pressure at which the pump needs to be capable of delivering the mRNA-LNP solution to the filter. During processing, a lesser, variable front-pressure is used with a control loop to maintain the constant TMP of 1.4 bar.

$$MAFP = MABP + TMP \tag{3.5.3-3}$$

where

MAFP = Maximum allowable front pressure (bar)

MABP = Maximum allowable back pressure for the filter cartridges (bar)

**2 bar for the Sartopore 2 XLG 1.6 m^2 cartridges*

TMP = Constant transmembrane pressure drop (bar),

** 1.4 bar (20 psi)*

A summative table for the process parameters of each sterile filter is displayed in Table 3.5.3-4.

Table 3.5.3-2. Sterile filtration filter specifications and operating parameters

Parameter	mRNA Sterile Filtration	LNP Sterile Filtration
Filter Cartridge	Sartopore 2 XLG	Sartopore 2 XLG
Cartridge Filtration Area (m^2)	1.6	1.6
Pore Size (µm)	0.2	0.2
Number of Filters	1	3
Constant Operating TMP (bar)	1.4	1.4
Batch Volume (L)	39.69	240
Processing Time (s)	11.9	28.8
Maximum Front Pressure (bar)	3.4	3.4

3.6 Cleaning

3.6.1 CIP/SIP

Each storage tank in the LNP-mRNA process undergoes a clean-in-place (CIP) cycle to remove residues from processing. A CIP skid, consisting of two tanks and two pumps, is utilized to complete the CIP cycle for each tank (Figure 3.6.1-1). Each storage tank is equipped with a fixed CIP spray ball to ensure the entire tank interior is cleaning throughout the process.[72]

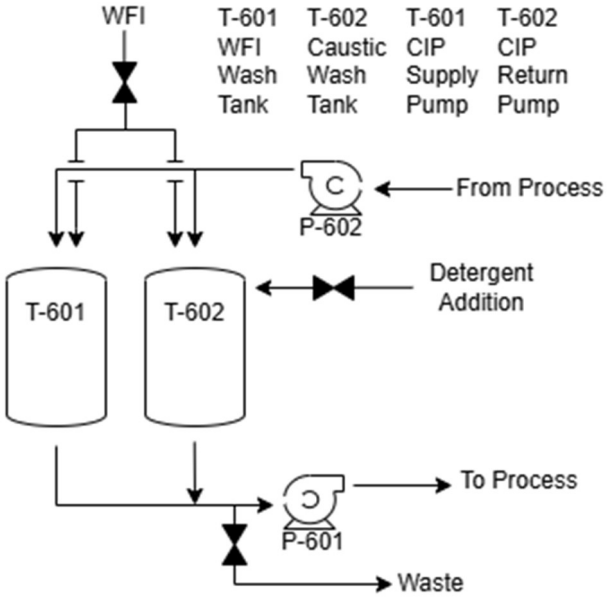

Figure 3.6.1-1. PFD of CIP skid

The CIP process consists of three phases: a pre-rinse, a caustic wash, and a final rinse. Each phase utilizes a wash volume equivalent to 10% of the tank's total capacity.[73] During the pre-rinse and final rinse phases, tank T-601 is filled with the required wash volume of WFI at 60°C, which is then circulated through the tank being cleaned. In the caustic wash phase, a 1% v/v solution of alkaline CIP detergent in WFI at the same temperature is prepared in tank T-602 and circulated through the cleaning route.[74] Throughout each cleaning phase, a flow velocity of 1.5 m/s is maintained to ensure turbulent conditions, maximizing cleaning effectiveness.[75] The wash volume for each phase circulates through the cleaning path 5 times, consistent with industry rule of thumb.[76] Since the exact length of piping associated with each tank is unknown, the minimum CIP duration is roughly estimated based on the total wash volume that must be cycled through the tank, assuming an average flow rate of 160 L/min. A time buffer is added when scheduling cleaning to account for drain and fill times.

$$t = \frac{5V}{Q} \tag{3.6.1-1}$$

where

$t =$ CIP Duration (min)

$V =$ Total Wash Volume of the 3 CIP Phases (L)

$Q = 160$ L/min (flow rate approximated based on 2 in pipe and 1.5 m/s flow velocity)

Following each CIP cycle, a sterilization or steam-in-place (SIP) process is conducted to ensure tank sterility. During SIP, the tank is filled with clean steam at 1.5 bar and 121°C.[77] Once steam has fully filled the tank, a sterilization time of 40 minutes is maintained. To account for filling times, the total SIP cycle is assumed to last approximately one hour. As with the CIP process, the exact piping length associated with each tank is unknown. Therefore, it is assumed that the amount of steam required for each SIP cycle is equal to the tank volume. A summary of the CIP and SIP cycle attributes for each tank is provided in Table 3.6.1-1.

Table 3.6.2.1-1. CIP and SIP process parameters

Tank	Tank Volume (L)	CIP Wash Volume (L)	Detergent Used (L)	WFI Used (L)	Clean Steam Used (L)	Total Cleaning Time (min)
T-101	68	6.8	0.07	20.33	68	60.64
T-201	322	32.2	0.32	96.28	322	63.01
T-202	144	14.4	0.14	43.06	144	61.35
T-301	68	6.8	0.07	20.33	68	60.64
T-302	68	6.8	0.07	20.33	68	60.64
T-401	627	62.7	0.63	187.47	627	65.86
T-501	322	32.2	0.32	96.28	322	63.01
T-502	6056	605.6	6.06	1810.74	6056	116.59
T-503	1552	155.2	1.55	464.05	1552	74.50
T-504	2801	280.1	2.80	837.50	2801	86.17
T-505	3066	306.6	3.07	916.73	3066	88.65
T-506	227	22.7	0.23	67.87	227	62.12
T-507	1173	117.3	1.17	350.73	1173	70.96
T-508	227	22.7	0.23	67.87	227	62.12
T-509	1987	198.7	1.99	594.11	1987	78.57
T-510	397	39.7	0.40	118.70	397	63.71
T-511	6056	605.6	6.06	1810.74	6056	116.59
T-512	6056	605.6	6.06	1810.74	6056	116.59

3.6.2 IVT Reactor Cleaning Protocol

The 5 L IVT bioreactor from the mRNA synthesis step requires a similar CIP cycle to that of the storage tanks (Section 3.6.1) to ensure the residual material is removed from the reactor. The same CIP skid is used (Figure 3.6.1-1), showing tank T-601 for WFI and T-602 for alkaline detergent, as well as pumps P-601/602.

The CIP process consists of three phases: a pre-rinse, caustic wash, and final rinse. Each phase uses a wash volume equal to the reactor's maximum working volume of 3.75 L.[78] During the two rinsing stages, WFI from tank T-601 is circulated through the reactor at 60 °C. During the caustic wash stage, a 1% v/v solution of alkaline CIP detergent in WFI at 60 °C is prepared in tank T-602 and circulates through the reactor. Throughout each cleaning phase, a turbulent flow rate is maintained, and the wash volume circulates through the cleaning path five times.[79] A static spray ball is employed within the reactor to simplify the CIP process, spraying at a flow rate of 18 L/min, calculated by multiplying the reactor circumference by 11.4.[80,81] The minimum CIP time is estimated based on the total wash volume cycled through the reactor, assuming a turbulence-inducing flow rate of 7.5 L/min based on the size of the reactor and its associated piping.[80] A time buffer is added to account for drain and fill times. The total time for the CIP process of the reactor is 40 minutes (Equation 3.5.1-1, Q = 7.5 L/min).

Following each CIP cycle, an SIP process is conducted to sterilize the reactor. During SIP, the reactor is filled with clean steam at 1.5 bar and 121 °C.[82] The amount of steam needed is estimated to be equal to the maximum working volume of the reactor, 3.75 L. Standard protocols recommend this step for 40 minutes. The total SIP cycle is approximated to be 60 minutes to account for filling times.

3.6.3 Chromatography Column Cleaning Protocol

At the end of each batch, both chromatography units undergo individual cleaning protocols. The AC unit, C-201, is cleaned using a 4-step process, each requiring 10 column volumes. The order of fluids being passed into the top of C-201 during the cleaning process are WFI, 0.5 M NaOH, WFI, equilibration buffer, taking a total time of 80 minutes to complete. The AEX unit, C-202, is cleaned using a 2-step process, consisting of 5 column volumes of 0.5 M NaOH, then 15 column volumes of buffer A1; this process takes a total time of 67 minutes.

3.6.4 Impinging Jet Mixer Cleaning Protocol

The confined impinging jet mixer (CIJM) in the LNP-mRNA process undergoes a similar CIP cycle to that of the storage tanks (Section 3.6.1) to remove residual material from processing. The same CIP skid (Figure 3.6.1-1), consisting of tanks T-601 and T-602 for WFI and alkaline detergent respectively and pipes P-601/602, is used to perform the CIP cycle. Due to the small internal volume of the mixing chamber, the CIP procedure includes a filling phase to ensure complete wetting of the mixer before continuous flow begins.

The CIP process consists of the same three phases: a pre-rinse, caustic wash, and final rinse. Each phase uses a wash volume equal to the mixing chamber internal volume + 10% of the associated piping to ensure the chamber is fully wetted.

Each phase begins with a filling phase, during which the outlet valve of the CIJM remains closed while the chamber is filled with cleaning solution (WFI or 1% v/v solution of alkaline CIP detergent at 60 ºC). Once the chamber is filled, the dwell phase begins. The cleaning solution remains in the mixing chamber for a brief period (typically 30–60 seconds) ensuring that any residual product is properly broken down before flushing.

After the dwell time, the continuous flushing is initiated. The outlet valve opens, allowing the cleaning solution to flow through the mixer and surrounding piping at a velocity of 1.5 m/s.[59] To ensure complete cleaning, the wash volume for each phase circulates through the cleaning path five times, consistent with industry best practices.[60] Since the internal volume of the CIJM and associated piping is small (estimated to be less than 1 mL), the total CIP duration is estimated to take a maximum of 30 minutes, included fill and drain times.

3.7 Ancillary Equipment

3.7.1 Heat Exchangers

3.7.1.1 Maintaining Constant Temperature for IVT Reactor (R-101)

Maintaining a stable reactor temperature is essential for optimizing enzyme activity and ensuring efficient mRNA synthesis during the *in vitro* transcription (IVT) process. To sustain a constant temperature of 37ºC throughout both the 6-hour reaction period and 2.25-hour DNase/EDTA treatment, a standard 110 VAC silicon heating jacket will be used. This heating method ensures uniform heat distribution, preventing temperature fluctuations that could negatively impact transcription yield and enzyme stability.

To confirm that a standard 110 VAC jacket can provide the necessary thermal energy, assuming a current of 15-20 amps, a maximum heat loss from the reactor was estimated under conservative conditions. Conservative assumptions included no external insulation (insulation of the jacket itself was not incorporated) and a natural convection coefficient of ~50 $W/m^2 \cdot K$ (estimated based on air flow rates for proper filtration in facility); the system was further simplified by assuming unidirectional flow of heat.[67] Additionally, the reactor vessel, made of borosilicate glass (pyrex) was estimated to have a thickness of 6.5 mm with a thermal conductivity of 1.4 $W/m \cdot K$.

The heat dissipation (Q) was calculated by combining equations for conductive and convective heat transfer, under steady state assumptions with uniform internal reactor wall temperature. Convective heat loss from the reactor's outer surface was estimated using Eq. 3.7.1.1-1, while conductive heat transfer through the borosilicate wall was determined by Eq. 3.7.1.1-2. Given that the inner and outer surface areas of the reactor are approximately equal, the surface area was estimated using the surface area of liquid in contact with the reactor vessel walls, assuming no heat is lost through the reactor headspace.

$$Q = A_o h(T_2 - T_1) \qquad 3.7.1.1\text{-}1$$

where

A_o=outer surface area of the reactor (m^2)

h= natural convective heat transfer coefficient=50 $\frac{W}{m^2 \cdot K}$

T_2=outer reactor wall temperature (K)

T_1=air temperature (K)

$$Q = \frac{A_i k}{\Delta}(T_3 - T_2) \qquad 3.7.1.1\text{-}2$$

where

A_i=inner surface area of the reactor (m^2)

k= thermal conductivity of borosilicate glass=1.4 $\frac{W}{m \cdot K}$

T_3=inner reactor wall temperature (K)

Δ =glass thickness (m)

$$A_o \approx A_i = \pi r_i^2 + 2 \pi r_i * H \qquad 3.7.1.1\text{-}3$$

where

r_i=reactor inner radius (m)

H = height of fluid in reactor (m

Solving these equations with the appropriate reactor dimensions, visualized in Figure 3.7.1.1-1, the maximum heat loss was determined to be 9.4 W. Given the jacket's expected voltage of 120 V and a current between 15-20 amps, which provides 1800-2400 W, it is expected to provide sufficient thermal energy to maintain a stable 37°C reaction environment throughout the IVT process, ensuring optimal enzyme performance and mRNA synthesis.

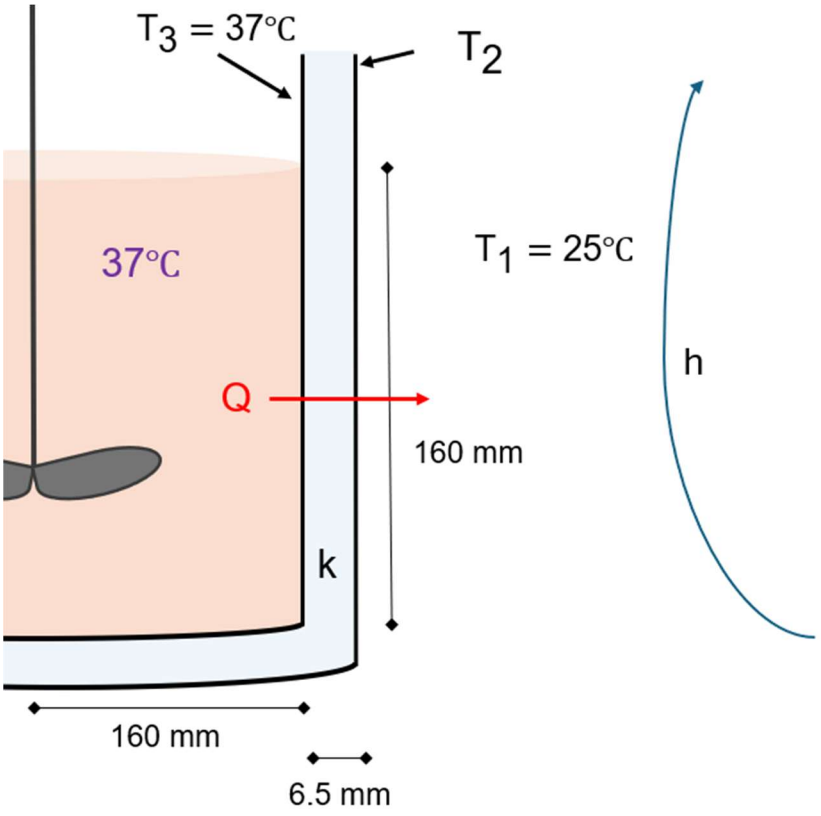

Figure 3.7.1.1-1. IVT bioreactor temperature diagram

3.7.1.2 E-301 Warming Ethanol/Lipid mixture

To ensure the solubility of supersaturated lipids in EtOH and promote uniform lipid nanoparticle (LNP) formation, the EtOH-lipid mixture is heated from 25°C to 60°C before rapid nanoprecipitation occurs upon mixing with a 4°C aqueous mRNA solution. This heating process will be achieved using low-pressure steam (1.5 barg) in a countercurrent, single-pass, shell-and-tube heat exchanger constructed from pharmaceutical-grade stainless steel (316L). The use of a shell-and-tube design enables efficient heat transfer while maintaining sterility required for regulatory compliance.

The required heating duty, 1.552 kW, was determined using Aspen Plus V14, under the assumption that the EtOH-lipid mixture has the properties of pure ethanol. While literature suggests that increased lipid content—such as the presence of glycerol in wine[68]—affects viscosity and therefore density, and heat capacity, the lack of numerical correlations means that experimental validation will be necessary for improved accuracy. Heat transfer calculations were performed using the log mean temperature difference method (Eq. 3.7.1.2-1&2) to determine the necessary surface area of the exchanger, and mass flow rate calculations (Eq. 3.7.1.2-3) were conducted to estimate steam consumption.

$$\Delta T_{LM} = \frac{\left(T_{H,in} - T_{C,out}\right) - \left(T_{H,out} - T_{C,in}\right)}{\ln\left(\frac{T_{H,in} - T_{C,out}}{T_{H,out} - T_{C,in}}\right)} \qquad 3.7.1.2\text{-}1$$

where

$T_{H,\,in}$= Temperature of hotter fluid entering heat exchanger (K)

$T_{H,\,out}$ = Temperature of hotter fluid exiting heat exchanger (K)

$T_{C,\,in}$=Temperature of colder fluid entering heat exchanger (K)

$T_{C,\,out}$=Temperature of colder fluid exiting heat exchanger (K)

$$Q = A \cdot U \cdot \Delta T_{LM} \qquad 3.7.1.2\text{-}2$$

where

A = surface area of heat transfer (m^2)

U = Universal heat transfer coefficient ≈ 850 $\frac{w}{m^2 \cdot K}$ (heuristic from Peters, et al.[84])

ΔT_{LM} = Log mean temperature (Eq. 3.4.1.2-1)

Q = Heat exchanged between fluids (W)

$$\dot{m} = \frac{Q}{\Delta H_{cond}} \qquad 3.7.1.2\text{-}3$$

where

$\dot{m}$ = Mass flow rate of steam $\left(\frac{kg}{s}\right)$

ΔH_{cond}=Heat of condensation $\left(\frac{kJ}{kg}\right)$

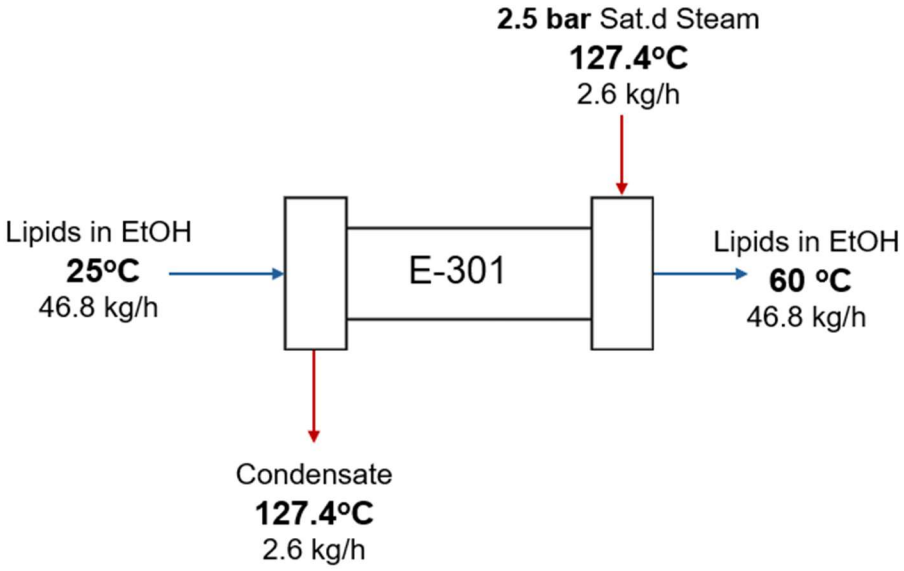

Figure 3.7.1.2-1. Diagram for heat exchanger E-301, used to heat EtOH-lipid stream entering CIJM

Based on this analysis, the necessary surface area was estimated to be 218 cm² with a steam flow rate of 2.56 kg/hr. The calculated temperature profiles and flow rates are visually represented in Figure 3.7.1.2-1, illustrating the exchange of heat between the steam and ethanol-lipid mixture.

3.7.1.3 E-302 Cooling LNP-mRNA solution

To ensure the stability of LNPs prior to filtration, the solution must be cooled back to room temperature (25^{o}C) after formation. This cooling process will be achieved using a countercurrent, single-pass, shell-and-tube heat exchanger constructed from pharmaceutical-grade stainless steel (316L). The coolant used is a 30% v/v mixture of refrigerated ethylene glycol and water, which maintains temperature differences across streams sufficient for efficient heat removal.

The required heat removal rate was determined using Aspen Plus, which calculated the heat duty to be 58.7 W. The analysis assumed that the LNP-mRNA solution had the same physical properties as an acetate buffer-ethanol mixture, without considering potential solubility effects of lipids or mRNA. The coolant inlet temperature was set to 10°C, and a mass flow rate of 56 kg/hr was used to ensure sufficient cooling capacity. Using the ELEC-NRTL property method, Aspen Plus estimated that the coolant mixture exits the exchanger at 20°C, maintaining a ~10°C temperature difference. Equation 3.7.1.2-1&2 were used to determine the required surface area to be 164 cm², which is within a feasible range for heat exchanger. A detailed diagram illustrating the heat exchanger setup, including flow rates and temperature values, is provided in Figure 3.7.1.3-1.

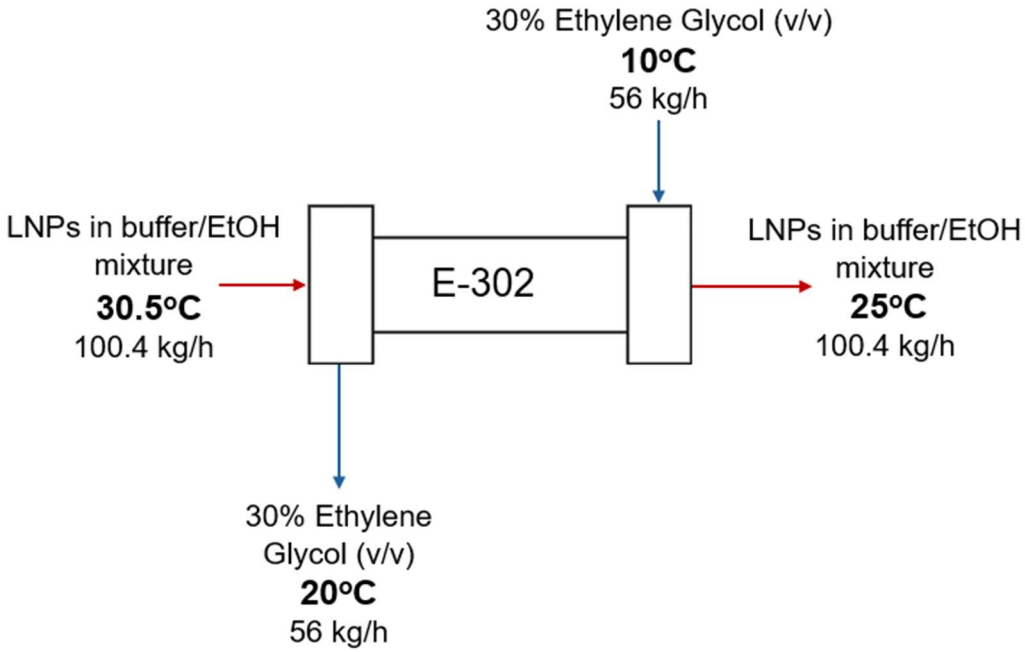

Figure 3.7.1.3-1. Diagram for heat exchanger E-302, used to cool LNP-mRNA stream leaving CIJM

By maintaining an appropriate coolant flow rate and temperature difference, this design ensures that the LNP-mRNA solution is rapidly cooled to a stable temperature, preventing particle aggregation or degradation before filtration.

3.7.1.4 E-303 Cooling purified mRNA solution

To ensure proper mixing and separation of phases during LNP formation, the aqueous mRNA solution leaving purification block must be cooled to 4°C. This cooling process will be achieved using a countercurrent, double pipe heat exchanger constructed from pharmaceutical-grade stainless steel (316L) with a chiller. The coolant used is a 30% v/v mixture of refrigerated ethylene glycol and water, which maintains temperature differences across streams sufficient for efficient heat removal.

The required heat removal rate was determined using Aspen Plus, which calculated the heat duty to be 1.3 kW. The analysis assumed that the mRNA solution had the same physical properties as

an acetate buffer-ethanol mixture, without considering potential effects of the mRNA. The coolant inlet temperature was set to -5°C, and a mass flow rate of 63 kg/hr was used to ensure sufficient cooling capacity. Using the ELEC-NRTL property method, Aspen Plus estimated that the coolant mixture exits the heat exchanger at 15°C, maintaining a ~10°C temperature difference. Equation 3.7.1.2-1&2 were used to determine the required surface area to be 0.483 m^2, which is within a feasible range for heat exchanger. A detailed diagram illustrating the heat exchanger setup, including flow rates and temperature values, is provided in Figure 3.7.1.4-1.

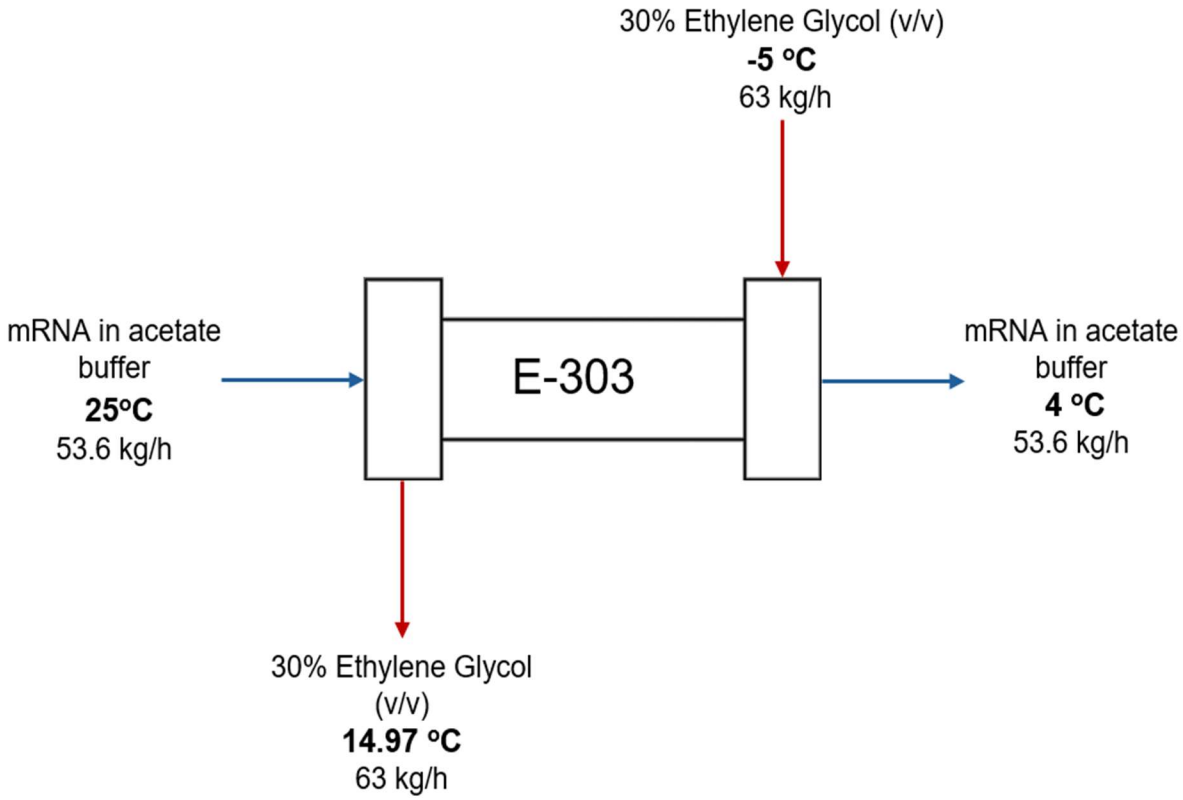

Figure 3.7.1.4-1. Diagram for heat exchanger E-303, used to cool mRNA stream entering CIJM

By maintaining an appropriate coolant flow rate and temperature difference, this design ensures that the mRNA solution is rapidly cooled to the proper temperature, preventing particle aggregation or degradation before filtration.

3.7.2 Pumps

Multiple pumps are required throughout the LNP-mRNA manufacturing process to facilitate fluid movement. Two primary types of pumps are utilized: centrifugal pumps and peristaltic pumps. Centrifugal pumps are employed in the TFF and CIP skids, while peristaltic pumps are used to transfer process fluid between batch operations. Each pump in the process has a spare available in the event of a mechanical failure. Since the buffer tanks are located on the second floor of the plant, gravity naturally drives buffer flow to the process, eliminating the need for additional pumps. The flowrate is regulated by flow control valves to ensure proper delivery.

3.7.2.1 TFF Pumps

Each of the two TFF skids is equipped with a centrifugal pump that drives each phase of the TFF process. These pumps must be appropriately sized to meet the flow rate and differential pressure requirements for concentration, diafiltration, and sterile filtration. The hydraulic power needed for each pump is estimated based on the flow rate and differential pressure of the process step (Equation 3.7.2.1-1). The differential pressure is calculated as the sum of frictional losses and the actual pressure difference between the source and destination (Equation 3.7.2.1-2). Gravity head is excluded from this calculation because the elevation change in the TFF process is negligible. The actual pressure difference between the pump source and destination during each TFF phase is determined based on the TMP of the filter. Frictional losses are estimated at 0.5 atm within the pipes, with an additional 0.5 atm loss through the control valve.

$$P = Q\Delta P \tag{3.7.2.1-1}$$

$$\Delta P = actual\ pressure\ difference + frictional\ losses + gravity\ head \tag{3.7.2.1-2}$$

where

$P =$ Hydraulic Power (W)

$Q =$ Volumetric Flowrate (m^3/s)

$\Delta P =$ Differential Pressure (Pa)

The pumps for each of the TFF skids were sized to meet the hydraulic power requirements of the most demanding process step, which is sterile filtration for both the mRNA and LNP TFF processes. A control valve is employed to regulate the pump's output flow rate during the concentration and diafiltration steps. A pump efficiency of 70% was assumed when determining the required power output. Capital costs of a API-610 horizontal centrifugal pump was estimated based on the required pump capacity factor using Figure 12-20 from *Plant Design and Economics for Chemical Engineers.*[84] Operating costs for each pump is estimated by multiplying the power

consumption of each pump, assuming 90% electrical driver efficiency, by the duration the pump operates. A summary of the pump attributes for the TFF skids is presented in Table 3.7.2.1-1.

Table 3.7.2.1-1. Attributes of TFF pumps

Pump ID	Operation	Output Flowrate (L/h)	Differential Pressure (atm)	Hydraulic Power (kW)	Energy Consumed* (kWh)
P-202	Concentration	225	3.361	0.021	0.056
P-202	Diafiltration	225	2.680	0.017	0.049
P-202	Sterile Filtration	4688	4.356	0.575	0.003
P-401	Concentration	1125	3.361	0.106	0.218
P-401	Diafiltration 1	1050	3.361	0.099	0.232
P-401	Diafiltration 2	1050	3.361	0.099	0.200
P-401	Sterile Filtration	3906	4.356	0.479	0.006

***per batch**

3.7.2.2 CIP Pumps

The CIP skid is equipped with two API-610 horizontal centrifugal pumps, each operating at 70% efficiency with a 90% efficient electrical driver. The CIP supply pump, P-601, delivers the cleaning solution into the tank via a spray ball, while the CIP return pump, P-602, removes the cleaning solution and returns it to the CIP skid. The hydraulic power required for each pump is estimated using the same method as for the TFF skid (Equation 3.7.2.1-1). The actual pressure difference for the CIP supply pump is determined based on a 25 psi pressure at the spray balls[85], while the CIP return pump is assumed to have no pressure difference between its source and destination. Frictional losses are estimated at 0.5 atm within the pipes, with an additional 0.5 atm loss through the control valve. For the CIP supply pump, the maximum possible gravity head is estimated based on the 5 m height needed to reach tanks on the second floor of the plant, while gravity head is neglected for the CIP return pump. The operating time of both pumps per batch is estimated by summing the CIP cleaning times for all tanks. This results in a conservative energy consumption calculation, as buffer tanks do not require CIP after every batch. A summary of the CIP pump attributes is provided in Table 3.7.2.2-1.

Table 3.7.2.1-1. Attributes of CIP pumps

Pump ID	**Output Flowrate (L/h)**	**Differential Pressure (atm)**	**Hydraulic Power (kW)**	**Energy Consumed* (kWh)**
P-601	9600	3.183	0.860	7.507
P-602	9600	1.000	0.270	2.358

***per batch**

3.7.2.3 Impinging Jet Mixer Pumps

Impinging jet mixing achieves efficient and rapid mixing through the collision of two high-velocity jet streams within a confined mixing zone. This requires pumps capable of generating high pressures to reach the necessary flow rates. In this system, three pumps are utilized to maintain flow control and stability, as summarized in Table 3.7.2.3-1.

Table 3.7.2.3-1. Attributes of CIJM pumps

Pump ID	Operation	Pump Type	Output Flowrate (L/h)	Hydraulic Power (kW)	Energy Consumed (kWh)*
P-301	R-301 inlet (aqueous)	Rotary piston	61	0.320	0.24
P-302	R-301 inlet (organic)	Rotary piston	54	0.320	0.24
P-303	R-301 outlet	Peristaltic micropump	115	.010	.0075

***per batch**

Rotary piston pumps (P-301 & P-302) are responsible for driving the inlet streams of lipids and mRNA solutions into the confined impinging jet mixer (CIJM). These pumps must generate sufficient pressure to accelerate the fluids to velocities of 22 m/s and 19 m/s, respectively, through the narrow mixing nozzles. Pumps supplied by KNAUER can deliver up to 320 W of power and generate a differential pressure of up to 95 bar, although the expected operational power requirement and operating pressures are significantly lower. To optimize performance and longevity, the pumps are ideally run at approximately 80% of their capacity, ensuring a buffer for energy requirements to accommodate any variations in flow resistance or process scaling needs. The exact differential pressure required is unknown due to the unknown diameter changes within the nozzles of the CIJM jets.

The outlet pump (P-303) will be a peristaltic pump responsible for transferring the newly formed mRNA-LNP mixture through a heat exchanger, cooling it to room temperature, before moving it to a holding tank for dilution. The suitability of a peristaltic pump was determined through an estimation of pressure drop (~0.7 bar) within the mixing chamber using a correlation with Reynolds number, as defined by Metzer and Kind (Figure 3.7.2.3-1).[86] Additional pressure drops from friction in the piping, control valves, and heat exchangers were estimated to be approximately 1.5 atm (1.52 bar). Both the total pressure drop (2.2 bar) and required volumetric flow rate (1.9 L/min) indicate a peristaltic pump with DW10-1 pump head and Tygon tubing (ID:1/16", OD: 3/16", thickness: 1/16" tubing) is sufficient.[87] The pump, using under 10 W, will be sufficient for maintaining stable product flow and transfer.

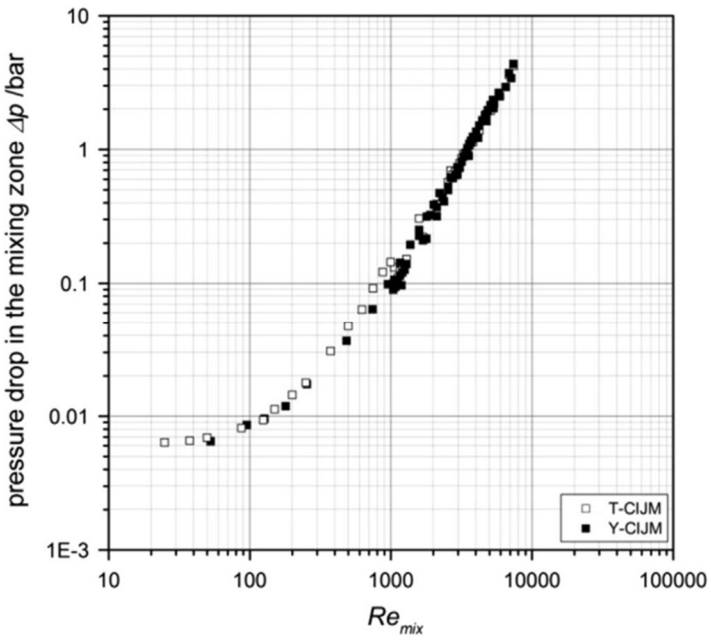

Figure 3.7.2.3-1. Pressure drop across the mixing chamber as a function of Reynolds number for mixing.

3.7.2.4 Peristaltic Transfer Pumps

Three peristaltic pumps are used in this process: P-101, P-102, and P-201. P-101 pumps the IVT mix from R-101 to T-101. P-102 pumps the IVT mix from T-101 to the top of the AC colums, C-201, during the sample loading step. P-201 pumps the AC product solution held in T-201 to the top of the AEX column, C-202, during the sample loading step. Peristaltic pumps were chosen for these processes as they offer the ability to operate at precise flow rates, which is necessary for maintaining the chromatographic procedures of both columns.

The differential pressure and hydraulic power for all peristaltic pumps are calculated using equations 3.7.2.1-2 and 3.7.2.1-1, respectively. Gravity head is neglected for each pump as the elevation change for each operation is negligible. The pressure loss for each pump is assumed to be 0.5 atm to account for frictional loss within the process tubing. The actual pressure difference for P-102 and P-201 are assumed to be equivalent to the calculated pressure drops across the AC and AEX columns, respectively. The actual pressure difference for P-101 is neglected as R-101 and T-101 are both held at atmospheric pressure. The flow rate, differential pressure, and power requirements for each peristaltic pump are available in Table 3.7.2.4-1.

Table 3.7.2.4-1. Attributes of peristaltic pumps

Pump ID	Operation	Flow Rate (L/h)	Differential Pressure (atm)	Hydraulic Power (kW)	Energy Consumed* (kWh)
P-101	IVT Mix Transfer	240.00	0.50	0.014	4.52E-05
P-102	AC Loading	240.00	5.78	0.156	5.21E-03
P-201	AEX Loading	83.16	4.94	0.012	3.56E-02

***per batch**

P-101, P-102, and P-103 are all VSH-A600, variable speed peristaltic pumps with A603 pump heads.[88] This pump type was selected due to its maximum flowrate (4700 mL/min) being suitable for all involved processes. Each will be operated using 3/8” bore PharMed® BPT tubing, the

tubing intended for use with the VSH-A600 pump.[89] Despite being autoclavable, the entire length of tubing used in peristaltic processes will be replaced between batches as to not risk aseptic containment. Operating costs for each pump are estimated by multiplying the power consumption of each pump, assuming 90% electrical driver efficiency, by the duration the pump operates.

3.7.3 Agitation and Storage Tanks

Storage tanks in the LNP-mRNA manufacturing process serve two primary purposes: holding process fluid between batch operations and storing the buffers used throughout the process. Tank sizing was determined by first calculating the volume each tank must hold for a single batch. Tanks designated for process fluids are sized to accommodate one batch, while buffer hold tanks are sized for eight batches, approximately two weeks of processing (Equation 3.7.3-1). For CIP tanks, sizing was based on the largest possible wash volume when cleaning. To prevent overfilling, a 20% buffer was added when determining the actual tank volume to purchase (Equation 3.7.3-2). Once the desired tank volume was established, tank dimensions were selected from the INDCO product catalog.[90] The storage tanks are constructed from grade 304 stainless steel, ensuring compliance with federal regulations.[91]

$$V_{total} = V_{batch} n \qquad (3.7.3-1)$$

$$V_{desired} = {}^{V_{total}}/_{p} \qquad (3.7.3-2)$$

where

$V_{batch} =$ Tank volume needed for single batch (L)

$n =$ Number of batches tank holds (1 for process storage tanks, 8 for buffer tanks)

$V_{total} =$ Maximum volume each tank needs to hold (L)

$p = 0.8 =$ Proportion of tank filled

$V_{desired} =$ Desired tank volume to purchase (L)

Nearly all storage tanks are equipped with a hydrofoil impeller to generate axial flow, ensuring that buffers and process fluid are evenly suspended.[92] Additionally, four vertical baffles are installed in each tank to enhance mixing. The specifications for the impeller and baffles are based on heuristics from *Plant Design and Economics for Chemical Engineers.*[84] The impeller diameter is set to one-third of the tank width, while each baffle measures one-tenth of the tank width. The

tip speed of each impeller is assumed to be 0.04 m/s, which is used to calculate the agitation rate in RPM (Equation 3.7.3-3). The power required to operate each impeller is estimated at 0.1 kW/m³. Using this power requirement, the energy consumption per batch can be calculated based on the duration the impeller operates (Equation 3.7.3-4). For tanks holding process fluid, the impeller is assumed to run continuously when the tank is full to maintain a well-mixed solution. For buffer tanks, the impeller is assumed to run for one hour before the buffer is needed in the process to ensure thorough mixing. To maintain a conservative estimate, it is assumed that the liquid level in the tank remains constant when calculating impeller energy consumption.

$$N = \frac{Tip\ speed}{\pi \cdot D} \qquad (3.7.3-3)$$

$$E = P \cdot V_{total} \cdot t \qquad (3.7.3-4)$$

where

$N =$ Agitation Rate (RPM)

$D =$ Impeller Diameter (m)

$Tip\ speed =$ Impeller Tip Speed (m/s)

$E =$ Impeller Energy Consumption (kJ)

$P = 0.1\ \mathrm{kW/m^3}$

$V_{total} =$ Volume of fluid in tank when full ($\mathrm{m^3}$)

$t =$ Length of time impeller runs (s)

Table 3.7.3-1 summarizes storage tank specifications.

Table 3.7.3-1. Storage tank specifications

Tank ID	Name	Volume (L)	Diameter (m)	Height (m)	Impeller Diameter (m)	Baffle Width (m)	Agitation Rate (RPM)	Mixing Time (min)	Energy Used* (kWh)
T-101	IVT Dilution Tank	68	0.46	0.46	0.15	0.05	5.01	60	0.003
T-201	Chromatography Holding Tank	322	0.77	0.76	0.26	0.08	2.96	185	0.079
T-202	mRNA TFF Holding Tank	144	0.58	0.61	0.19	0.06	3.96	190	0.038
T-301	mRNA Holding Tank	68	0.46	0.46	0.15	0.05	5.01	660	0.044
T-302	Lipid Holding Tank	68	0.46	0.46	0.15	0.05	5.01	660	0.048
T-401	LNP TFF Holding Tank	852	0.97	1.22	0.32	0.10	2.37	516	0.539
T-501	IVT Dilution Buffer	322	0.77	0.76	0.26	0.08	2.96	60	0.023
T-502	Affinity Binding Buffer	6056	2.11	1.83	0.70	0.21	1.09	60	0.461
T-503	Affinity Washing Buffer	1552	1.32	1.22	0.44	0.13	1.74	60	0.102
T-504	Affinity Elution Buffer	2801	1.42	1.83	0.47	0.14	1.61	60	0.205
T-505	Buffer A1 Holding Tank	3066	1.52	1.78	0.51	0.15	1.50	60	0.269
T-506	Buffer A2 Holding Tank	227	0.58	0.91	0.19	0.06	3.96	60	0.018
T-507	Buffer B1 Holding Tank	1173	1.14	1.22	0.38	0.11	2.01	60	0.083
T-508	0.5M NaOH Holding Tank	227	0.58	0.91	0.19	0.06	3.96	60	0.018
T-509	50mM NaOAc Holding Tank	1987	1.32	1.52	0.44	0.13	1.74	60	0.146
T-510	Ethanol Holding Tank	397	0.77	0.91	N/A	N/A	N/A	N/A	N/A
T-511	35mM NaOAc Holding Tank	6056	2.11	1.83	0.70	0.21	1.09	60	0.442
T-512	Final Formulation	6056	2.11	1.83	0.70	0.21	1.09	60	0.380
T-601	WFI Wash Tank	852	0.97	1.22	N/A	N/A	N/A	N/A	N/A
T-602	Caustic Wash Tank	852	0.97	1.22	N/A	N/A	N/A	N/A	N/A

***per batch**

3.7.4 Utilities

The utilities utilized in the LNP-mRNA manufacturing process consist of Water for Injection (WFI), clean steam, ethylene glycol, and electricity. WFI is required for all processing as well as CIP cycles. Clean steam is utilized during the SIP cycles as well as providing energy to E-301. Ethylene glycol is used to remove heat from E-302 and E-303. Low pressure steam, refrigeration system for ethylene glycol/water mixture. Electricity powers all pumps and agitators in the process as well as the freezers and steam generators used elsewhere in the plant.

All utilities except for clean steam are purchased directly from outside suppliers. Clean steam is produced within the plant by purchasing WFI and vaporizing it using an electric steam generator.[93] As a result, the cost of steam is estimated based on the amount of WFI that must be purchased and the electricity required to vaporized the WFI. Energy required to produce clean steam is calculated by summing the heat needed to raise the WFI temperature from 25C to 100C with the heat needed to vaporize the WFI at 100C (Equation 3.7.4-1). This energy requirement is then converted to an electricity demand by considering the 97% efficiency of the electric steam generator.

$$E = mc\Delta T + mH_{vap} \qquad (3.7.4-1)$$

where

$E =$ Energy (kJ)

$m =$ Mass of WFI (kg)

$c =$ Specific Heat of Water (kJ/kgK)

$\Delta T =$ Temperature Difference (K)

$H_{vap} =$ Heat of Vaporization of Water (kJ/kg)

3.8 Batch Schedule

As outlined in the plant capacity section, the manufacturing schedule consists of 24 batches per year, each yielding 24 g of mRNA, to achieve the annual production target of 576 g of mRNA. Table 3.8-1 presents the processing and cleaning times for each process unit and storage tank. The production time for buffer tanks is excluded from the table, as they function solely in conjunction with other process units.

Table 3.8-1. Processing and cleaning time for each process unit

Unit	Name	Processing Time (hr)	Cleaning Time (hr)	Total (hr)
R-101	In Vitro Transcription Reactor	6.00	1.62	7.62
T-101	IVT Dilution Tank	N/A	1.01	1.01
T-501	IVT Dilution Buffer	N/A	1.05	1.05
C-201	Affinity Chromatography	1.03	1.33	2.37
T-502	Affinity Binding Buffer	N/A	1.94	1.94
T-503	Affinity Washing Buffer	N/A	1.24	1.24
T-504	Affinity Elution Buffer	N/A	1.44	1.44
T-201	Chromatography Holding Tank	N/A	1.05	1.05
C-202	AEX Chromatography Column	5.58	1.12	6.70
T-505	Buffer A1 Holding Tank	N/A	1.48	1.48
T-506	Buffer A2 Holding Tank	N/A	1.04	1.04
T-507	Buffer B1 Holding Tank	N/A	1.18	1.18
T-508	0.5M NaOH Holding Tank	N/A	1.04	1.04
T-202	mRNA TFF Holding Tank	3.48	1.02	4.50
T-509	Sodium Acetate (50mM)	N/A	1.31	1.31
T-510	Ethanol Holding Tank	N/A	1.06	1.06
T-301	mRNA Holding Tank	N/A	1.01	1.01
T-302	Lipid Holding Tank	N/A	1.01	1.01
R-301	Impinging Jet Mixer	0.74	0.50	1.24
T-401	LNP TFF Holding Tank	5.03	1.10	6.13
T-511	Sodium Acetate (35mM)	N/A	1.94	1.94
T-512	Final Formulation	N/A	1.94	1.94
	Total (hr)	21.86	27.44	49.30

From in-vitro transcription to the final LNP-mRNA sterile filtration, the process requires a minimum of 21.86 hours to complete. One hour is allocated to transfer process fluid between each unit operation, resulting in a total processing time of slightly over one day per batch. Because the plant operates with a single CIP skid, cleaning cycles are staggered to ensure only one tank is scheduled to undergo a CIP at a time.

Production follows a 2-week cycle, with four batches completed per week. At the beginning of week one, each buffer tank undergoes a CIP and SIP cycle. Following cleaning, eight batches worth of each buffer are prepared and stored in their respective holding tank. In-vitro transcription for batch one begins in parallel with the CIP of IVT dilution buffer tank (T-501). Upon IVT completion, the IVT reactor (R-101) immediately begins a CIP and SIP cycle. R-101 sits in a sterile state for approximately 3 hours before beginning IVT for batch two. A three-hour gap between batches is necessary to prevent overlapping CIP cycles between tanks. By staggering batches in this manner, it takes roughly 66 hours to complete four batches. As a result, this plant only operates Monday through Friday, with no production taking place during the weekends. Figure 3.8.-1 illustrates the schedule for a single week. The second week of the production cycle mirrors the first, except buffer preparation at the beginning of the week is not required.

Given the completion of four batches per week, the facility achieves its annual production goal of 24 batches in six weeks. This schedule allows the plant to pivot to manufacturing mRNA vaccines targeting other diseases for the remainder of the year. However, for the scope of this project, it is assumed that the facility only produces the LNP-mRNA vaccine for tuberculosis, as the process modifications required for other mRNA products are beyond the scope of this project.

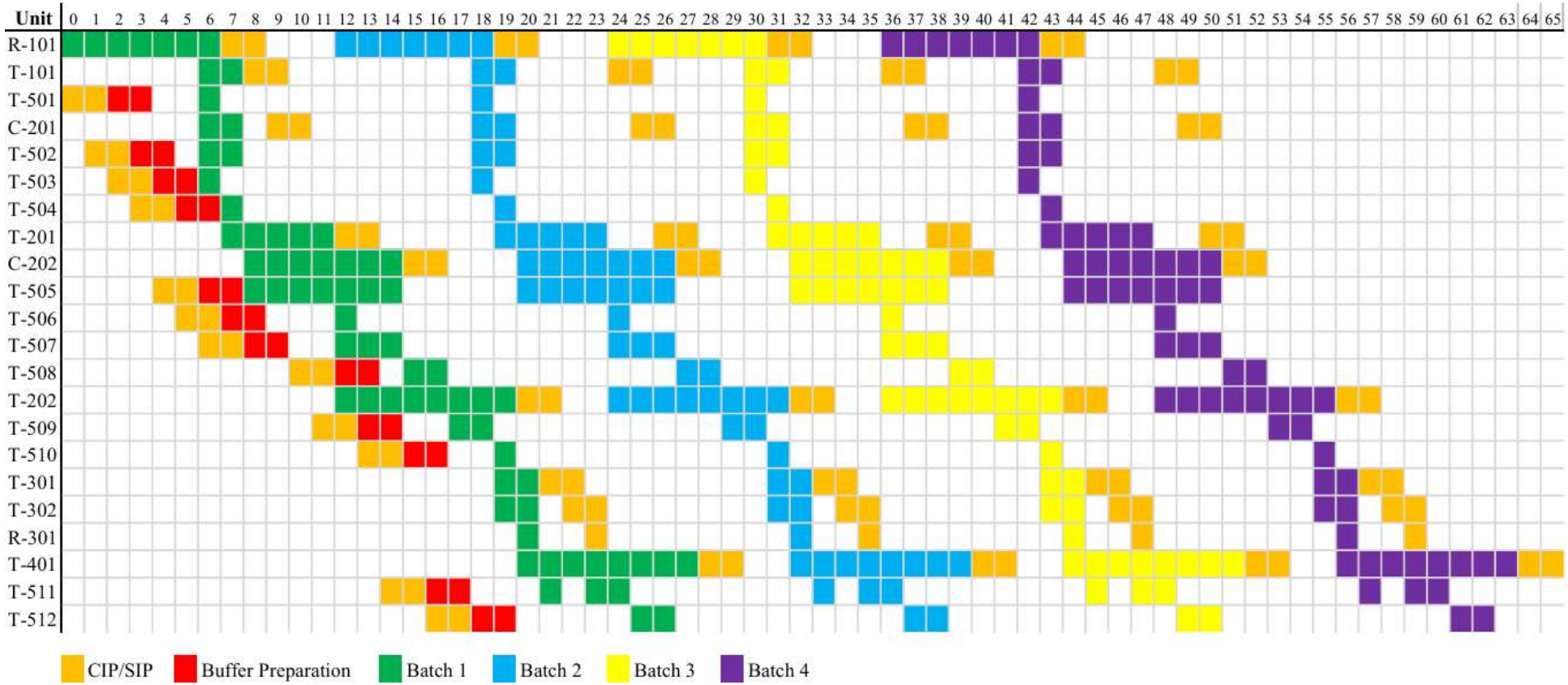

Figure 3.8-1. Batch schedule for LNP-mRNA production process

3.9 Waste Treatment and Disposal

Proper waste treatment and disposal are critical for ensuring environmental safety and regulatory compliance in vaccine manufacturing. Waste management practices are governed by the EPA's Resource Conservation and Recovery Act (RCRA) as well as by local/state government agencies, which outline how hazardous and non-hazardous waste must be handled to minimize risks to public health and ecosystems.

Hazardous waste generated during mRNA vaccine production includes materials contaminated with enzymes, nucleic acid fragments, nucleotides and coolant mixtures. This category encompasses streams from mRNA purification, diafiltration and concentration steps which may contain chemicals (DTT, spermidine), enzymes and other biologically derived materials. Additionally, waste from the pre-rinse phase of CIP processes—excluding that of the confined impinging jet mixer (CIJM)—are classified as hazardous due to potential contamination.

Flammable waste, ethanol containing waste streams, is another category of waste generated during LNP purification. These streams include the concentration step following the dilution of the CIJM outlet stream as well as the diafiltration step replacing remaining ethanol with acetate buffer (as described in section 3.5.2). Additionally, the pre-rinse from the ethanol storage tank and CIJM during its CIP cycle contributes to this waste stream, requiring controlled disposal.

Both hazardous and flammable waste streams, totaling 2757 L/batch, will be disposed of through licensed waste management companies that specialize in handling biopharmaceutical waste.[94,95] On the other hand, non-hazardous waste−including condensed steam from SIP processes and caustic detergent diluted with waste water from CIP rinse phases−can be safely discharged to

standard wastewater treatment facilities. However, the pH of the diluted caustic detergent must be confirmed to be between 6-9 to meet EPA standards for disposal to wastewater treatment facilities.

4 Final Design

4.1 Unit Operations

The manufacturing process for the formulated, high-purity mRNA-LNP solution requires eight key unit operations: in vitro transcription, affinity chromatography, anion exchange chromatography, two tangential flow filtrations, confined impinging jet mixing, and two sterile filtrations. The specifications and process for each unit operation are detailed in the following sections.

4.1.1 *in vitro* Transcription (R-101)

The *in vitro* transcription (IVT) process is a critical step in mRNA manufacturing, taking place within the 5L bioreactor (R-101), equipped with a silicone heating jacket for temperature control (Figure 4.1.1-1). To achieve the target annual production, each batch must yield 24 g of mRNA, requiring an IVT output of approximately 50.6 g per batch to account for downstream losses. This production target can be met using a 3.21 L working volume within the reactor.

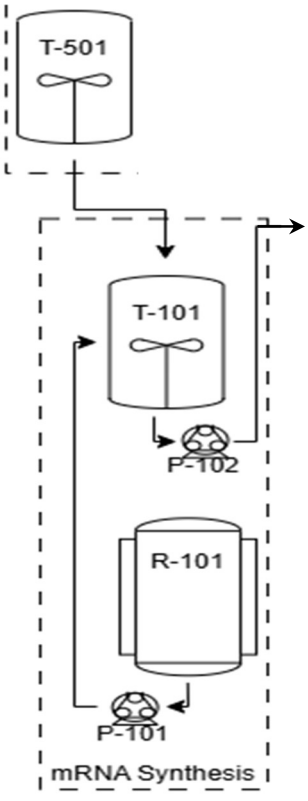

Figure 4.1.1-1. PFD of *in vitro* transcription

The process begins with the addition of Tris-HCl buffer to R-101, from buffer preparation tank T-501; the buffer is then heated to 37ºC, creating optimal conditions for enzymatic activity. Once heated essential reagents—including nucleotides (ATP, ΨTP, CTP, and GTP at 10 mM final concentration), capping reagents, dithiothreitol (DTT), and spermidine—are introduced to the reactor. The enzyme mixture, comprising RNA polymerase, pyrophosphatase, and capping RNA polymerase transcribes mRNA

from a linearized DNA template, while co-transcriptional capping ensures the proper 5' end modification ensuring mRNA stability. The poly-A tail, necessary for both stability and purification steps, is encoded into the DNA template to ensure correct 3' end processing.

Once transcription is complete, DNase is introduced to degrade remaining DNA template, while EDTA is added as a chelating agent to halt further transcription reactions. The resultant mRNA and excess reagents are then pumped through P-101 to holding tank, T-101, prior to processing in the mRNA purification block, as seen in Figure 4.1.1-1, where impurities are removed to ensure product quality before downstream processing.

4.1.2 Affinity Chromatography (C-201)

Following *in vitro* transcription, the reaction mixture, held in T-101, is passed through affinity chromatography unit C-201 to remove contaminants from the IVT reaction, like reaction enzymes, oligonucleotides, and uncapped or incomplete mRNA strands. C-201 consists of four CIMmultus Oligo dT18 8 L monolithic columns operated in parallel, corresponding to a total resin volume of 32 L. The AC process is performed in five steps: equilibration, sample loading, binding, washing, and elution. The exact buffer compositions and chromatographic procedure for the AC process are available in Table 3.3.1.1-1 and Table 3.3.1.1-2, respectively. As to not require a high volumetric throughput peristaltic pump, the chromatographic procedures for each column in C-201 will be staggered by two minutes so only a single column is being loaded with sample at a time; therefore, the fourth column will be done processing six minutes after the first column. The column being loaded in C-201 will be decided by the selective opening and closing of diaphragm valves in the tubing after P-102 (Figure 4.1.2-1). All process steps are performed using an

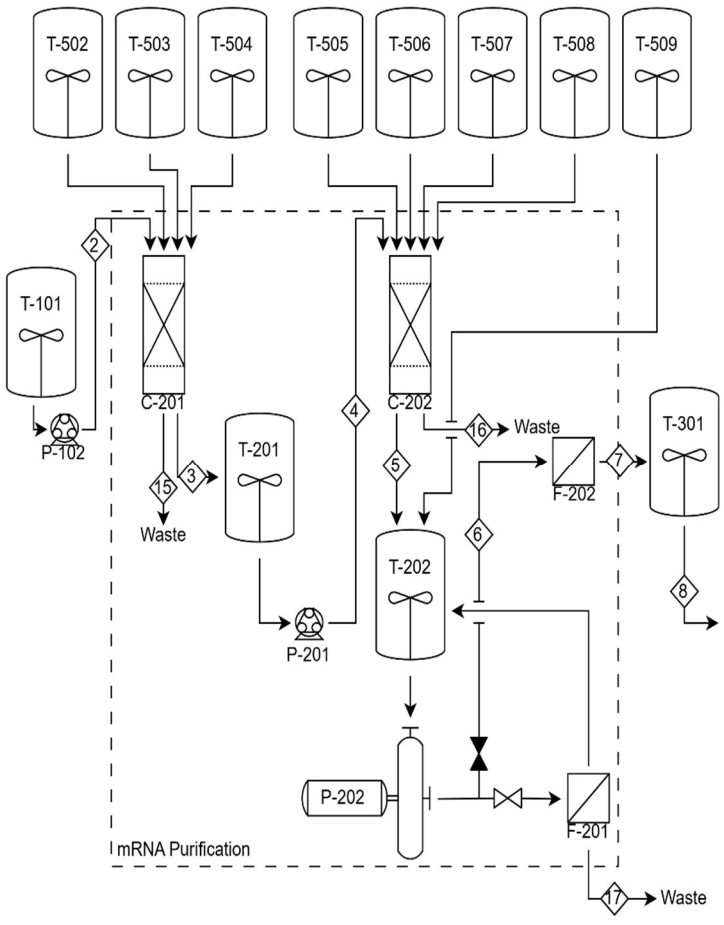

Figure 4.1.2-1 PFD of mRNA purification process

operating flow rate of 0.5 CV/min, which leads to a complete processing time for AC of 68 minutes, including the staggered operation.

All buffers supplied to C-201 are held in tanks T-502, T-503, and T-504, which are in the second-floor buffer preparation area. Flow from these tanks to C-201 is driven by gravity, with a flow controller guaranteeing the correct flow rate is provided. During the sample loading step, the IVT mix is pumped from T-101 using P-102 to top of the monolithic columns. During the first four steps of the AC chromatographic procedure, all buffers that flow through C-201 are sent directly to a waste stream, including any contaminants that don't bind to the columns. Once the elution step begins, flow from C-201, which contains the product mRNA and any mRNA-associated contaminants that bind and elute alongside the product mRNA, is directed into tank T-201 for storage. The estimated yield for this process is 80.0%, so the 48.03 grams of target mRNA per batch entering C-201 is reduced to 38.43 grams of target mRNA per batch, which is stored in T-201 before use in the next chromatography step.

The monolithic columns used in the process are stable for 10 cycles before a drop in yield is observed; therefore, each column will be replaced after 10 batches of operation.[79] Rather than replace all columns at once, one column will be replaced every 2-3 batches to maintain that at least 3 columns are always operational.

4.1.3 Anion Exchange Chromatography (C-102)

To remove any mRNA-associated contaminants that may have eluted alongside the product mRNA during the AC process, anion exchange column C-202 is used. C-202 consists of a single Cytiva Axichrom column with a 140 mm inner diameter and 300 mm bed height, manually packed with 4.62 L of Eshmuno Q resin. The AEX process is performed in eight steps: equilibration, sample loading, two washes, and four step-elutions. The exact buffer compositions and chromatographic procedure for the AEX process are available in Table 3.3.1.2-1 and Table 3.3.1.2-3, respectively. All process steps are performed using an operating flow rate of 0.3 CV/min, which leads to a complete processing time for AEX of 335 minutes.

The mRNA solution held in T-201 is pumped to the top of C-202 by pump P-201 for the sample loading step, while all other buffers flow into the column from second-floor tanks T-505, T-506, T-507, and T-508 using gravity with an automated flow controller to maintain the operating flow rate (Figure 4.1.2-1). During equilibration, loading, and wash steps, all flow through C-202 is sent directly to waste. During all elution steps, flow from C-201, which contains the product mRNA, is directed into tank T-202 for storage. The collection range for this process will need to be reduced once the precise product mRNA residence time is found through facility testing. The estimated yield for this process is 75.3%, so the 38.43 grams of target mRNA per batch entering C-202 is reduced to 28.94 grams of target mRNA per batch, which is stored in T-202 before tangential flow filtration.

The Eshmuno Q resin has proven stability for over 100 cycles; therefore, as a conservative measure, the resin in C-202 will be replaced every 100 batches.[96]

4.1.4 mRNA Tangential Flow Filtration (F-201)

Prior to the target mRNA solution from AEX being used for LNP encapsulation, the buffer solution must be exchanged with sodium acetate and concentrated to achieve the design specifications for the CIJM process. This buffer exchange and concentration is accomplished through a two-step process: concentration and diafiltration. This tangential flow unit, pictured in Figure 4.1.2-1, is connected directly to T-202, where the mRNA solution is held. P-202 pumps the mRNA solution from T-202 through either F-202, the sterile filter, or F-201, the tangential flow filter; the direction of flow is decided by two diaphragm valves. For TFF, the diaphragm valves are open and closed such that the mRNA solution is passed through F-201 and returned to T-202 in a closed loop.

F-201 consists of a single, delta regenerated cellulose membrane with a filtration area of 0.5 m^2, and MWCO of 100. Therefore, in both the concentration and diafiltration, the target mRNA is maintained in the retentate and constantly passed through the closed loop, while any buffer components exit the system in the permeate stream and are sent to waste.

In the concentration step of mRNA TFF, the 138.54 L of mRNA solution held in T-202 after AEX is concentrated to 39.69 L. This process operates at a constant feed flow rate of 225 L/h and trans-membrane pressure drop of 1.38 bar. These operating conditions correspond to a time-average permeate flow rate of 60 L/h; therefore, the time required to remove the necessary 98.86 L is 99 minutes.

In the diafiltration step of mRNA TFF, the 39.69 L of buffer in T-202 is exchanged with sodium acetate buffer through the addition of sodium acetate buffer to T-202 from T-509, driven by gravity. This process operates at constant feed flow rate of 225 L/h and trans-membrane pressure drop of 0.69 bar. These operating conditions correspond to a permeate flow rate of 100 L/h, therefore, to

maintain a constant volume, sodium acetate buffer is added to T-202 at a flow rate of 100 L/h. 4.61 diavolumes of sodium acetate buffer are necessary to achieve a 99% exchange of the buffer in T-202, requiring 182.76 L of sodium acetate buffer from T-509 and takes 110 minutes to complete.

The time required for both the concentration and diafiltration steps is 209 minutes. As the MWCO for F-201 is significantly smaller than the size of the target mRNA, the expected yield of mRNA for both processes is 100.0%, so the 28.94 g mRNA per batch is maintained. Once the TFF process is completed, the mRNA in sodium acetate buffer is held in T-202 before sterile filtration.

4.1.5 mRNA Sterile Filtration (F-202)

Prior to LNP encapsulation, the product mRNA in sodium acetate buffer is passed through sterile filtration unit F-202 to guarantee the solution being encapsulated is free from any non-sterile contaminants, as well as to maintain regulatory compliance. F-202 consists of a single Sartopore 2 XLG cartridge with a filtration area of 1.6 m^2, consisting of a 0.8-micron prefilter and a 0.2-micron final filter, contained in its designed housing. In this process, P-202 pumps the solution in T-202 directly through F-202 to T-301, with any contaminants or trapped mRNA remaining in the filter cartridge. Prior to beginning sterile filtration, the diaphragm valve directing the flow to F-201 is closed and the diaphragm valve directing the flow to F-202 is opened. F-202 is operated at a constant trans-membrane pressure drop of 1.4 bar, which is maintained by a pressure indicator controller system around F-202 that increases or decreases the output of P-202. For the selected operating conditions, the average filtrate flow rate for this process is 3.33 L/s, therefore, the 39.69 L of solution in T-202 requires 12 seconds to filter. The expected yield for this process is 96.0%; the 28.94 g of mRNA per batch in T-202 is reduced to 27.78 g after sterile filtration, with 1.16 g of mRNA remaining in F-202 per batch. The filter cartridge in F-202 will be replaced following every batch.

4.1.6 Confined Impinging Jet Mixing (R-301)

From the mRNA purification block, following sterile filtration, the mRNA solution (0.7 mg/mL in acetate buffer) is cooled to 4ºC in holding tank T-301. It is then pumped by rotary piston pump P-301 into R-301, a confined impinging jet mixer (CIJM), where it will be combined with the lipid phase.

The lipids for the process are suspended in ethanol and stored in T-302. They are then pumped by rotary piston pump P-302 through a heat exchanger, where they are heated to 60ºC before entering R-301. Within the CIJM, the mRNA stream (0.9 L/min) and lipid stream (1.0 L/min) collide at high velocity, ensuring rapid and efficient mixing. This process facilitates self-assembly between the lipids and mRNA, resulting in the formation of lipid nanoparticles (LNPs) with a high encapsulation efficiency (~90%).

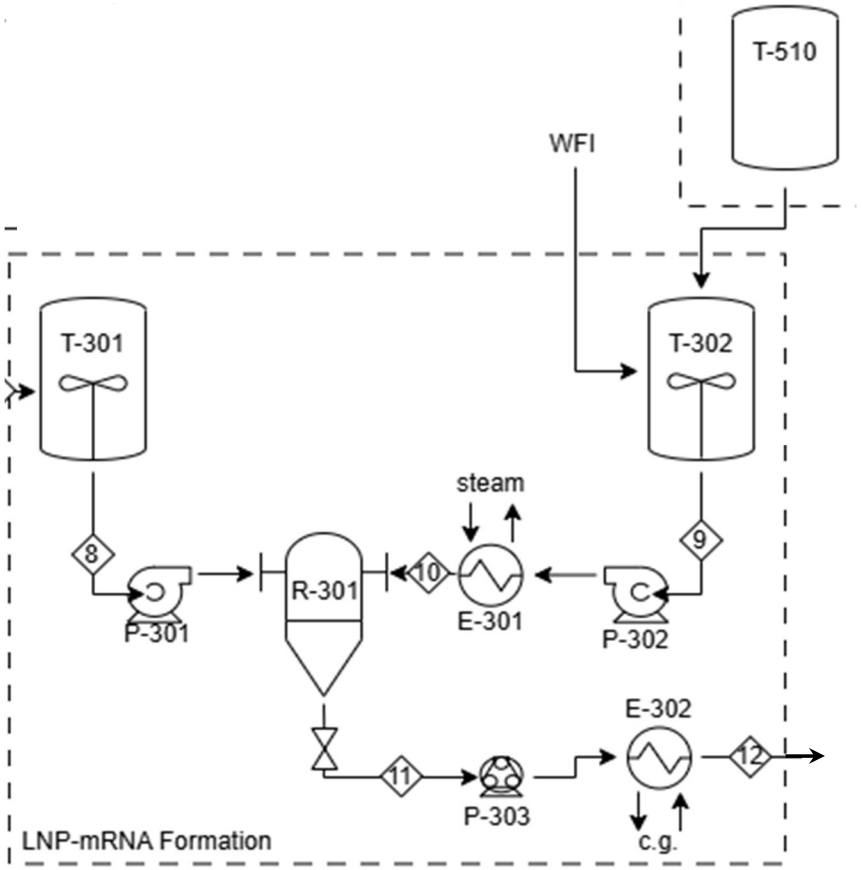

Figure 4.1.6-1 PFD of LNP-mRNA formation process

Following encapsulation, the LNP-mRNA suspension exits the mixer and is cooled to 25ºC in heat exchanger E-302 before being pumped, using peristaltic micropump P-303, to the LNP-mRNA purification block for filtration and formulation.

4.1.7 LNP Tangential Flow Filtration (F-401)

Immediately following CIJM, the 83.78 L of LNP-mRNA solution held in T-401 is diluted with 542.46 L of 35 mM sodium acetate from T-511 to achieve 5 %w/v ethanol. T-511 is in the second-floor buffer preparation area, thus the flow to T-401 is gravity driven and controlled by an automated flow controller. This rapid dilution increases the stability of the LNPs and increases encapsulation efficiency.

Following dilution, the LNP-mRNA solution undergoes three sequential TFF steps using F-401 as the filter: concentration, diafiltration with sodium acetate buffer, and diafiltration with cryoprotectant. In all steps, solution from T-401 is pumped in a closed loop through F-401 by P-401 and returned to T-401 (Figure 4.7-1). In this unit, flow to F-401 or sterile filter F-402, which is also attached to the stream after P-401, is controlled by opening or closing two diaphragm valves that are placed before the filters. In diafiltration steps, buffers held in T-511 and T-512, which are in the second-floor buffer preparation area, are added to T-401 using gravity.

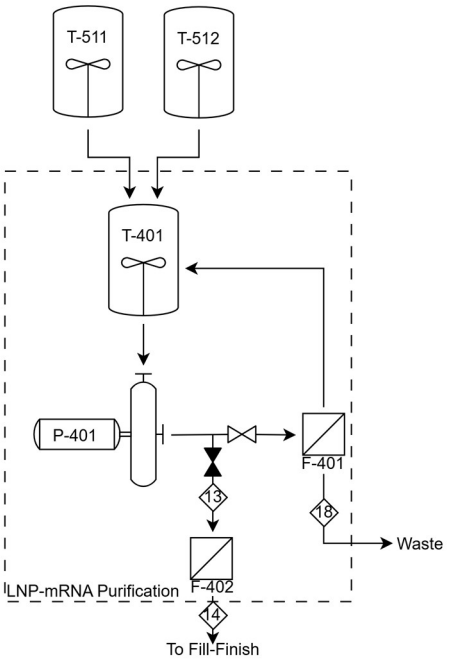

Figure 4.1.7-1 PFD of LNP purification process

F-401 consists of a single, delta regenerated cellulose membrane with a filtration area of 2.5 m^2, and MWCO of 100. Therefore, in both the concentration and diafiltration, the mRNA-LNPs are maintained in the retentate and constantly passed through the closed loop, while any buffer components exit the system in the permeate stream and are sent to waste.

In the concentration step, the 626.24 L of mRNA-LNP solution held in T-401 is concentrated to 240.00 L. This process operates at a constant feed flow rate of 1125 L/h and trans-membrane pressure drop of 1.38 bar. These operating conditions correspond to a time-average permeate flow rate of 300 L/h; therefore, the time required to remove the necessary 386.24 L is 77.3 minutes.

In the first diafiltration step, the 240.00 L of buffer in T-401 is exchanged with 35mM sodium acetate buffer through the addition of buffer from T-511.This process operates at constant feed flow rate of 1050 L/h and trans-membrane pressure drop of 1.38 bar. These operating conditions correspond to a permeate flow rate of 375 L/h, therefore, to maintain a constant volume, sodium acetate buffer is added to T-401 at a flow rate of 375 L/h. 2.30 diavolumes of sodium acetate buffer are used in this process (552.62 L), taking a total time of 88.4 minutes.

In the second diafiltration step, the 240.00 L of buffer in T-401 is exchanged with cryoprotectant buffer (0.15 w/v% Tris-HCl, 5 w/v% sucrose) through the addition of buffer from T-512. This process operates at constant feed flow rate of 1050 L/h and trans-membrane pressure drop of 1.38 bar. These operating conditions correspond to a permeate flow rate of 375 L/h, therefore, to maintain a constant volume, cryoprotectant buffer is added to T-401 at a flow rate of 375 L/h. 1.98 diavolumes of cryoprotectant buffer are used in this process (475.42 L), taking a total time of 76.1 minutes.

The time required for all TFF steps is 241.8 minutes. As the MWCO for F-401 is significantly smaller than the size of the mRNA-LNPs, the expected yield of mRNA for all processes is 100.0%, so the 25.00 g mRNA per batch is maintained. Once the TFF process is completed, the mRNA-LNP solution is held in T-401 before sterile filtration.

4.1.8 LNP Sterile Filtration (F-402)

Prior to being sent out of the facility for final filling and formulation processes, the LNP-mRNA solution is passed through sterile filtration unit F-402 to guarantee the absence of any non-sterile contaminants, as well as to maintain regulatory compliance. F-402 consists of three Sartopore 2 XLG cartridges with filtration areas of 1.6 m^2, consisting of a 0.8-micron prefilters and a 0.2-micron final filters, in parallel with each contained in its designed housing. In this process, P-401 pumps the solution in T-401 directly through F-402 (Figure 4.1.7-1). The mRNA-LNP that passes through F-402 is filled into three 100L single-use sterile bags where it will await fill-to-finish operations.[97] Each bag will contain 80L of the final LNP-mRNA formulation. Prior to beginning sterile filtration, the diaphragm valve directing the flow to F-401 is closed and the diaphragm valve directing the flow to F-402 is opened. F-402 is operated at a constant trans-membrane pressure drop of 1.38 bar, which is maintained by a pressure indicator controller system around F-402 that increases or decreases the output of P-401. For the selected operating conditions, the average filtrate flow rate for this process is 2.78 L/s, therefore, the 80.00 L of solution in T-401 requires 28.8 seconds to filter. The expected yield for this process is 96.0%; the 25.00 g of mRNA per batch in T-401 is reduced to 24.00 g after sterile filtration, with 1.00 g of mRNA remaining in F-402 per batch. The filter cartridges in F-402 will be replaced following every batch.

5 Process Economics

The following sections outline the projected capital and operating expenses associated with the facility and present a cash flow analysis over its operational lifespan.

5.1 Purchased Equipment

Costs associated with all purchased equipment are based on vendor quotes, if available, or through linear interpolation/extrapolation using similar equipment to best match the equipment necessary for the plant. All equipment costs were adjusted to the current economic conditions using the CEPCI from January 2025 of 800. A breakdown of all purchased equipment, leading to a total purchased equipment cost of $643,985, in Table 5.1-1.

Table 5.1-1: Purchased equipment

Equipment	Cost/Unit	Units	Total
CIJM (including pumps)	$ 6,500	2	$ 13,000
68L Stainless Steel Tank	$ 2,670	3	$ 8,009
144L Stainless Steel Tank	$ 3,553	1	$ 3,553
227L Stainless Steel Tank	$ 3,826	2	$ 7,651
322L Stainless Steel Tank	$ 4,223	2	$ 8,446
397L Stainless Steel Tank	$ 4,519	1	$ 4,519
852L Stainless Steel Tank	$ 5,469	3	$ 16,407
1173L Stainless Steel Tank	$ 7,144	1	$ 7,144
1552L Stainless Steel Tank	$ 11,342	1	$ 11,342
1987L Stainless Steel Tank	$ 12,647	1	$ 12,647
2801L Stainless Steel Tank	$ 16,769	1	$ 16,769
3066L Stainless Steel Tank	$ 18,744	1	$ 18,744
6056L Stainless Steel Tank	$ 23,985	3	$ 71,955
6" Diameter Hydrofoil Impeller	$ 581	3	$ 1,743
7" Diameter Hydrofoil Impeller	$ 583	3	$ 1,749
10" Diameter Hydrofoil Impeller	$ 661	2	$ 1,322
13" Diameter Hydrofoil Impeller	$ 773	1	$ 773
15" Diameter Hydrofoil Impeller	$ 849	1	$ 849
17" Diameter Hydrofoil Impeller	$ 936	2	$ 1,872
19" Diameter Hydrofoil Impeller	$ 1,092	1	$ 1,092
20" Diameter Hydrofoil Impeller	$ 1,138	1	$ 1,138
28" Diameter Hydrofoil Impeller	$ 1,634	3	$ 4,902
TFF Membrane Cassette Holder	$ 5,843	2	$ 11,686
API-610 Horizontal Centrigufal Pump	$ 18,200	8	$ 145,602
Fixed CIP Sprayball	$ 47	21	$ 986
316 Steel Heat Exchangers (<1 m2)	$ 7,078	3	$ 21,234
VSH A600R Peristaltic Pump (300 rpm)	$ 1,024	6	$ 6,144
VSH A600R Peristaltic Pump (150 rpm)	$ 899	1	$ 899
Freezer (-80C)	$ 18,269	9	$ 164,421

Equipment	Cost/Unit	Units	Total
Cytiva Axichrom Columns	$ 2,250	2	$ 4,500
VSH A600 Pumps (P-101, P-102, P-103)	$ 1,124	4	$ 4,496
Eshumuno Q AEX Resin	$ 34,775	1	$ 34,775
In Vitro Transcription Reactor	$ 13,190	1	$ 13,190
Sterile Filter Housing	$ 1,620	4	$ 6,480
Electric Steam Generator	$ 6,975	2	$ 13,950
Total Equipment Cost	-	-	**$ 643,985**

5.2 Capital Investment

Fixed capital investment (FCI) represents the amount of money that has been invested in long-term assets necessary to begin production, including expenses like equipment delivery, piping installation, and process instrumentation, and is the sum of direct and indirect plant costs. To effectively estimate all direct and indirect costs that compose FCI, estimation rules from Plant Design and Economics for Chemical Engineers[98], were used. These rules estimate standard components of FCI as a percentage of purchased equipment cost, however these percentages may have errors of ± 20% or higher depending on various factors. The final estimation of FCI is $3,245,687, a breakdown for which is available in Table 4.5.2-1.

Working capital refers to the amount of money necessary to fund the plant's day-to-day operations and is estimated as 15% of total capital investment (TCI), which is the sum of FCI and working capital.[99] Working capital is estimated to be $573,147. Combining FCI and working capital, the TCI for the plant is estimated to be $3,818,834 (Table 4.5.2-1).

Table 5.2-1: Total capital investment breakdown

Cost	Percent of Delivered Equipment Cost (%)	Actual Cost ($)
Direct Costs		
Purchased equipment delivered	100	643,985
Purchased equipment installation	47	302,673
Instrumentation and controls	36	231,835
Piping (installed)	68	437,910
Electrical systems (installed)	11	70,838
Buildings (including services)	18	115,917
Yard improvements	10	64,399
Service facilities	70	450,790
Total direct plant cost	360	2,318,348
Indirect Costs		
Engineering and supervision	33	212,515
Construction Expenses	41	264,034
Legal Expenses	4	25,759
Contractor's fee	22	141,677
Contingency	44	283,354
Total indirect plant cost	144	927,339
Fixed Capital Investment (FCI)	504	3,245,687
Working capital (15% of TCI)	89	573,147
Total capital investment (TCI)	593	3,818,834

5.3 Operating Costs

The cost of manufacture (COM) for the plant was estimated using Equation 4.5.3.[100]

$$COM = 0.280FCI + 2.73\ C_{OL} + 1.23(C_{UT} + C_{WT} + C_{RM}) \quad (4.5.3)$$

where

$C_{OL} =$ Labor cost

$C_{UT} =$ Utilities cost

$C_{WT} =$ Waste treatment cost

$C_{RM} =$ Raw material cost

The COM for the first year of production is $43,789,964; however, the plant is estimated to increase its production from the first to the second year by 20% to achieve the production goal of 10 million doses annually, so 8.33 million doses are estimated to be produced in the first year of production. In subsequent years, the COM increases by 20% to account for the 20% increase in production necessary to achieve the production goal, leading to a COM of $52,547,957. Breakdowns for how raw material, utilities, labor, and waste treatment costs were estimated are detailed in sections 4.5.3.(1-4).

5.3.1 Raw Material Costs

The yearly cost of raw materials was calculated using the grams per batch, cost per gram, and number of batches per year (24). The cost breakdown was mostly found using past cost modeling done for the COVID-19 mRNA-1273 vaccine production, with the numbers being scaled to represent a bulk price per gram of reagent.[101] Other costs were found through supplier websites and were scaled to model a bulk price. The cost of buffers was accounted for by considering the dry buffer salts as a raw material cost while the WFI added to prepare each buffer was a utility cost. The total cost of raw materials was found to be $ 24,341,355, with a breakdown of each

reagent used shown in Table 5.3.1-1, other single-use materials are incorporated into the yearly cost of manufacturing.

Table 5.3.1-1: Cost of raw materials

Raw Material	g/batch or U/batch	$/g or $/U	Annual Cost $/(24 batches)
Block 1: mRNA synthesis			
Tris-HCl	20.8	0.65	326.28
$MgCl_2$	15.7	0.01	2.47
DTT	5.1	5.93	726.14
ATP	16.28	243.61	95182.93
ψTP	15.54	4668.74	1741253.38
CTP	15.51	255.22	95001.31
GTP	16.79	236.17	95166.60
Spermidine	0.96	8.31	191.43
Pyrophosphatase[102] (U)	3300	5.90	467280.00
DNA template	0.165	108706.59	430478.08
RNase inhibitor[103] (U)	3300000	0.06	4498560.00
RNA polymerase[104] (U)	41250000	0.01	11959200.00
Clean Cap	15.1	3953.95	1432912.12
DNase[105] (U)	165	0.33	1288.29
EDTA[106]	4.8	0.11	12.70
Block 2: mRNA purification			
Tris-HCl	4058.4	0.65	63662.45
EDTA	411.5	0.11	1088.83
Na_3PO_4[107]	5817.9	0.15	21586.74
NaCl[108]	23882.8	0.02	13756.49
Arginine[109]	11061.6	0.67	176847.37
Sodium Acetate	741.8	0.02	291.19
Block 3: mRNA-LNP formulation			
Cholesterol	855.54	27.00	554394.64
Ionizable lipid	1838.97	54.00	2383359.44
PEG lipid	216.09	21.54	111710.64
Phospholipid	454.23	16.19	176459.73
Ethanol	31560	0.01	5989.56

Raw Material	g/batch or U/batch	$/g or $/U	Annual Cost $/(24 batches)
Block 4: mRNA-LNP purification			
Sodium Acetate	1586	0.02	622.58
Tris-HCl	713	0.65	11184.54
Sucrose	23771	0.005	2819.79

A breakdown of cost per production block is shown in Figure 5.3.1-1. The predominant cost of raw materials comes from the mRNA synthesis step of the process, taking up 86% of raw material costs. Compared to IVT, the purification steps end up being a negligible cost, consisting of 1% and 0% of total cost for mRNA and mRNA-LNP purification respectively.

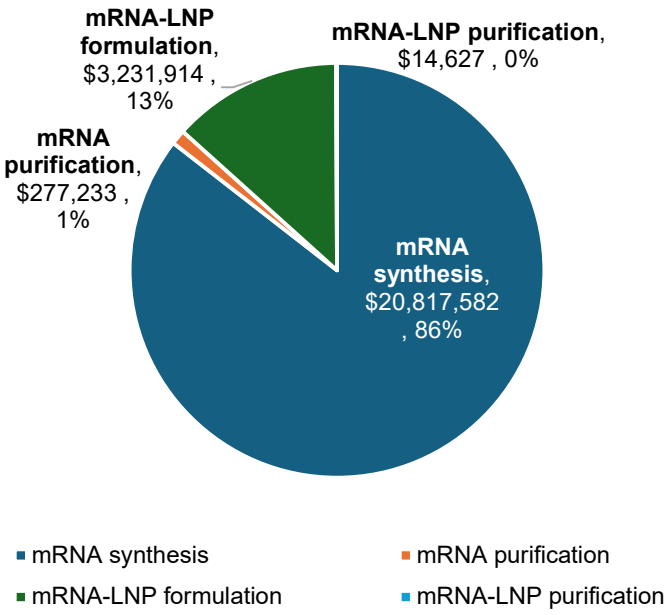

Figure 5.3.1-1: Total cost breakdown of raw materials per production block

5.3.2 Utilities Cost

Plant utilities include WFI, clean steam, ethylene glycol, and waste disposal. Apart from clean steam, all utilities are sourced from external vendors. Clean steam is generated on-site by vaporizing WFI using a steam generator, as detailed in Section 3.7.4. As a result, the cost of

clean steam is incorporated into the utility expenses for both WFI and the electricity required to operate the steam generator.

WFI is procured from a vendor in 200L bags at a unit price of $7.14 per liter.[110] The largest consumer of WFI in the facility is the CIP process, followed by processing operations. WFI is primarily used in the mRNA-LNP manufacturing process to prepare buffers. Table 5.3.2-1 provides a summary of WFI consumption across the plant.

Table 5.3.2-1: Breakdown of WFI consumption

Purpose	Per Batch (L)	Per Year (L)
CIP	9354	224498
Process	2957	70963
Clean Steam	28	664
Total	12339	296126

The price of electricity was estimated using the average electricity cost for the industrial sector in North Carolina.[111] The primary electricity consumers in the plant consist of pumps, agitators, the steam generator, and -80ºC freezers (Table 5.3.2-2). Energy consumption of pumps, agitators, and -80ºC freezers was estimated by multiplying their power consumption by their time in operation. It is conservatively assumed that the freezers will be running for the entire year. For the steam generator, electricity consumption is estimated based on the energy required to vaporize room temperature water as outlined in Section 3.7.4.

Table 5.3.2-2: Breakdown of electricity usage

Purpose	Per Batch (kWh)	Per Year (kWh)
Pumps	11.16	267.78
Agitators	2.90	69.55
Steam Generator	20.53	492.62
Freezers	-	181332.00
Total	34.58	182161.95

A 30% (v/v) mixture of ethylene glycol and water is used to cool fluids in heat exchangers E-302 and E-303 at 10 and -5℃ respectively. The cost of refrigerant is based on temperature and approximated using an exponential regression from 2003 estimated costs, Figure 5.3.2-1, and updated using a dated CECPI (325) and current CECPI (800) to estimate changes in costs over time. The final cost estimates of EG mixture per GJ of energy removed is $17.91 and $26.71 for the refrigerants at 10 and -5℃ respectively.

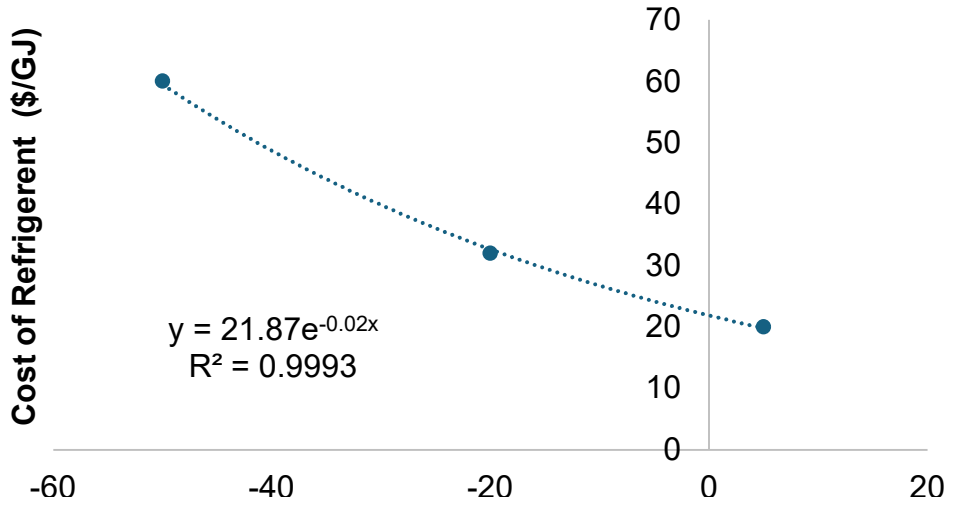

Figure 5.3.2-1: Exponential regression of the cost of refrigerant in 2003.[76]

In total, utility costs for the plant sum to $2,150,883 with the vast majority being attributed to WFI expenses (Table 5.3.2-3).

Total waste treatment costs are estimated, assuming on site treatment, on an annual basis with the additional hazardous waste fees imposed by the state of North Carolina. These fees include an annual Large Quantity Generator fee of $1400 and a Treater fee of $1680.[112] Hazardous waste treatment was estimated to cost $145.00/1000 kg of waste generated in 2003, using a CECPI of 325 from 2003 and current CECPI of 800, the new estimated cost of hazardous waste treatment is expected to be $293.22/1000 kg.[99] The amount of hazardous waste per batch is 2756.52 L/batch

or 2756.52 kg/batch, using a conservative assumption that all waste has a similar density to water, resulting in an annual cost of $22,479, as detailed in table 5.3.2-3.

Table 5.3.2-3: Summary of annual utility expenses

Utility	Amount Per Batch	Amount Per Year	Unit Price	Total Price
WFI	12339 L	296126 L	$7.14 / L	$2,114,336.28
Electricity	-	182162 kWh	$0.0772 / kWh	$14,063
EG (10C)	155320 J	3727685 J	$3.6E-08 / J	$0.14
EG (-5C)	3458322 J	82999728 J	$5.4E-08 / J	$4.48
Waste Treatment	2756.52 kg	66156.48 kg	$0.2932 / kg	$22,478.77
			Total	**$2,150,883**

5.3.3 Labor Cost

The labor cost for the manufacturing facility designed in this report was calculated by first determining the number of operators necessary per shift to operate the processes in the facility, using Equation 4.5.3.3.

$$N_{OL} = (6.29 + 31.7{N_P}^2 + 0.23N_{NP})^{0.5} \quad (4.5.3.3)$$

where

$N_{OL} =$ Number of operators per shift

$N_P =$ Number of particulate-handling processes

$N_{NP} =$ Number of non-particulate processes

The manufacturing process designed in this report utilizes a single particulate handling process, buffer preparation, and six non-particulate processes, mRNA transcription, AC, AEX, mRNA TFF/sterile filtration, CIJM, and LNP TFF/sterile filtration. Both TFF/sterile filtration processes are considered one non-particulate process each as both the TFF and sterile filters are present on a

single skid. Therefore, using Equation 4.5.3.3, 7 operators are necessary per shift (rounding up from 6.27). Assuming 4.5 shifts are necessary to achieve our production schedule, the facility requires the hiring of 32 operators.[100] Using the mean annual wage for pharmaceutical plant operators reported from the Bureau of Labor Statistics as of May 2023 of $54,490,[113] the total operator labor costs for the facility is $1,743,680. Direct supervisory and clerical costs are estimated to be 25% of the total operator labor costs, and direct salary overhead is estimated as 25% of the sum of both operator and supervisory costs. Additionally, laboratory costs are estimated to be an additional 15% of all of these costs combined, leading to a labor cost of $3,759,810.[114]

5.3.4 Miscellaneous Material Costs

Additional products contributing to the yearly cost of manufacturing include other items/equipment that must be replaced or purchased more than once per year. These costs primarily consist of filter membranes/cartridges, storage bags and tubing as outline in Table 5.3.4-1.

Table 5.3.4-1. Miscellaneous Material Costs

Material	**Amount/batch**	**Unit**	**Unit Price**	**Total Price**
CIP 100 Alkaline Process Cleaner	31.22	L	$ 40.00	$ 29,971.20
0.5m2 Delta RC Membrane	1		$ 2,210.00	$ 53,040.00
2.5m2 Delta RC Membrane	1		$ 4,420.00	$106,080.00
1.6m2 0.2 Micron Filter Cartridge	4		$ 1,440.00	$138,240.00
ReadyCircuit™ single-use 3-D bag assemblies	3		$ 750.00	$ 54,000.00
ANKO Ultra Class Tubing | PharMed	8	25 ft / roll	$ 205.00	$ 39,360.00
CIMmultus™ Oligo dT18 8000 mL Monolithic Columns	0.4	columns	$ 1,300.00	$ 12,480.00

5.4 Financial Analysis

To determine the profitability of the vaccine manufacturing plant designed in this report, an internal rate of return (IRR) is calculated using a discounted cash flow analysis. During this calculation, numerous assumptions were made:

1. Construction and validation take one year to complete, production begins at the beginning of year two.
2. Production of the vaccine is continued for 20 years at a constant production of 10 million doses annually, other than the first year, where 8.33 million doses are produced.
3. All components of FCI are depreciated linearly for 7 years once production begins
4. 74.5% of doses are sold to LMICs at a cost of $6.00 per dose. 25.5% of doses are sold on the domestic market for $15.00 per dose. Annual revenue is calculated by multiplying these prices by the number of doses sold domestically and internationally each year. These prices are less than comparable standards of care in their respective regions, thus only a single scenario is necessary for this analysis.
5. The combined state and federal corporate tax rate is 30%.

Table 5.4-1 summarizes the cash flow for the life of the plant. After 20 years of production, the cumulative cash flow (CCF) for the plant is $196,047,136. As explained in section 4.5.3, the COM increases by 20% after the first year of production, explaining the different COM for year 2 in Table 5.4-1. The other estimated expenses included in the cash flow analysis are:

1. Rent expense: 2% of FCI
2. Fill-to-Finish expense: $0.30 per dose
3. R&D expenses: 15% of gross revenue
4. Insurance expense: 1% of FCI

5. Maintenance expense: 7% of FCI

6. Laboratory expense: 15% of FCI

Table 5.4-1: Cash Flow Analysis

Year	Doses (millions)	Revenue	COM	Other Expenses	Cash Flow	CCF
1				$ (64,914)	$ (64,914)	$ (64,914)
2	8.33	$ 66,360,000	$ (43,789,964)	$(15,894,285)	$ 6,675,751	$ 6,610,837
3	10.00	$ 82,950,000	$ (52,547,957)	$(20,336,537)	$ 10,065,506	$ 16,676,343
4	10.00	$ 82,950,000	$ (52,547,957)	$(20,336,537)	$ 10,065,506	$ 26,741,849
5	10.00	$ 82,950,000	$ (52,547,957)	$(20,336,537)	$ 10,065,506	$ 36,807,354
6	10.00	$ 82,950,000	$ (52,547,957)	$(20,336,537)	$ 10,065,506	$ 46,872,860
7	10.00	$ 82,950,000	$ (52,547,957)	$(20,336,537)	$ 10,065,506	$ 56,938,366
8	10.00	$ 82,950,000	$ (52,547,957)	$(20,336,537)	$ 10,065,506	$ 67,003,872
9	10.00	$ 82,950,000	$ (52,547,957)	$(20,475,638)	$ 9,926,405	$ 76,930,277
10	10.00	$ 82,950,000	$ (52,547,957)	$(20,475,638)	$ 9,926,405	$ 86,856,682
11	10.00	$ 82,950,000	$ (52,547,957)	$(20,475,638)	$ 9,926,405	$ 96,783,087
12	10.00	$ 82,950,000	$ (52,547,957)	$(20,475,638)	$ 9,926,405	$ 106,709,492
13	10.00	$ 82,950,000	$ (52,547,957)	$(20,475,638)	$ 9,926,405	$ 116,635,897
14	10.00	$ 82,950,000	$ (52,547,957)	$(20,475,638)	$ 9,926,405	$ 126,562,302
15	10.00	$ 82,950,000	$ (52,547,957)	$(20,475,638)	$ 9,926,405	$ 136,488,707
16	10.00	$ 82,950,000	$ (52,547,957)	$(20,475,638)	$ 9,926,405	$ 146,415,112
17	10.00	$ 82,950,000	$ (52,547,957)	$(20,475,638)	$ 9,926,405	$ 156,341,517
18	10.00	$ 82,950,000	$ (52,547,957)	$(20,475,638)	$ 9,926,405	$ 166,267,922
19	10.00	$ 82,950,000	$ (52,547,957)	$(20,475,638)	$ 9,926,405	$ 176,194,327
20	10.00	$ 82,950,000	$ (52,547,957)	$(20,475,638)	$ 9,926,405	$ 186,120,731
21	10.00	$ 82,950,000	$ (52,547,957)	$(20,475,638)	$ 9,926,405	$ 196,047,136

Using a CCF of $196,047,136 after 21 years, the IRR is calculated to be 105%, indicating the plant is a highly profitable investment.

Year	Doses (millions)	Revenue	COM	Other Expenses	Cash Flow	CCF
0					**$(3,818,833.58)**	**-$3,818,833.58**
1				$ (64,914)	$ (64,914)	-$3,883,747
2	8.33	$ 66,360,000	$ (43,789,964)	$ (15,894,285)	$ 6,675,751	$2,792,003
3	10.00	$ 82,950,000	$ (52,547,957)	$ (20,336,537)	$ 10,065,506	$12,857,509
4	10.00	$ 82,950,000	$ (52,547,957)	$ (20,336,537)	$ 10,065,506	$22,923,015
5	10.00	$ 82,950,000	$ (52,547,957)	$ (20,336,537)	$ 10,065,506	$32,988,521
6	10.00	$ 82,950,000	$ (52,547,957)	$ (20,336,537)	$ 10,065,506	$43,054,027
7	10.00	$ 82,950,000	$ (52,547,957)	$ (20,336,537)	$ 10,065,506	$53,119,533
8	10.00	$ 82,950,000	$ (52,547,957)	$ (20,336,537)	$ 10,065,506	$63,185,038
9	10.00	$ 82,950,000	$ (52,547,957)	$ (20,475,638)	$ 9,926,405	$73,111,443
10	10.00	$ 82,950,000	$ (52,547,957)	$ (20,475,638)	$ 9,926,405	$83,037,848
11	10.00	$ 82,950,000	$ (52,547,957)	$ (20,475,638)	$ 9,926,405	$92,964,253
12	10.00	$ 82,950,000	$ (52,547,957)	$ (20,475,638)	$ 9,926,405	$102,890,658
13	10.00	$ 82,950,000	$ (52,547,957)	$ (20,475,638)	$ 9,926,405	$112,817,063
14	10.00	$ 82,950,000	$ (52,547,957)	$ (20,475,638)	$ 9,926,405	$122,743,468
15	10.00	$ 82,950,000	$ (52,547,957)	$ (20,475,638)	$ 9,926,405	$132,669,873
16	10.00	$ 82,950,000	$ (52,547,957)	$ (20,475,638)	$ 9,926,405	$142,596,278
17	10.00	$ 82,950,000	$ (52,547,957)	$ (20,475,638)	$ 9,926,405	$152,522,683
18	10.00	$ 82,950,000	$ (52,547,957)	$ (20,475,638)	$ 9,926,405	$162,449,088
19	10.00	$ 82,950,000	$ (52,547,957)	$ (20,475,638)	$ 9,926,405	$172,375,493
20	10.00	$ 82,950,000	$ (52,547,957)	$ (20,475,638)	$ 9,926,405	$182,301,898

6 Regulatory, Health, Safety and Environmental Considerations

6.1 Regulatory Compliance

Patient health and safety is the top priority in vaccine manufacturing. It is therefore crucial to adhere to regulatory standards set by the U.S. Food and Drug Administration (FDA) and

international authorities in the Southeast Asian and African regions–including the ASEAN Pharmaceutical Regulatory Policy (APRP), ASEAN Pharmaceutical Product Working Group (PPWG), African Medicines Agency (AMA), and African Medicines Regulatory Harmonization (AMRH) initiative. Compliance with regulations will maintain product quality, efficacy, and safety for the patients and employees.

The FDA enforces Current Good Manufacturing Practices (cGMP) regulations to ensure high quality and safety of drug products. These regulations include establishing strong quality management systems, obtaining quality raw materials, establishing robust operating procedures, investigating product quality deviations, and maintaining reliable testing.[115] Additionally, collaboration with the APRP and PPWG will ensure compliance and distribution in Southeast Asia; similarly, working with the AMA and AMRH initiative will strengthen compliance and distribution across African nations.

The plant will also implement rigorous quality control systems (Section 5.2.1), employee training, and regular facility and equipment maintenance. The goal is to produce safe, effective, and high-quality vaccines while fostering patient health and regulatory and public trust.

6.2 Health and Safety Considerations

6.2.1 Quality Control Framework

To ensure consistent production of safe and effective mRNA vaccines, manufactures we will implement a structured quality control plan that spans the entire production process. Following current World Health Organization guidelines, put forth in 2022, this plan includes rigorous testing at each stage of manufacturing, from verification of materials to product characterization prior to

release, with additional opportunities for improvement based on recent advancements in analytical techniques.[116–118]

The first step in ensuring a quality product is raw material verification, where all nucleotides, enzymes, plasmid DNA (pDNA) templates and lipid components are tested prior to use. Plasmid DNA integrity, physical structure, will be confirmed through restriction enzyme mapping, a method that cuts DNA at specific sites, followed by gel electrophoresis. Plasmid sequence accuracy is to be validated using Sanger sequencing or short-read Illumina sequencing. Lipid components will also be analyzed using high-performance liquid chromatography (HPLC) to ensure they meet required purity and composition specifications. Additionally, all materials will be tested for contaminants like endotoxins and microbes using standard sterility tests. A potential improvement is the use of long-read sequencing (VAX-seq) to more accurately check for DNA errors before manufacturing begins.[116]

Once the raw materials are confirmed, IVT and mRNA purification processes are carefully monitored with multiple quality control tests. The mRNA sequence and integrity are to be verified using reverse transcription-polymerase chain reaction (RT-PCR) and capillary gel electrophoresis. Additionally, 5’ capping efficiency and poly(A) tail length will be assessed during chromatography runs to ensure purified mRNA strands have the proper modifications for immunogenicity. Ensuring the removal of contaminants is another critical step—residual template DNA should be identified using high performance liquid chromatography, while immunoblotting techniques can confirm the removal of double-stranded RNA (dsRNA), which triggers an undesirable immune response. Residual T7 RNA polymerase will be measured using an enzyme-linked immunosorbent assay (ELISA). A key opportunity for process improvement at this stage is the adoption of VAX-

seq (long-read nanopore sequencing), which enables a single, streamlined analysis of mRNA sequence identity, length, and integrity, reducing reliance on multiple time-consuming methods.[116]

During mRNA synthesis and purification, in-process quality checks are essential. These include RNA integrity analysis, sequencing verification, and purity assessments. Traditional industry methods like capillary electrophoresis, a technique that separates molecules based on size and charge using narrow capillaries, are commonly used to evaluate mRNA fragment distribution and detect degradation.[118] High-performance liquid chromatography (HPLC) is another standard method used to assess the removal of unwanted byproducts, such as unreacted nucleotides and template DNA, from the final mRNA product.

As purified mRNA must be encapsulated within lipid nanoparticles (LNPs) for delivery, LNP formulation quality control is crucial to maintaining efficacy. Particle size and uniformity will be assessed using dynamic light scattering (DLS), a method that measures how light scatters to determine nanoparticle dimensions, as well as transmission electron microscopy (TEM) imaging to confirm LNP structure and uniformity. Fluorescence-based assays will evaluate encapsulation efficiency, while zeta potential analysis will evaluate LNP surface charge to predict formulation stability. Another possible process improvement would be the introduction of real-time monitoring using Process Analytical Technology (PAT), which would track LNP size and encapsulation efficiency continuously, minimizing batch failures and enhancing consistency.[118]

Before a vaccine batch is released, final sterility, potency, and stability testing will be conducted. Sterility will be confirmed following USP 71 guidelines, while potency and efficacy will be assessed using cell-based expression assays to verify mRNA translation. Stability studies will also be conducted under different storage conditions, including freeze-thaw cycles and long-term storage at -80°C, to ensure the vaccine maintains its efficacy over time. Additional tests for residual

solvents and endotoxins will also be performed to confirm the vaccine's purity and safety. Furthermore, implementing a Quality by Design framework, which identifies critical quality attributes (CQAs) and critical process parameters (CPPs), would enhance process control and ensure consistent batch-to-batch quality.[118]

To help ensure consistent product quality, we will use engineering runs to help identify critical quality attributes—key characteristics that affect vaccine safety and efficacy—and critical process parameters—the specific conditions that must be controlled to ensure reproducibility. This will allow us to optimize process parameters like reaction temperatures, mixing speeds, and purification methods, ensuring that each batch meets strict quality criteria.

6.2.2 Process Safety

Several chemicals used in mRNA vaccine manufacturing require strict handling procedures to ensure the safety of plant personnel. Steam, alkaline detergents, ethanol, ethylenediaminetetraacetic acid (EDTA), dithiothreitol (DTT), spermidine, and adenosine triphosphate (ATP) all present potential hazards. Steam, used in SIP processes, poses a burn risk, while alkaline detergents in CIP systems are highly corrosive and can cause severe skin and eye irritation. Ethanol, used in LNP formulation, is highly flammable, requiring proper ventilation and fire suppression measures. EDTA, ethylene glycol, DTT, and spermidine are toxic or irritant chemicals that necessitate proper protective equipment such as gloves, safety glasses, and long-sleeved clothing when handling. ATP, while essential in certain reactions, poses an additional hazard as a flammable dust, meaning it should never be stored in large powder quantities to avoid dust explosion risks. To mitigate these hazards, all employees will undergo comprehensive safety training in chemical handling, emergency response, and PPE usage. Additionally, a spill response

plan will be implemented, ensuring that appropriate chemical spill kits, eyewash stations, and emergency showers are available throughout the facility.

A key component of process safety is safe plant design, which ensures that incompatible materials are properly separated to reduce the risk of accidental reactions. Flammable and corrosive chemicals will be stored in designated, ventilated areas with proper secondary containment, and static discharge prevention measures will be in place for any powder-handling operations. To further assess the potential risks associated with chemical handling, a Maximum Credible Event (MCE) analysis was conducted.

One identified hazard is the release of 320 liters of ethanol, a flammable solvent, which could result in a fire if ignited. A simulation using ALOHA modeling software (Figure 5.2.2-1), based on stable atmospheric conditions in the Research Triangle Park (RTP) area, indicated that such a release could reach areas almost 150 yards away, affecting nearby personnel safety and plant operations. To mitigate this risk, the facility will install fire suppression systems, explosion-proof ventilation, and flame arrestors in ethanol storage areas. Additionally, ethanol handling procedures will include regular leak inspections, restricted access zones, and grounding of all equipment to prevent static ignition. Fire extinguishers and sprinkler systems will be placed at critical locations to ensure immediate response capabilities in case of an emergency. By

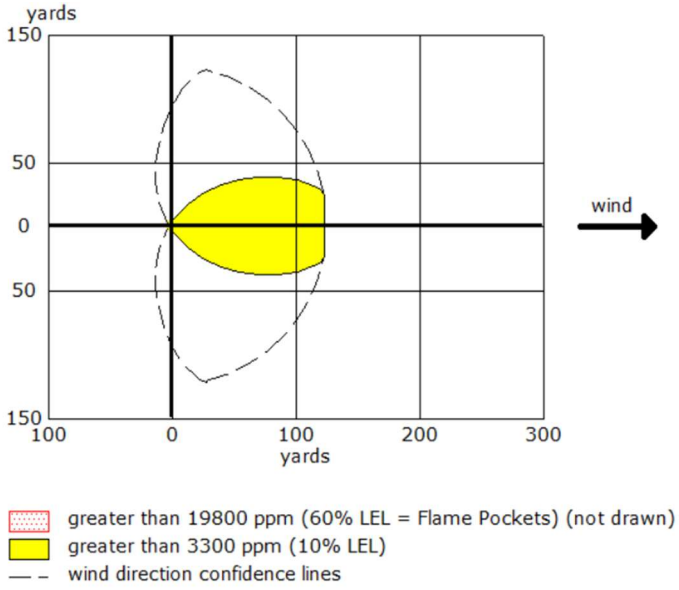

Figure 5.2.2-1: ALOHA model of flammable area of ethanol vapor cloud, post release

implementing these process safety measures, the facility will minimize hazards, protect personnel, and ensure continuous safe operation in mRNA vaccine production.

6.3 Environmental Considerations

The facility is in the Research Triangle Park (RTP), chosen for its existing relevance in biotechnology and pharmaceutical industries. Strict compliance with federal and local environmental regulations is crucial, given its proximity to research institutions, industrial buildings, and protected natural areas. To ensure environmental safety, plant employees will undergo extensive training on chemical handling, waste disposal procedures, and emergency spill response. Regular maintenance, inspections, and testing of equipment will be conducted to minimize the risk of system leaks and other hazards.

Waste streams from vaccine production will be properly managed to prevent contamination of the area's water systems and surrounding ecosystem. The plant handles chemicals including ethanol, EDTA, DTT, and spermidine, all of which pose environmental risks and must be fully broken down or neutralized before release into the wastewater system. Ethanol waste from LNP formation will be properly treated to avoid flammability hazards (see Section 5.2.2) and volatile organic compound (VOC) emissions. Hazardous waste, such as unused enzymes and nucleic acid fragments, will be disposed of through reputable pharmaceutical waste management companies. Non-hazardous waste, such as condensed steam, will be treated onsite before being safely discharged into the local sewer system. Routine verification of pH levels and chemical content will be conducted to meet local wastewater treatment regulations.

To reduce environmental impact, the plant will implement sustainability initiatives such as energy-efficient equipment and building design, as well as green training for employees. The integration

of these environmental safety and sustainability methods will allow the facility to meet regulatory compliance and maintain a commitment to the RTP ecosystem and its residents.

7 Social and Ethical Considerations

There are several social and ethical issues associated with vaccine manufacturing. A key concern is equitable access to treatment. This is especially critical in lower-income regions with high TB rates, specifically in Southeast Asia and Africa. The vaccine pricing will therefore reflect our commitment to global healthcare equity by offering affordable vaccines for these high-burden regions, achieved by raising domestic pricing to offset costs and maintain financial stability.

Beyond affordability, challenges such as cold-chain requirements, last mile delivery, and regulatory barriers must be addressed to ensure successful, widespread distribution. We will work closely with governments, non-governmental organizations (NGOs), and international health organizations to strengthen supply chain infrastructure and ensure doses reach all high-burden areas, including those that are remote and underserved. Leveraging existing vaccine delivery programs will maximize distribution efficiency while reducing costs.

There is widespread skepticism toward Western pharmaceutical companies in many parts of the world due to historical exploitation, affordability concerns, and a lack of transparency. To address these issues, we will engage in community education efforts to communicate the benefits of our vaccine and how it will support public health. Establishing transparent dialogue with local governments, healthcare providers, and community leaders will be crucial to building trust and demonstrating our commitment to ethical healthcare practices.

Internally, the workplace culture will be built on respect, safety, and ethical responsibility to ensure the highest standards in manufacturing and patient care. Comprehensive safety and ethical training for employees will emphasize the importance of understanding and respecting the values, beliefs, and healthcare practices of the populations the product serves. There is also a need to provide clear

and accessible information on TB prevention, vaccines, and affordable healthcare solutions. This will involve collaborating with public health officials, NGOs, and local government leaders to develop educational materials that empower and inform communities.

By upholding these ethical standards, we will not only deliver a life-saving vaccine but also foster trust, improve global health outcomes, and contribute to sustainable, responsible business practices.

8 Conclusions and Final Recommendations

Our proposed mRNA vaccine manufacturing facility has been designed to product approximately 10 million doses of an mRNA-based TB vaccine, targeting populations in low-income countries, where infection rates are highest, primarily across Southeast Asia and Africa, as well as United States healthcare workers and those traveling abroad to at risk countries. The facility is expected to be economically viable with an IRR of 105% and an expected yearly cash flow of approximately $10 million dollars after the first two years of operation.

Several cost-saving measures could be implemented and investigated to further enhance profitability. One of the largest utility expenses, WFI, currently purchased from outside suppliers, could be reduced by producing it on site. The reduction in the cost of manufacturing would offset initial capital costs and result in long-term increased cash flow. Additionally, optimizing CIP and SIP cycles, for example reusing caustic detergent for multiple cycles, could farther lower operational costs. Another potential cost-saving measure involves reducing freezer (and outsourcing) costs by incorporating fill-to-finish processes, by decreasing the amount of time material needs to be held at -80^{o}C. Additionally, exploring enzyme recycling methods as well as techniques and equipment required to produce the linearized plasmid for our target sequence could further reduce costs.

To further refine the manufacturing process and improve efficiency, additional studies and optimizations, outside the scope/capabilities of this initial work are recommended. More precise modeling of viscosity in highly concentrated solutions is needed, rather than assuming behavior similar to pure substances (as done for modeling the CIJM, R-302). Additionally, improved estimates for mRNA yield, filtration losses, and encapsulation efficiency would provide more

accurate cost and production projections. Further experimentation regarding the ratio of mRNA to lipid solution in R-302 (CIJM) will provide incite into the impact of flow rate and ratio on the size of LNP particles produced as well as the number of non-mRNA containing LNPs, possibly impacting vaccine efficacy. Pending future market sizes, using a multi-inlet vortex mixer may allow for better control and throughput of mRNA containing LNPs. Investigating these areas of interest may allow for platform improvements in efficiency, profitability and greater social impact.

Furthermore, extensive studies must be performed on both chromatography units prior to operation. First, the permeability of both columns and the viscosity of the flowing buffers must be determined experimentally to better evaluate the pressure drop across both columns; the operating flow rate must be adjusted accordingly. Second, the specific elution region for the target mRNA during AEX must be determined. In the design of this step, a larger volume than necessary is collected and optimization of the automated collection period will lead to higher purities and decreased downstream volumes.

While this project and facility is promising, there are risks that could impact production and market viability. Competing TB vaccines may enter the market before the completion of clinical trials, and the efficacy of the vaccine against drug-resistant TB remains uncertain. However, further clinical trials may reveal efficacy against latent TB, which could significantly expand the potential market size, particularly in the U.S., where an estimated 13 million people have latent TB.

References

(1) Al Fayez, N.; Nassar, M. S.; Alshehri, A. A.; Alnefaie, M. K.; Almughem, F. A.; Alshehri, B. Y.; Alawad, A. O.; Tawfik, E. A. Recent Advancement in mRNA Vaccine Development and Applications. *Pharmaceutics* **2023**, *15* (7), 1972. https://doi.org/10.3390/pharmaceutics15071972.

(2) Hwang, T. *Progress Deferred: Lessons From mRNA Vaccine Development | IFP*. Institute for Progress. https://ifp.org/progress-deferred-lessons-from-mrna-vaccine-development/ (accessed 2025-03-23).

(3) Gote, V.; Bolla, P. K.; Kommineni, N.; Butreddy, A.; Nukala, P. K.; Palakurthi, S. S.; Khan, W. A Comprehensive Review of mRNA Vaccines. *Int. J. Mol. Sci.* **2023**, *24* (3), 2700. https://doi.org/10.3390/ijms24032700.

(4) Larsen, S. E.; Baldwin, S. L.; Coler, R. N. Tuberculosis Vaccines Update: Is an RNA-Based Vaccine Feasible for Tuberculosis? *Int. J. Infect. Dis.* **2023**, *130*, S47–S51. https://doi.org/10.1016/j.ijid.2023.03.035.

(5) *Tuberculosis (TB)*. World Health Organization. https://www.who.int/news-room/fact-sheets/detail/tuberculosis (accessed 2025-03-23).

(6) Yuh, B. *BCG Treatment for Bladder Cancer and Side Effects*. City of Hope. https://www.cancercenter.com/cancer-types/bladder-cancer/treatments/bcg-treatment (accessed 2025-03-23).

(7) *Facing global shortage, Merck commits to meeting patient demand*. Merck.com. https://www.merck.com/stories/facing-a-global-shortage-merck-commits-to-meeting-patient-demand/ (accessed 2025-03-23).

(8) Looney, M. M.; Hatherill, M.; Musvosvi, M.; Flynn, J.; Kagina, B. M.; Frick, M.; Kafuko, Z.; Schmidt, A.; Southern, J.; Wilder-Smith, A.; Tippoo, P.; Paradkar, V.; Popadić, D.; Scriba, T. J.; Hanekom, W.; Giersing, B. Conference Report: WHO Meeting Summary on mRNA-Based Tuberculosis Vaccine Development. *Vaccine* **2023**, *41* (48), 7060–7066. https://doi.org/10.1016/j.vaccine.2023.10.026.

(9) *BNT-164 by BioNTech for Tuberculosis: Likelihood of Approval*. Pharmaceutical Technology. https://www.pharmaceutical-technology.com/data-insights/bnt-164-biontech-tuberculosis-likelihood-of-approval/ (accessed 2025-03-23).

(10) MacNeil, A. Global Epidemiology of Tuberculosis and Progress Toward Achieving Global Targets — 2017. *MMWR Morb. Mortal. Wkly. Rep.* **2019**, *68*. https://doi.org/10.15585/mmwr.mm6811a3.

(11) CDC. *Latent TB Infection in the United States – Published Estimates*. Tuberculosis Data. https://www.cdc.gov/tb-data/latent-tb-infection-estimates/index.html (accessed 2025-03-23).

(12) *News: Healthcare accounted for 24% of all new U.S. jobs in 2023 | ACDIS*. https://acdis.org/articles/news-healthcare-accounted-24-all-new-us-jobs-2023 (accessed 2025-03-23).

(13) *Healthcare Occupations*. Bureau of Labor Statistics. https://www.bls.gov/ooh/healthcare/ (accessed 2025-03-23).

(14) *Power BI Report*. https://app.powerbi.com/view?r=eyJrIjoiZWFlY2RlYzktMWI5NC00NDNlLWFkYTEtMGU1M2MyNjAzN2ZiIiwidCI6IjgzNjY2NmM2LWM2NDQtNDYwYS1iYTBlLTg1NmNjMWQwNTU5ZCIsImMiOjEwfQ%3D%3D (accessed 2025-03-23).

(15) Gomez, P. L.; Robinson, J. M.; Rogalewicz, J. A. 4 - Vaccine Manufacturing. In *Vaccines (Sixth Edition)*; Plotkin, S. A., Orenstein, W. A., Offit, P. A., Eds.; W.B. Saunders: London, 2013; pp 44–57. https://doi.org/10.1016/B978-1-4557-0090-5.00019-7.
(16) *ABS Ultra Low Temperature Freezers | LabFreezers.net*. Laborator Supply Network. https://labfreezers.net/collections/all-freezers/products/ultra-low-temperature-freezers (accessed 2025-03-24).
(17) Beckert, B.; Masquida, B. Synthesis of RNA by In Vitro Transcription. In *RNA: Methods and Protocols*; Nielsen, H., Ed.; Humana Press: Totowa, NJ, 2011; pp 29–41. https://doi.org/10.1007/978-1-59745-248-9_3.
(18) Perenkov, A. D.; Sergeeva, A. D.; Vedunova, M. V.; Krysko, D. V. In Vitro Transcribed RNA-Based Platform Vaccines: Past, Present, and Future. *Vaccines* **2023**, *11* (10), 1600. https://doi.org/10.3390/vaccines11101600.
(19) Morais, P.; Adachi, H.; Yu, Y.-T. The Critical Contribution of Pseudouridine to mRNA COVID-19 Vaccines. *Front. Cell Dev. Biol.* **2021**, *9*, 789427. https://doi.org/10.3389/fcell.2021.789427.
(20) *(PDF) Messenger RNA (mRNA) Vaccine Large Scale Manufacturing – Process Modeling and Techno-Economic Assessment (TEA) using SuperPro Designer.* https://www.researchgate.net/publication/356474248_Messenger_RNA_mRNA_Vaccine_Large_Scale_Manufacturing_-_Process_Modeling_and_Techno-Economic_Assessment_TEA_using_SuperPro_Designer (accessed 2025-03-07).
(21) Davidopoulou, C.; Kouvelas, D.; Ouranidis, A. COMPARING Vaccine Manufacturing Technologies Recombinant DNA vs in Vitro Transcribed (IVT) mRNA. *Sci. Rep.* **2024**, *14* (1), 21742. https://doi.org/10.1038/s41598-024-67797-x.
(22) *mRNA capping: biological functions and applications | Nucleic Acids Research | Oxford Academic*. https://academic.oup.com/nar/article/44/16/7511/2460195 (accessed 2025-03-07).
(23) *Co-transcriptional capping*. https://www.takarabio.com/learning-centers/mrna-and-cdna-synthesis/mrna-synthesis/5-prime-capping-of-mrna/co-transcriptional-capping (accessed 2025-03-07).
(24) Hengelbrock, A.; Schmidt, A.; Strube, J. Digital Twin Fundamentals of mRNA In Vitro Transcription in Variable Scale Toward Autonomous Operation. *ACS Omega* **2024**, *9* (7), 8204–8220. https://doi.org/10.1021/acsomega.3c08732.
(25) Stover, N. M.; Ganko, K.; Braatz, R. D. Mechanistic Modeling of in Vitro Transcription Incorporating Effects of Magnesium Pyrophosphate Crystallization. *Biotechnol. Bioeng.* **2024**, *121* (9), 2636–2647. https://doi.org/10.1002/bit.28699.
(26) Arnold, S.; Siemann, M.; Scharnweber, K.; Werner, M.; Baumann, S.; Reuss, M. Kinetic Modeling and Simulation of in Vitro Transcription by Phage T7 RNA Polymerase. *Biotechnol. Bioeng.* **2001**, *72* (5), 548–561. https://doi.org/10.1002/1097-0290(20010305)72:5<548::AID-BIT1019>3.0.CO;2-2.
(27) Young, J. S.; Ramirez, W. F.; Davis, R. H. Modeling and Optimization of a Batch Process for in Vitro RNA Production. *Biotechnol. Bioeng.* **1997**, *56* (2), 210–220. https://doi.org/10.1002/(SICI)1097-0290(19971020)56:2<210::AID-BIT10>3.0.CO;2-K.
(28) Whitley, J.; Zwolinski, C.; Denis, C.; Maughan, M.; Hayles, L.; Clarke, D.; Snare, M.; Liao, H.; Chiou, S.; Marmura, T.; Zoeller, H.; Hudson, B.; Peart, J.; Johnson, M.; Karlsson, A.; Wang, Y.; Nagle, C.; Harris, C.; Tonkin, D.; Fraser, S.; Capiz, L.; Zeno, C. L.; Meli, Y.; Martik, D.; Ozaki, D. A.; Caparoni, A.; Dickens, J. E.; Weissman, D.; Saunders, K. O.;

Haynes, B. F.; Sempowski, G. D.; Denny, T. N.; Johnson, M. R. Development of mRNA Manufacturing for Vaccines and Therapeutics: mRNA Platform Requirements and Development of a Scalable Production Process to Support Early Phase Clinical Trials. *Transl. Res.* **2022**, *242*, 38–55. https://doi.org/10.1016/j.trsl.2021.11.009.

(29) Guo, L.; Liu, Z.; Song, S.; Yao, W.; Yang, M.; Chen, G. Maximizing the mRNA Productivity for in Vitro Transcription by Optimization of Fed-Batch Strategy. *Biochem. Eng. J.* **2024**, *210*, 109412. https://doi.org/10.1016/j.bej.2024.109412.

(30) Skok, J.; Megušar, P.; Vodopivec, T.; Pregeljc, D.; Mencin, N.; Korenč, M.; Krušič, A.; Celjar, A. M.; Pavlin, N.; Krušič, J.; Mueller, M.; McHugh, K.; Štrancar, A.; Sekirnik, R. Gram-Scale mRNA Production Using a 250-mL Single-Use Bioreactor. *Chem. Ing. Tech.* **2022**, *94* (12), 1928–1935. https://doi.org/10.1002/cite.202200133.

(31) He, W.; Zhang, X.; Zou, Y.; Li, J.; Wang, C.; He, Y.; Jin, Q.; Ye, J. Effective Synthesis of High-Integrity mRNA Using In Vitro Transcription. *Molecules* **2024**, *29* (11), 2461. https://doi.org/10.3390/molecules29112461.

(32) Hou, X.; Zaks, T.; Langer, R.; Dong, Y. Lipid Nanoparticles for mRNA Delivery. *Nat. Rev. Mater.* **2021**, *6* (12), 1078–1094. https://doi.org/10.1038/s41578-021-00358-0.

(33) Rosa, S. S.; Prazeres, D. M. F.; Azevedo, A. M.; Marques, M. P. C. mRNA Vaccines Manufacturing: Challenges and Bottlenecks. *Vaccine* **2021**, *39* (16), 2190–2200. https://doi.org/10.1016/j.vaccine.2021.03.038.

(34) Nitika; Wei, J.; Hui, A.-M. The Delivery of mRNA Vaccines for Therapeutics. *Life* **2022**, *12* (8), 1254. https://doi.org/10.3390/life12081254.

(35) *Lipid Nanoparticles for Drug Delivery - Xu - 2022 - Advanced NanoBiomed Research - Wiley Online Library*. https://advanced.onlinelibrary.wiley.com/doi/full/10.1002/anbr.202100109 (accessed 2025-02-14).

(36) Haque, Md. A.; Shrestha, A.; Mikelis, C. M.; Mattheolabakis, G. Comprehensive Analysis of Lipid Nanoparticle Formulation and Preparation for RNA Delivery. *Int. J. Pharm. X* **2024**, *8*, 100283. https://doi.org/10.1016/j.ijpx.2024.100283.

(37) Zhao, L.; Xu, Z.; Li, H.; Liu, L.; Chen, S.; Peng, Z.; Wang, G. A Review of Confined Impinging Jet Reactor (CIJR) with a Perspective of mRNA-LNP Vaccine Production. *Rev. Chem. Eng.* **2024**, *40* (8), 887–916. https://doi.org/10.1515/revce-2024-0016.

(38) Kong, W.; Wei, Y.; Dong, Z.; Liu, W.; Zhao, J.; Huang, Y.; Yang, J.; Wu, W.; He, H.; Qi, J. Role of Size, Surface Charge, and PEGylated Lipids of Lipid Nanoparticles (LNPs) on Intramuscular Delivery of mRNA. *J. Nanobiotechnology* **2024**, *22* (1), 553. https://doi.org/10.1186/s12951-024-02812-x.

(39) Maeki, M.; Uno, S.; Niwa, A.; Okada, Y.; Tokeshi, M. Microfluidic Technologies and Devices for Lipid Nanoparticle-Based RNA Delivery. *J. Controlled Release* **2022**, *344*, 80–96. https://doi.org/10.1016/j.jconrel.2022.02.017.

(40) Marchisio, D. L.; Rivautella, L.; Barresi, A. A. Design and Scale-up of Chemical Reactors for Nanoparticle Precipitation. *AIChE J.* **2006**, *52* (5), 1877–1887. https://doi.org/10.1002/aic.10786.

(41) Schober, G. B.; Story, S.; Arya, D. P. A Careful Look at Lipid Nanoparticle Characterization: Analysis of Benchmark Formulations for Encapsulation of RNA Cargo Size Gradient. *Sci. Rep.* **2024**, *14* (1), 2403. https://doi.org/10.1038/s41598-024-52685-1.

(42) Kon, E.; Elia, U.; Peer, D. Principles for Designing an Optimal mRNA Lipid Nanoparticle Vaccine. *Curr. Opin. Biotechnol.* **2022**, *73*, 329–336. https://doi.org/10.1016/j.copbio.2021.09.016.
(43) Li, S.; Hu, Y.; Li, A.; Lin, J.; Hsieh, K.; Schneiderman, Z.; Zhang, P.; Zhu, Y.; Qiu, C.; Kokkoli, E.; Wang, T.-H.; Mao, H.-Q. Payload Distribution and Capacity of mRNA Lipid Nanoparticles. *Nat. Commun.* **2022**, *13* (1), 5561. https://doi.org/10.1038/s41467-022-33157-4.
(44) Subraveti, S. N.; Wilson, B. K.; Bizmark, N.; Liu, J.; Prud'homme, R. K. Synthesizing Lipid Nanoparticles by Turbulent Flow in Confined Impinging Jet Mixers. *J. Vis. Exp. JoVE* **2024**, No. 210, e67047. https://doi.org/10.3791/67047.
(45) Lee, Y.; Jeong, M.; Park, J.; Jung, H.; Lee, H. Immunogenicity of Lipid Nanoparticles and Its Impact on the Efficacy of mRNA Vaccines and Therapeutics. *Exp. Mol. Med.* **2023**, *55* (10), 2085–2096. https://doi.org/10.1038/s12276-023-01086-x.
(46) Nguyen, M. *Turbulent Mixing: Scaling Up Nanoparticle Manufacturing for the Future*; Helix Biotech, 2023. https://www.helixbiotech.com/post/turbulent-mixing-scaling-up-nanoparticle-manufacturing-for-the-future.
(47) Nguyen, M. *Scale-Up Lipid Nanoparticle (LNP) Manufacturing | Turbulent Mixing*. Helix Biotech. https://www.helixbiotech.com/post/turbulent-mixing-scaling-up-nanoparticle-manufacturing-for-the-future (accessed 2025-02-14).
(48) Devos, C.; Mukherjee, S.; Inguva, P.; Singh, S.; Wei, Y.; Mondal, S.; Yu, H.; Barbastathis, G.; Stelzer, T.; Braatz, R. D.; Myerson, A. S. Impinging Jet Mixers: A Review of Their Mixing Characteristics, Performance Considerations, and Applications. *AIChE J.* **2025**, *71* (1), e18595. https://doi.org/10.1002/aic.18595.
(49) Brito, M. S. C. A.; Dias, M. M.; Lopes, J. C. B.; Santos, R. J.; Fonte, C. P. A General Design Equation for Confined Impinging Jets Mixers. *Chem. Eng. J.* **2023**, *465*, 142892. https://doi.org/10.1016/j.cej.2023.142892.
(50) Gavi, E.; Marchisio, D. L.; Barresi, A. A. CFD Modelling and Scale-up of Confined Impinging Jet Reactors. *Chem. Eng. Sci.* **2007**, *62* (8), 2228–2241. https://doi.org/10.1016/j.ces.2006.12.077.
(51) Demongeot, J.; Fougère, C. mRNA COVID-19 Vaccines—Facts and Hypotheses on Fragmentation and Encapsulation. *Vaccines* **2022**, *11* (1), 40. https://doi.org/10.3390/vaccines11010040.
(52) Hardianto, A.; Muscifa, Z. S.; Widayat, W.; Yusuf, M.; Subroto, T. The Effect of Ethanol on Lipid Nanoparticle Stabilization from a Molecular Dynamics Simulation Perspective. *Mol. Basel Switz.* **2023**, *28* (12), 4836. https://doi.org/10.3390/molecules28124836.
(53) QYAOBIO. Affinity Chromatography Purification. https://www.qyaobio.com/protein/protein-purification/affinity-chromatography/ (accessed 2025-04-02).
(54) Purification of mRNA With CIMmultus® Oligo dT. https://dcvmn.org/wp-content/uploads/2023/03/Purification-of-mRNA-With-CIMmultus-Oligo-dT-Technical-Note-en-B-Sartorius.pdf.
(55) Purification of Messenger RNA by Affinity Chromatography on CIMmultus™ Oligo dT Column, 2019. https://web.archive.org/web/20221029000157/http:/www.rubiconscience.com.au/wp-content/uploads/2022/02/AN062-Purification-of-messenger-RNA-by-affinity-chromatography-on-CIMmultus-Oligo-dT-column.pdf.

(56) Mencin, N.; Cernigoj, U.; Pelijhan, S.; Persic, S.; Gagnon, P.; Strancar, A. Extraction of mRNA From IVT Mixtures With CIMmultus® Oligo dT Column, 2022. https://www.sartorius.com/download/751776/cimmultus-oligo-dt-affinity-column-based-poster-en-a0-b-sart-1--data.pdf.
(57) Lee, J.; Woodruff, M. C.; Kim, E. H.; Nam, J.-H. Knife's Edge: Balancing Immunogenicity and Reactogenicity in mRNA Vaccines. *Exp. Mol. Med.* **2023**, *55* (7), 1305–1313. https://doi.org/10.1038/s12276-023-00999-x.
(58) Tian, B.; Bevilacqua, P. C.; Diegelman-Parente, A.; Mathews, M. B. The Double-Stranded-RNA-Binding Motif: Interference and Much More. *Nat. Rev. Mol. Cell Biol.* **2004**, *5* (12), 1013–1023. https://doi.org/10.1038/nrm1528.
(59) mRNA Purification Using Anion Exchange Chromatography at Ambient Temperature, 2024. https://www.sigmaaldrich.com/deepweb/assets/sigmaaldrich/marketing/global/documents/352/385/mrna-purification-app-note-an14134en-ms.pdf?srsltid=AfmBOooHgYDe-f29-K-t26S9mS5bXNKP8xjnyFcv76HG45c1hxBpw0Kc.
(60) SaniSure. *What is Tangential Flow Filtration (TFF) and Where is it Used?* https://tblplastics.com/tangential-flow-filtration-tff/ (accessed 2025-03-05).
(61) Uppu, D.; Auger, M.; Kondra, R.; Hejmowski, A.; Marchand, N. *T-series TFF cassettes with Delta 100 kDa membranes for RNA and LNP applications*. Cytiva. https://www.cytivalifesciences.com/en/us/solutions/bioprocessing/knowledge-center/tff-membranes-for-rna-and-lnp-applications (accessed 2025-02-14).
(62) *T-Series cassettes with Delta regenerated cellulose membranes*. Cytiva. https://www.cytivalifesciences.com/en/us/shop/bioprocessing-filtration/tangential-flow-filtration/cassettes/t-series-centramate-cassettes-w-delta-regenerated-cellulose-membranes-p-36679 (accessed 2025-02-14).
(63) Frost, O. *Advanced characterization of LNP-mRNA therapeutics via FFF-MALS and DLS techniques*. News-Medical. https://www.news-medical.net/whitepaper/20241120/Advanced-characterization-of-LNP-mRNA-therapeutics-via-FFF-MALS-and-DLS-techniques.aspx (accessed 2025-02-14).
(64) Schoenmaker, L.; Witzigmann, D.; Kulkarni, J. A.; Verbeke, R.; Kersten, G.; Jiskoot, W.; Crommelin, D. J. A. mRNA-Lipid Nanoparticle COVID-19 Vaccines: Structure and Stability. *Int. J. Pharm.* **2021**, *601*, 120586. https://doi.org/10.1016/j.ijpharm.2021.120586.
(65) ThermoFisher. *DNA and RNA Molecular Weights and Conversions - US*. https://www.thermofisher.com/us/en/home/references/ambion-tech-support/rna-tools-and-calculators/dna-and-rna-molecular-weights-and-conversions.html (accessed 2025-03-05).
(66) Geng, C.; Zhou, K.; Yan, Y.; Li, C.; Ni, B.; Liu, J.; Wang, Y.; Zhang, X.; Wang, D.; Lv, L.; Zhou, Y.; Feng, A.; Wang, Y.; Li, C. A Preparation Method for mRNA-LNPs with Improved Properties. *J. Controlled Release* **2023**, *364*, 632–643. https://doi.org/10.1016/j.jconrel.2023.11.017.
(67) Q3C — Tables and List Guidance for Industry, 2017. https://www.fda.gov/media/71737/download.
(68) Urru, S. A. M.; Maines, E.; Campomori, A.; Soffiati, M. Safety of Sars-Cov-2 Vaccines Administration for Adult Patients with Hereditary Fructose Intolerance. *Hum. Vaccines Immunother. 17* (11), 4112–4114. https://doi.org/10.1080/21645515.2021.1943992.

(69) Critical Process Filtration. *Sterilizing & Bioburden Reduction Filtration in Biopharmaceutical Processes*. https://www.criticalprocess.com/knowledge/sterilizing-and-bioburden-reduction-filtration-in-biopharmaceutical-processes (accessed 2025-03-06).
(70) STERILE DRUG PROCESS INSPECTIONS, 2015. https://www.fda.gov/media/75174/download#:~:text=(a)%20Aseptic%20Processing%20Equipment.,of%20batches%20to%20contamination%20risk.
(71) Messerian, K. O.; Zverev, A.; Kramarczyk, J. F.; Zydney, A. L. Pressure-Dependent Fouling Behavior during Sterile Filtration of mRNA-Containing Lipid Nanoparticles. *Biotechnol. Bioeng.* **2022**, *119* (11), 3221–3229. https://doi.org/10.1002/bit.28200.
(72) *Fixed CIP Spray Ball | Tri Clamp 2 in. w/ 3 in. Ball - SS304*. Glacier Tanks. https://www.glaciertanks.com/tank-cip-spray-balls-sb-fx-200-300.html (accessed 2025-03-19).
(73) *How much CIP detergent needed?*. TechNotes – Critical Cleaning Advice from Alconox Inc. https://technotes.alconox.com/detergents/solujet/how-much-cip-detergent-needed/ (accessed 2025-03-18).
(74) *STERIS CIP 100 Alkaline Process and Research Cleaner - Facility Safety and Maintenance, Cleaning Supplies and Equipment*. Fischer Scientific. https://www.fishersci.com/shop/products/cip-100-alkaline-process-research-cleaner-2/5001172 (accessed 2025-03-20).
(75) Bowser, T. *What is Clean in Place (CIP)? - Oklahoma State University*. https://extension.okstate.edu/fact-sheets/what-is-clean-in-place-cip.html (accessed 2025-03-18).
(76) Bailey, J. *Clean-In-Place (CIP) Best Practices in 2023*. InterTech. https://inter-techltd.com/clean-in-place-cip-best-practices-2021/ (accessed 2025-03-18).
(77) Clean and Pure Steam Systems Biopharmaceutical Industry, 2010. https://606473.app.netsuite.com/core/media/media.nl?id=275911&c=606473&h=sowcabPOnS79LYXfyL-dvS70GgGQXkTq_5vr-ykoFnafkZIV&_xt=.pdf.
(78) *5 Liter Bioreactor Assembly (Cell Culture) - Broadley-James*. https://www.broadleyjames.com/product/5-liter-bioreactor-assembly-cell-culture/ (accessed 2025-03-23).
(79) PMP, J. B., PE. *Clean-In-Place (CIP) Best Practices in 2023*. InterTech. https://inter-techltd.com/clean-in-place-cip-best-practices-2021/ (accessed 2025-03-23).
(80) McNulty, C. Cleaning Bioreactors and Fermenters with CIP Systems.
(81) *CIP Spray Balls | Rotating & Fixed*. https://www.glaciertanks.com/tank-systems/tank-accessories/cip-spray-balls.html?srsltid=AfmBOopTFLmMKFuhr5cyVvB84QjXxni68F7becItErz7gzkaGdcT13pH (accessed 2025-03-23).
(82) Clean and Pure Steam Systems Biopharmaceutical Industry: Technical Reference Guide, 2010.
(83) *McGraw-Hill Education - Access Engineering*. https://www.accessengineeringlibrary.com/highwire_display/entity_view/node/12248373/focus_view (accessed 2025-03-17).
(84) Peters, M. S.; Timmerhaus, K. D.; West, R. E. *Plant Design and Economics for Chemical Engineers*; McGraw-Hill Education, 2003.

(85) Static Spray Ball & Supply Tube Operation and Installation Instructions. https://www.craneengineering.net/hubfs/Product%20Documents/sani-matic-static-spray-balls-iom.pdf.
(86) Metzger, L.; Kind, M. On the Transient Flow Characteristics in Confined Impinging Jet Mixers - CFD Simulation and Experimental Validation. *Chem. Eng. Sci.* **2015**, *133*, 91–105. https://doi.org/10.1016/j.ces.2014.12.056.
(87) *AN800017 Tygon® by Saint Gobain | 1/4" I.D. x 3/8" O.D. x 1/16" Wall | XL-60 | Pump Tubing | 50' Package Length*. HoseWarehouse. https://hosewarehouse.com/products/tygon-an800017-1-4-i-d-x-3-8-o-d-x-1-16-wall-xl-60-50-package-length-pump-tubing (accessed 2025-03-22).
(88) VSH A600R Variable Speed High Flow Peristaltic Pump. https://ankoproducts.com/products/vsh-a600r?srsltid=AfmBOoo6Oiy7OGmXyu3yBqxtHhGGNZrzct23jTXLI0tiPzzQzP4yC1e3.
(89) PharMed BPT Biocompatible Peristaltic Pump Tubing, 2024. https://www.biopharm.saint-gobain.com/sites/imdf.biopharm.com/files/pharmed_bpt_tubing_data_sheet.pdf.
(90) INDCO. *Digital Catalog*. https://www.indco.com/catalog/digital-catalog (accessed 2025-03-16).
(91) Shah, H. *Why Is Stainless Steel Widely Used In The Pharmaceutical Industry?*. Vishwa Stainless. https://www.vishwastainless.com/role-of-stainless-steel-in-pharmaceutical-industry/ (accessed 2025-03-16).
(92) *Pharmaceutical mixers*. GMM Pfaudler. https://www.gmmpfaudler.com/mixing-technology/applications-4/pharmaceuticals (accessed 2025-03-16).
(93) *Sussman Low-Capacity Electric Steam Generators - Cole-Parmer*. Cole-Parmer. https://www.coleparmer.com/p/sussman-low-capacity-electric-steam-generators/5554 (accessed 2025-03-24).
(94) US EPA, O. *Defining Hazardous Waste: Listed, Characteristic and Mixed Radiological Wastes*. https://www.epa.gov/hw/defining-hazardous-waste-listed-characteristic-and-mixed-radiological-wastes (accessed 2025-03-21).
(95) *Environmental Programs NIH Drain Discharge Guide*. https://nems.nih.gov/environmental-programs/Pages/NIH-Drain-Disposal-Guide.aspx (accessed 2025-03-21).
(96) Eshmuno Q, 2023. https://www.sigmaaldrich.com/deepweb/assets/sigmaaldrich/product/documents/169/342/eshmuno-q-techinfo-millipr-20130828lp-ms.pdf.
(97) *ReadyCircuit™ single-use 3-D bag assemblies*. Cytiva. https://www.cytivalifesciences.com/en/us/shop/liquid-preparation-and-management/liquid-handling-bags-and-assemblies/disposable-bags/readycircuit-single-use-3-d-bag-assemblies-p-05846 (accessed 2025-03-21).
(98) Peters, M.; Timmerhaus, K.; West, R. *Plant Design and Economics for Chemical Engineers*, Fifth.; McGraw-Hill, 2002.
(99) Peters, M. S.; Timmerhaus, K. D.; West, R. E.; West, R. E. *Plant Design and Economics for Chemical Engineers*, 5. ed, international ed. 2004.; McGraw-Hill chemical engineering series; McGraw-Hill: Boston, 2004.
(100) Turton, R.; Bailie, R. C.; Whitling, W. B.; Shaeiwitz, J. A.; Bhattacharyya, D. *Analysis, Synthesis, and Design of Chemical Processes*, Fourth.; Prentice Hall, 2012.

(101) Kis, Z. Process-Cost Modelling for Producing 100 Million COVID-19 mRNA Vaccine Doses per Year at Injectable Medicines Manufacturing Sites. *msfaccess.org* **2021**.
(102) *Pyrophosphatase, Inorganic (E. coli) | NEB*. https://www.neb.com/en-us/products/m0361-pyrophosphatase-inorganic-e-coli?srsltid=AfmBOorq0njiVwE3MMcu1rkSBZ7Oj6EKvrgNXgWBCdPe_KYBC3N3YGoU (accessed 2025-03-30).
(103) *SUPERase·In™ RNase Inhibitor (20 U/μL)*. https://www.thermofisher.com/order/catalog/product/AM2696 (accessed 2025-03-30).
(104) *T7 RNA Polymerase*. https://www.promega.com/products/cloning-and-dna-markers/molecular-biology-enzymes-and-reagents/t7-rna-polymerase/ (accessed 2025-03-30).
(105) *DNase, a powerful research tool for DNA manipulations - US*. https://www.thermofisher.com/us/en/home/references/ambion-tech-support/nuclease-enzymes/general-articles/dnase-i-demystified.html (accessed 2025-03-30).
(106) *E58100-1000.0 - Ethylenediaminetetraacetic acid [EDTA], 1 Kilogram*. https://www.rpicorp.com/products/biochemicals/biochemical-reagents/edta-free-acid-1-kg.html (accessed 2025-03-30).
(107) *Sodium phosphate, monobasic monohydrate, 98+%, ACS reagent, Thermo Scientific Chemicals - Chemicals, Salts and Inorganics*. https://www.fishersci.com/shop/products/sodium-phosphate-monobasic-monohydrate-98-acs-reagent-thermo-scientific/AC424390250 (accessed 2025-03-30).
(108) *Sodium chloride ReagentPlus , = 99 7647-14-5*. https://www.sigmaaldrich.com/US/en/product/sigald/s9625?utm_source=google&utm_medium=cpc&utm_campaign=21902440230&utm_content=&gad_source=1&gclid=Cj0KCQjwhYS_BhD2ARIsAJTMMQZVtiJA1uGdqQkWyYxsC1TEfbltswLIPsdgiXGY9gG1KMfTPv0CkPQaAtH-EALw_wcB (accessed 2025-03-30).
(109) *Products List*. Pfanstiehl. https://pfanstiehl.com/en/products-list/ (accessed 2025-03-30).
(110) *WFI Quality Water, 200L bag | Teknova*. https://www.teknova.com/en/products/product-page.html/20143.html (accessed 2025-04-02).
(111) *North Carolina Profile*. https://www.eia.gov/state/print.php?sid=NC (accessed 2025-04-02).
(112) *Hazardous Waste Fees | NC DEQ*. https://www.deq.nc.gov/about/divisions/waste-management/hazardous-waste-section/fees-and-records-management/hazardous-waste-fees (accessed 2025-03-26).
(113) *Chemical Plant and System Operators*. Bureau of Labor Statistics. https://www.bls.gov/oes/2023/may/oes518091.htm (accessed 2025-03-30).
(114) Towler, G.; Sinnott, R. *Chemical Engineering Design: Principles, Practice and Economics of Plant and Process Design*; Elsevier, 2008.
(115) Research, C. for D. E. and. Facts About the Current Good Manufacturing Practice (CGMP). *FDA* **2025**.
(116) Gunter, H. M.; Idrisoglu, S.; Singh, S.; Han, D. J.; Ariens, E.; Peters, J. R.; Wong, T.; Cheetham, S. W.; Xu, J.; Rai, S. K.; Feldman, R.; Herbert, A.; Marcellin, E.; Tropee, R.; Munro, T.; Mercer, T. R. mRNA Vaccine Quality Analysis Using RNA Sequencing. *Nat. Commun.* **2023**, *14* (1), 5663. https://doi.org/10.1038/s41467-023-41354-y.

(117) *WHO Expert Committee on Biological Standardization: Seventy-Fourth Report*, 1st ed.; Technical Report Series - World Health Organization Series; World Health Organization: Geneva, 2022.
(118) Hu, C.; Bai ,Yu; Liu ,Jianyang; Wang ,Yiping; He ,Qian; Zhang ,Xuanxuan; Cheng ,Feiran; Xu ,Miao; Mao ,Qunying; and Liang, Z. Research Progress on the Quality Control of mRNA Vaccines. *Expert Rev. Vaccines* **2024**, *23* (1), 570–583. https://doi.org/10.1080/14760584.2024.2354251.